AD NUMBER

AD872139

LIMITATION CHANGES

TO:

Approved for public release; distribution is unlimited.

FROM:

**Distribution authorized to U.S. Gov't. agencies and their contractors;
Administrative/Operational Use; 31 MAY 1970.
Other requests shall be referred to Air Force Materials Lab., Wright-Patterson AFB, OH 45433.**

AUTHORITY

AFML ltr 29 Mar 1972

AFML-TR-70-124

20

THE EARLY DETECTION OF FATIGUE DAMAGE

George Martin
Schillings Tsang

Los Angeles Division of
North American Rockwell Corporation

TECHNICAL REPORT AFML-TR-70-124

May 1970

The views and conclusions contained in this document are those of the authors and should not be interpreted as necessarily representing the official policies, either expressed or implied, of the Advanced Research Projects Agency or the U. S. Government.

Air Force Materials Laboratory
Air Force Systems Command
Wright-Patterson Air Force Base, Ohio

133

NOTICE

When Government drawings, specifications, or other data are used for any purpose other than in connection with a definitely related Government procurement operation, the United States Government thereby incurs no responsibility nor any obligation whatsoever; and the fact that the government may have formulated, furnished, or in any way supplied the said drawings, specifications, or other data, is not to be regarded by implication or otherwise as in any manner licensing the holder or any other person or corporation, or conveying any rights or permission to manufacture, use, or sell any patented invention that may in any way be related thereto.

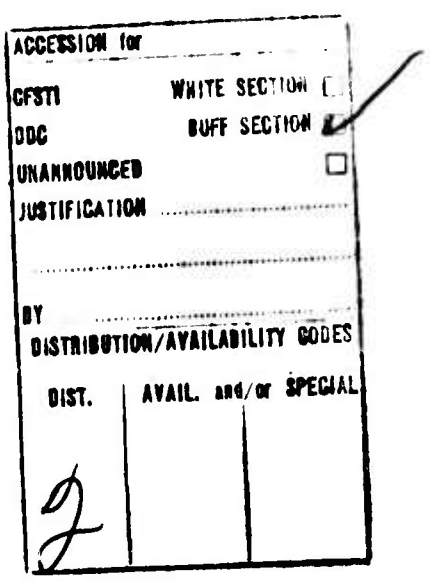

Copies of this report should not be returned unless return is required by security considerations, contractual obligations, or notice on a specific document.

AFML-TR-70-124

THE EARLY DETECTION OF FATIGUE DAMAGE

George Martin
Schillings Tsang

Los Angeles Division of
North American Rockwell Corporation

TECHNICAL REPORT AFML-TR-70-124

May 1970

Air Force Materials Laboratory
Air Force Systems Command
Wright-Patterson Air Force Base, Ohio

BLANK PAGE

FOREWORD

This is the final report on a study for the development of methods for the early detection of fatigue, carried out by the Los Angeles Division of North American Rockwell Corporation. This research was supported by the Advanced Research Project Agency of the Department of Defense and was monitored by the Air Force Materials Laboratory, MAMN, under Contract No. F33615-68-C-1706, initiated under ARPA Order 1244, Program Code 8D10. Mr. R. R. Rowand (MAMN) was Project Engineer. This report covers the period from 1 July 1968 to 28 February 1970.

The program was conducted by the Materials and Producibility Department, N. Klimmek, Manager, under the direction of Dr. George Martin, Program Manager. The work described in this report was carried out by Dr. George Martin, Dr. S. Tsang, Mr. J. F. Moore, Mr. F. Coate, Mr. H. Harvey, and Mr. R. Brose (of the Los Angeles Division of North American Rockwell Corporation), and Dr. L. K. Hanson (of the Power Systems Divisions of North American Rockwell Corporation).

This technical report was submitted by the authors on 31 March 1970.

This technical report has been reviewed and is approved.

THOMAS D. COOPER
Chief, Processing and
Nondestructive Testing Branch
Metals and Ceramics Division

ABSTRACT

The fatigue process of 1100-0 aluminum was studied by means of exoelectron emission and ultrasonic surface wave measurements, and correlated with metallographic examination. Measurement of exoelectrons was accomplished by emission counts, amplified by a Channeltron electron multiplier and integrated over short time intervals. It appears that very early in the fatigue process there is an exoelectron emission peak, whose intensity is related to the intensity of the applied stress, coinciding with initial surface layer slip. The emission event lasts not more than a few percent of the fatigue life. No emission occurs thenceforth until in the final stages of fatigue, just prior to failure, when another emission period is observed. It was further noted that, at least at room temperature, light stimulation is necessary for exoelectron emission from 1100-0 aluminum. Preliminary ultrasonic surface wave measurements disclose a change in material response at about 50 percent of the fatigue life, which so far could not be correlated with metallographic observations.

BLANK PAGE

TABLE OF CONTENTS

LIST OF ILLUSTRATIONS

SECTION I

INTRODUCTION

The phenomena of fatigue of metals and alloys and particularly the early detection of material damage due to these phenomena have always been high on the list of material problems. Our present understanding of the problem comprises a large number of phenomenological observations of the metallurgical events in a great variety of materials during the fatigue progress. There is a very large collection of fatigue test data mainly confined to often unspecified ambient conditions; there are a few tentative theories based on phenomenological observations, and a number of empirical rules based on fatigue test data; and there are comparatively few studies relating fatigue phenomena to physical effects which could serve as indicators of the extent of fatigue damage.

There appear to be two principal reasons for this lack of data required for developing methods for nondestructively determining early fatigue damage. The first reason is the gap between the fundamental investigations into the fatigue mechanism and the fatigue test data. This gap is caused by the difference in scale of approach (fundamental investigations being confined to the atomic scale and fatigue test data to the engineering scale), by the fact that different types of materials are usually chosen for the two groups of investigations, by the lack of coordination between the types of investigators, and because there are too few studies conducted which represent a multidisciplinary approach. The second reason arises from the nature of the fatigue phenomena, which are generally confined to a surface layer. Bulk methods of investigation, such as fatigue tests and overall damping studies, are only able to measure the very diluted effect of these surface phenomena on the bulk properties. Because bulk properties are generally affected by a number of other factors, the sensitivity of these tests to surface phenomena is relatively low. Tests using surface layer sensitive properties have been more successful. However, they have rarely considered the fact that the depth of surface layer affected by progressive fatigue may vary, and if signals from a fixed surface layer depth are investigated, a distortion of the signal-to-fatigue damage effect ratio occurs. Therefore, a rational approach must consider the metal surface layer depth-of-fatigue phenomena in relation to physical and engineering effects. The objective of the study program was the development of methods suitable for the early detection of fatigue damage.

The principal method developed in this program was a measurement method for exoelectron emission. Preliminary investigations into the measurement of propagation of ultrasonic waves were also carried out. Results were correlated with extensive metallographic observations.

SECTION II

SUMMARY

This report covers the work on the investigation into the fatigue process of 1100-0 aluminum by studying exoelectron emission and propagation of ultrasonic surface waves. Exoelectron observations during tension-tension loading were by means of emission counts amplified by a Channeltron electron multiplier and integrated over short time intervals. The exoelectron emission occurred in two stages. The initial stage started soon after the application of the stress and lasted not longer than 10 percent of the fatigue life. The final stage occurred near the end of test when cracks formed and propagated to cause failure of the test specimen. There was a long period of emission quiescence between the two stages. Both the peak intensity of emission and the emission period of the initial stage depended strongly on the applied stress. The higher the applied stress, the stronger was the peak emission and the longer the emission lasted. Exoelectrons still emitted from specimens subject to cyclic stressing at or slightly below the tentatively determined fatigue limit (based on 6 x 10^6 cycles), even though the intensity was quite weak. The emission was also affected by light conditions. At least at room temperature, no emission was observed if the deformation took place in complete darkness. On the other hand, the emission intensity was increased considerably when the specimen was illuminated with long-wave ultraviolet light during test.

Comparison between metallographic observations and the initial stage of emission reveals that this stage of emission coincided with the formation of fatigue-affected layer and surface slip striations. Prolonging the fatigue process beyond this stage of emission appeared to change the depth of attack but little.

The frequencies (1 to 5 MHz) chosen for the ultrasonic tests were dictated by the availability of suitable transducers. The test results for fatigued 1100-0 aluminum indicated a gradual reversing trend for both fatigue life to surface wave velocity and fatigue life to attenuation ratios at about 50 percent of the fatigue life, which could not yet be correlated with metallographic observations.

SECTION III

REVIEW OF PERTINENT DATA

THE FATIGUE PROCESS

GENERAL PHENOMENA IN THE FATIGUE PROCESS

It has been suggested that fatigue damage of face-centered cubic metals at high and low stress levels occurs by different mechanisms (Wood, 1959). The H mechanism at high stress level occupies the steeper portion of the S-N curve where fatigue life increases slowly with decreasing stress. The F mechanism at low stress level operates in the flatter portion of the S-N curve where fatigue life increases rapidly with decreasing stress. It has also been suggested that there is no very clear-cut distinction between the mechanisms at high and low stress levels (Laird and Smith, 1962; Forsyth, 1963). In addition, experiments on aluminum and copper having different texture and ductility reveal that, regardless of the stress level, the operating mechanisms may be influenced to a great extent by texture and ductility (Nair and May, 1968).

It is not the purpose here to make a critical review of the fatigue mechanisms. But it is a concern to know in a specimen the successive events that take place in the fatigue process, leading to permanent damage and ultimate failure of the specimen. The H and F mechanisms concerning the formation of microcracks are briefly described to aid in such understanding, since they shed some light on how fatigue damage in the form of cracks develops.

Cyclic-stressing of face-centered cubic metals at large plastic amplitudes, those corresponding mainly to the H part of the S-N curve, produces coarse slip. At the early stage, severe local strains develop within grain boundaries, resulting in the breakdown of each grain into regions of different lattice orientation separated by irregular subboundaries. As cycling continues, micropores develop on the subboundaries. In copper or brass, these micropores appear during about 1/200 of the specimen life. The micropores multiply and coalesce into cavities which, with continued stressing, multiply and link into microcracks. These microcracks remain smaller than the grains for the greater part of the remaining life. An increase in the number of cycles of amplitudes only starts more cracks in other parts of a grain. The stage of crack formation encompasses the appearance of micropores, cavities, and microcracks in each grain. This stage occupies most of the time of the fatigue process of an annealed metal.

The specimens become structurally unsound early in the formation of micropores. Tests show, however, that there is no loss of mechanical strength, which remains constant, although microcracks develop and multiply. Microcracks can be considered centers of fatigue damage, but they are harmless as long as they are confined in grains and are not self-propagating.

Cyclic-stressing of face-centered cubic metals at small plastic amplitudes produces fine slip zones or bands corresponding to the F part of the S-N curve. They are readily shown as traces brought up by etching and begin to appear after approximately 1/1000 of the specimen life. Though the existing bands are intensified by adding fine slip movements, they are limited in length and are usually shorter than a grain. Such bands are zones of abnormal distortion resulting from the to-and-fro slip movements and show up clearly in grains undergoing cross-slip. Surface notches and peaks, often called intrusions and extrusions respectively, may also form at the end of a slip band where slip bands meet the surface. These surface disturbances, which are about 10^{-4} cm in depth, have been considered responsible for forming fatigue cracks. However, they do not seem to develop with continued cycling. Isolated micropores then form in the interior of slip zones (Wood et al, 1963); They multiply and coalesce to elongated cavities along the zones as cycling continues further. These pores, however, are recently believed to be spurious interpretations of normal extrusions (Dover and Jones, 1967); they are tubular holes extending into the metal from the surface. These holes which constitute the crack front grow and link up to complete the failure of a grain in a direction compatible with the applied stress.

The S-N curve for a body-centered cubic metal, such as iron, generally consists of an inclined portion, called the H part, and a horizontal portion, called the S part, giving rise to a sharp knee (Wood et al, 1964). The basic structural change in iron above the knee in the H part is a pronounced cell formation in the grains, which determines irregular microcracks. At amplitudes below the knee in the S part, slip produces in the surface the form of dense clouds of short, faint markings. The clouds are composed of short, fine slip. Pores form but they are dispersed widely and cannot readily link into microcracks. The fine dispersed slip and dispersed pore formation is therefore an example of fatigue damage in its least effective form.

FATIGUE DAMAGE

Fatigue damage is assessed in different ways. The residual static strength after cracks grow to a certain size is one criterion, while another is the prediction of accumulations of damage when a specimen or a structure is subjected to a number of cycles at one or several different amplitudes. Both criteria have important practical aspects in engineering applications, but neither is suitable for developing early fatigue damage detecting techniques by nondestructive means. The few prominent cracks which may influence the

residual static strength are not of primary concern. Of greater concern is the damage which may occur before a macrocrack develops, so that its detection will prevent formation and growth of additional macrocracks that could cause sudden or catastrophic failure of a structure in service.

The micropores that develop very early in fatigue deformation at subboundaries and the intrusion extension by means of tubular hole growth in a grain are the smallest centers of damage since they eventually multiply and link up to form microcracks. However, even the microcracks existing in the confines of a grain may still be harmless because tests at this stage show no loss of mechanical strength of the specimen. Microcrack damage becomes apparent when the cracks multiply and extend beyond the confines of a grain to link together forming macrocracks.

Since X-ray experiments have shown that nearly all of the small angle X-ray scattering is due to the double-Bragg reflection process, an evidence of the existence of disoriented subgrains (Grosskreutz and Rollins, 1959), the micropores are not actual cavities. Since they show up by etching, they might be regions of concentrated plastic deformation. Transmission electron micrographs indicate that the apparently microporous areas shown in optical micrographs correspond to abnormally dense regions of loops and debris left by oscillating screw dislocations along etched-up slip zones or along subgrain boundaries (Grosskreutz et al, 1966). The slip zones are dense regions of loops and unresolved debris. The subgrain boundaries are dislocation arrays. Thus, micropores are only regions of high internal strain.

It should be noted that micropores, tubular holes, and microcracks are harmless only when the test specimen is subjected to pure fatigue with zero mean plastic strain. They become centers of mechanical weakness that can be pulled apart by a static tensile load which is superimposed on the pure fatigue (Wood and Bendler, 1962). Since structures are often subjected to combined static and cyclic loading, microcracks must be considered potentially dangerous.

Ideally, the early fatigue damage zone is then a few grains deep with each grain containing microcracks within its confines. Since it is difficult to determine this depth, a method of measuring the damage depth is to estimate the amount of surface layer that must be removed by electropolishing or other means to cause the disappearance of persistent slip bands because extrusion and intrusion form at the end of a slip band where the band meets the surface. For example, the persistent slip bands of copper (Thompson et al, 1956) and iron (Klesnil and Lukas, 1965; Sullivan et al, 1961) are 10 to 30 μm and 6 to 10 μm deep respectively.

Transmission electron micrography technique using thin foils reveals that the dislocation structure in regions near the fatigued iron specimen surface (less than 25 μm) is characterized by bands of intense dislocation tangling, individual dislocations within the bands being unresolved, and arrays of parallel rows of dislocation loops, the arrays often extending for considerable distances across a given grain (Wei and Baker, 1965). On the other hand, micrographs of the interior show isolated clusters of dislocations and scattered dislocation loops and loop trails. Since the dislocation structure in the surface region is completely different from the dislocation structure in the interior and since thickness of the foil (less than 25 μm) taken from the fatigued iron specimen surface is of the same order of magnitude as the amount of surface layer (6-10 μm for iron and 10-30 μm for copper) removed by electropolish to eliminate persistent slip bands, the observed dislocation structure must be correlated with the fatigue damage zone because the damage occurs only at the surface layer.

PHYSICAL PROPERTIES RELATED TO FATIGUE DAMAGE

It is known that most physical properties of metallic materials change with plastic deformation. Some of the properties would also be influenced by cyclic stressing. It is then possible to utilize such changes to indicate fatigue damage. Though fatigue cracks on a macroscale in metals can be detected by various nondestructive techniques, detection or evaluation of the early damage prior to the formation of macrocracks is not simple or easy. Some knowledge of the change in physical phenomena in the course of fatigue deformation is needed for the development of techniques to detect early fatigue damage. Such knowledge, together with some other characteristics which might be useful, is described in the following paragraphs.

MAGNETIC HYSTERESIS AND EDDY CURRENT LOSSES

In the majority of ferromagnetic materials, magnetic hysteresis is caused by a delay in the change of magnetization. Loss of energy to magnetic hysteresis depends on the average amplitude of internal stresses. Internal stresses also have influence on the resistance of the metal, both magnetic and nonmagnetic, to alternating current. Changes in resistance and disturbance of continuity result in eddy current losses. The region having high internal stresses could be a nucleation site of fatigue crack since transmission electron micrographs of foils prepared from specimens subject to cyclic stressing reveal that the region of abnormally high dislocation density corresponds to the fatigue zone in the specimen (Grosskreutz et al, 1966).

The variation of the total losses in steels in fatigue process has been investigated by Gushcha (1965). The change of the losses in the course of deformation above the fatigue limit can be divided into four stages. In the

first stage, the losses decrease with number of cycles while work-hardening revealed by microhardness measurement intensifies. Slip lines appear in some grains. In the second stage, there is an increase in the losses, but microhardness is lowered. These changes are attributed to relaxation or softening of the most stressed grains. As the number of cycles increases, further softening becomes intensified while work-hardening is slowed down. When the process of softening is more intensified, microhardness is lowered even more and more. The slip lines become wider and longer, and the number of slip lines increases. The rise of the losses continues but at a lower rate in the third stage. Microcracks form and some of them link together and develop to a fatigue macrocrack. Formation of a macrocrack is marked by a certain lowering of the losses at the end of the third stage. A steep climb of the losses in the fourth stage indicates a rapid growth of the fatigue crack. Duration of each of these stages differs and depends on the material and the level of the cyclic stresses. The duration of each stage relative to the total fatigue life for a given material, however, is about the same for all stress levels.

Below fatigue limit, microhardness increases while the losses decrease with the increasing number of cycles. Softening can occur in weak grains, but this process does not spread to other grains because of low cyclic stresses.

Since the maximum of the losses vs number of cycles curve indicates the formation of a macrocrack, detection of earlier fatigue damage must then rely on the determination of the onset of the third stage when the rate of the losses is lowered due to the formation of microcrack.

It should be noted that the magnetic hysteresis and eddy current losses are not entirely caused by internal stresses. Inclusions, voids, cracks, and chemical segregation can also influence these losses.

Magnetic tests measuring perturbation in the magnetic field have been employed to detect fatigue damage in the form of cracks (Kusenberger et al, 1964 and 1966). The perturbation is caused by the change of magnetic permeability by internal stresses or the other factors mentioned previously. The crack is indicated by a sudden increase in peak-to-peak signal amplitude in a record. The detection of cracks is primarily a function of signals caused by the stressed volume adjacent to the crack and not by the material separation. The minimum crack length that can be detected in 4340 steel is 0.006 to 0.008 inch.

ELECTRIC IMPEDANCE

The electric impedance at a fixed frequency of a metallic specimen whose dimensions remain unchanged during measurement depends on electric conductivity and magnetic permeability. To make the use of the skin effect of

high-frequency currents, it is possible to study the change of electric impedance during fatigue deformation. When Armco iron wire is subject to torsional fatigue, no change in impedance at 35 kHz is observed if the shear strain is below a critical value which is less than the fatigue limit (Shlyapin et al, 1967). The impedance hysteresis loop also does not change its form. If the cycling strain exceeds the critical value but is below the fatigue limit, the impedance decreases gradually with an increasing number of cycles. Though the hysteresis loop changes in the process, it tends to approach the stable form below the critical strain. The impedance decreases more rapidly with an increasing number of cycles when the cycling strain is above fatigue limit. Shortly before failure, some increase in the impedance is observed, probably due to the appearance of fatigue cracks. The rate of change in the hysteresis loop during test differs little from the change at the fatigue limit. However, the loop cannot become stabilized because of failure of the specimen. Early fatigue damage must then be detected by analyzing the change in the form of the hysteresis loop and the trend of the impedance vs number-of-cycles curve before the rise of impedance due to the formation of macrocracks.

Another approach is to make the specimen after fatigue deformation one end of a low-loss cylindrical cavity resonator (Benson et al, 1968). The transmission loss of the cavity is mainly due to the loss of the specimen. The system must be operated at the exact resonant frequency of the resonator in order to make the magnitude of the signal transmitted through the cavity meaningful. The loss curve for a 2024-T3511 aluminum alloy specimen shows little change until approximately 80 percent of the fatigue life is spent. It then rises rather sharply before failure of the specimen.

Cylindrical specimens have also been made in the form of a low-loss, half-wave linear resonator operated at frequencies near 1 GHz (Benson et al, 1968). The increase in electric resistivity at the surface layer due to the presence of microcracks results in an increase in bandwidth of the resonator when it is considered as a band-pass filter. When fatigue deformation in aluminum alloys is measured, the surface resistivity does not change in the first one-fourth of fatigue life. Afterwards, the measured resistivity can be either above or below the previous constant value. The scatter is so wide that it is difficult to correlate fatigue damage with surface resistivity.

OPTICAL PHENOMENA

An optical correlation technique has been used to detect changes in surface structure resulting from fatigue deformation (Chuang, 1968). The correlation function for a given surface area is measured before and after cyclic stressing in terms of light intensity output of a coherent optical system.

Change in surface structure produces a decrease in correlation intensity. The surface strain that can be detected is of the order of 1 micron.

The correlation intensity vs number-of-cycles curve can generally be divided into three stages. A sharp loss of the correlation intensity (as much as 80 percent) in the first few minutes constitutes the first stage. The loss then becomes relatively steady in the second stage. Finally, a sharp loss before a visible crack appears starts the third stage. Early fatigue damage must therefore occur in the first two stages.

INTERNAL FRICTION

Internal friction of solution-treated aluminum alloys containing magnesium subject to cyclic stressing below the fatigue limit is practically constant. Above the fatigue limit, internal friction decreases with an increasing number of cycles. The formation of a fatigue crack is indicated by an increase in internal friction (Hanstock, 1947). However, tests on solution-treated and aged aluminum alloys containing mainly copper reveal that above but near the fatigue limit, the internal friction increases almost imperceptibly during many millions of cycles, followed then by a rapid rise before specimen failure. The rise is mainly due to precipitation induced by cyclic stressing and not to the formation of cracks (Hanstock, 1954). In pure metals, such as aluminum, cadmium, and copper, above the fatigue limit the internal friction first increases and remains practically constant with continued cyclic stressing. Near the end, there is again a rise which is attributed to the appearance of a fatigue crack (Gorshkov and Postnikov, 1965).

Both internal friction and early fatigue damage are related to the movement of dislocations and their interaction with point defects. Their relationship, however, is complex because internal friction is associated with bulk-property-type measurement while fatigue damage occurs only at the surface layer.

PROPAGATION OF ULTRASONIC WAVES

In addition to detecting flaws, propagation of ultrasonic waves in metal parts has also been employed to investigate early fatigue damage by means of noting the changes in ultrasonic attenuation and velocity. Measurement of the ultrasonic attenuation in aluminum specimens subject to tension-tension or tension-compression cyclic loading reveals that the attenuation starts to decrease from the beginning, reaching a minimum value between 100 and 1000 cycles or approximately at 1/100 to 1/1000 fatigue life (Truell et al, 1959 and 1961). Subsequently, the attenuation rises again as deformation continues.

This variation in attenuation with time is attributed to a dislocation effect. A large increase in the dislocation density can be expected within a few cycles at the beginning. The dislocation density increases with continued cycling until dislocation damping, which contributes to attenuation, is reduced both from the shortening of loop lengths, due to increased intersection and defect pinning, and from direct interference or interaction of the dislocations among themselves.

Another phenomenon also causes a rise in attenuation as the dislocation density increases with continued cycling. Regions of dense dislocation form because of the shortening loop lengths and their mutual interference. High internal strains are present in these regions within each grain. These regions are therefore scattering centers, causing increased attenuation as their size and number increase with number of cycles. The minimum of the attenuation vs number of cycles curve is a result of competition between the decrease in dislocation damping loss and the increase in the scattering loss. The increase in attenuation by scattering eventually becomes large and dominant.

Under fatigue deformation, either in tension or in compression, the velocity of wave propagation starts to decrease at the beginning with respect to the initial value before deformation. This decrease is characteristic of dislocation damping behavior. The change in velocity becomes smaller as deformation continues until the range of cycling for the attenuation minimum is reached. The change then again begins to increase rather rapidly with an increasing number of cycles.

The regions of high internal strain in a grain, which serve as scattering centers to the propagation of ultrasound, could be identified with the regions of abnormally high dislocation density revealed by transmission electron micrographs. Such regions are therefore the potential nucleation sites of microcracks.

The wave modes employed by Truell and his associates were mainly longitudinal waves. A longitudinal wave is a volume-type wave, but fatigue damage develops only at or near the surface of a test specimen. Rayleigh waves or surface waves therefore seem more appropriate for studying the change in attenuation and velocity of propagation. Moreover, depth of wave penetration is controllable.

The change in attenuation as well as velocity of propagation of a Rayleigh wave in mild steel subject to fatigue deformation has been investigated by Herlescu and his coworkers (1967). Both attenuation and velocity tend to increase slightly at the early stage of fatigue (about 1/100 to 1/1000 life). They then drop considerably and become somewhat constant as

cycling proceeds. Finally, there is a pronounced increase of attenuation as a result of dispersion of ultrasound at the microcracks. Velocity in this interval changes relatively little.

Relaxation and work-hardening are thought to cause such changes in the propagation of ultrasound waves. Relaxation is assumed dominant in the beginning. Later, work-hardening intensifies, and relaxation ceases to play an important role. Search of fatigue damage should thus be concentrated in the period prior to the formation of microcracks when both attenuation and velocity first decrease and then become constant.

EXOELECTRON EMISSION

The term exoelectron has been used to describe electrons emitted from both metals and nonmetals which have been subjected to various treatments, such as abrasion, mechanical deformation, irradiation with ultraviolet light, X-rays or ultrasonic waves, electron bombardment, electric gas discharge, chemical interaction between the material surface and the ambient gas, phase transformation upon heating or cooling, etc. The first comprehensive discussion of this subject took place in an exoelectron conference held in 1956 in Austria. A number of reviews (Grunberg, 1958; Mueller, 1961; Bohun, 1963; Bohun, 1965; Ramsey, 1965; Brotzen, 1967) have been published since then. Because exoelectron emission can be excited in a variety of ways, there is much confusion in the literature on the mechanism of emission. The present survey will therefore not be devoted either to examining the mechanisms or to reviewing the present state of the art. Rather, the objective is to make a concise report on the exoelectron emission arising mainly from abrasion or plastic deformation of metallic materials. Such knowledge is essential to developing new testing techniques based upon exoelectron emission for assessing the damage of metals subjected to cyclic stressing. An annotated bibliography containing articles dealing mainly with exoelectron emission from abraded or plastically deformed metals and published after 1956 is presented in appendix I.

The emission of electrons from abraded or deformed metal surfaces has been interpreted in several ways: (1) The interaction of gas with the freshly worked surface resulting either in the release of energy due to chemisorption of oxygen (Haxel et al, 1952; Lohff, 1956) or the absorption of water vapor (Ramsey, 1967) or in the formation of a layer of defected structure containing trapping sites which produce a surface of lower work of function (Grunberg and Wright, 1955; Ramsey and Garlick, 1964), (2) the release of energy associated with the vacancies reaching the surface by diffusion (von Voss and Brotzen, 1959; Ku and Pimbley, 1961), and (3) the transfer of energy associated with the stress field around dislocation to electrons (Krogstad and Moss, 1965). The active emission centers are assumed

to be chemisorbed atoms, vacancy clusters, points of emergence of dislocations on the surface, etc. Therefore, exoelectron emission can occur by the interaction between the metal surface and the ambient gas as well as by the deformation of the metal lattice. It is also found that the effect of the former can be weakened by localized and dynamic loading in vacuum (Mints and Kortov, 1967).

Emission caused by the deformation of the lattice must be associated with dislocations or point defects. This is demonstrated by the correspondence between the darkened spots on the emulsion applied to a statically strained zinc single crystal and dislocation etch pits along the slip lines (Meleka and Barr, 1960), and by the emission of electrons from aluminum after quenching from temperatures between 300° and 450° C (Claytor et al, 1966). The release of electrons can be facilitated by lowering the work function of the metal surface, since change in the contact potential with strain in molybdenum and tantalum indicates that the work function of these metals is reduced as a result of plastic deformation (Andreev and Paligé, 1962 and 1964). The work function changes are associated with surface structure modifications.

The kinetic characteristics of emission is influenced by the mobility of point defects. The time for ground aluminum to reach the maximum emission before decay sets in is shorter than the time for ground gold at a pressure about 10^{-4} torr (Mints and Kortov, 1967). Shorter time to peak emission is attributed to higher mobility of point defects because time is required for dislocations and point defects moving to the metal surface. By the same reasoning, decay of the emission from the metal surface having point defects of lower mobility should be slower. This phenomenon is observed in the experiment with ground silicon and germanium (Kryuk et al, 1966). The slower decay for silicon is due to lower mobility of vacancies, indicated by a greater activation energy for self-diffusion in silicon.

The mobility of point defects increases with temperature. The emission from abraded metal surfaces (Ku and Pimbley, 1961; Ramsey, 1965; Williams, 1966) or strained metal specimens (Hempel et al, 1964) has been found to increase with rising temperature. However, the relation between exoelectron emission and migration of the point defects to the surface is still not well understood because it is difficult to avoid the influence of ambient gas exerted on the surface. Freshly abraded aluminum specimens and those that were abraded and aged at room temperature for 8 days exhibited similar emission when their surfaces were etched (Mueller and Pontinen, 1964). Defects in the aged specimens had ample time to migrate to the surface and to internal sinks. The observed emission from abraded, aged, and etched specimens is probably due to interaction between the ambient gas and the new surface produced by etching.

In addition to surface conditions, structure of the metal surface can influence exoelectron emission. Local indentation on metallurgical phases of steels results in varying emission intensity (Kortov and Mints, 1965; Bogachev et al, 1966). The intensity of ferrite is greater than that of austenite which in turn has more intense emission than either martensite or epsilon carbide. Grains and grain boundary may also have different exoelectron emission.

Emission from most abraded or otherwise deformed metals is not observed in total darkness. Light is necessary, and the photoelectric threshold is shifted (Conrad and Levy, 1961). The explanation is that the energy of impinging photons is needed to add to the energy which is released by vacancies at the surface in order to exceed the work function of the surface (Pimbley and Francis, 1961). However, emission without photostimulation has been observed during plastic deformation of aluminum coated with a thick (over 50 μm) oxide layer (Gieroszynski and Sujak, 1965). Two emission peaks occur at a strain of 0.01-0.02 and 0.03-0.04. The emission is considered to originate from the oxide layer and is attributed to large electric fields (about 10^7 v/cm) when the cracks in the oxide layer are formed.

Deceleration methods have been used to determine the average kinetic energy of exoelectrons (Lohff, 1957; Bathow, 1958). The value for abraded metals in vacuum varies from 0.13 to 0.20 ev. The highest energy that can be determined depends on the emission intensity and the sensitivity of the measuring apparatus. The emission intensity prior to saturation relates to the grid potential by the equation:

$$N = N_o \exp\left(\frac{U - U_k}{\bar{U}}\right)$$

where N = number of emitting electrons per second
N_o = saturated number of emitting electrons per second
U = grid potential
U_k = contact potential between grid and the specimen
$\bar{U}$ = a constant

A design of a spectrometer to measure electron energy is shown in appendix II.

Since exoelectrons emit at the surface of a material, it is essential to know the thickness of the surface responding to emission. Experiments on emission excited by electron bombardment reveal that the estimated thickness varies from 2×10^2 Å at 1 kv for tungsten and germanium (Seeger, 1955 and 1957) to 5×10^3 Å at 5 kv for $CaSO_4$ containing manganese (Vogel, 1960).

Successive removal by etching of surface layers from an abraded aluminum specimen shows that emission dies out at approximately a depth of 0.2 μm or 2×10^3 Å (Mueller and Pontinen, 1964).

Since fatigue cracks usually start at or near the surface, both fatigue damage and exoelectron emission belong to surface phenomena. Furthermore, cyclic stressing can accumulate rather large amounts of plastic strain, and the emission intensity increases with increasing amount of deformation (von Voss and Brotzen, 1959). Therefore, exoelectron emission could be a measure of cumulative fatigue damage.

Exoelectron emission by fatigue deformation has been reported (Grosskreutz and Bensen, 1963; Hempel et al, 1964; Krogstad and Moss, 1965; Bogachev et al, 1966; Mints and Kortov, 1967; Mints et al, 1968). The intensity generally increases with the number of cycles. After it reaches a saturated value, it slowly decreases until specimen failure. A rapid rise of intensity shortly before failure has also been observed. This rise is attributed to the formation of fatigue cracks, but it cannot be used to assess fatigue damage because the damage occurs and grows at the early stage of fatigue deformation. Therefore, the progressively changing emission events during the test before the final rise should be analyzed.

OTHER PHENOMENA

Acoustic emission has been associated with the formation and growth of macrocracks. This phenomenon might also be useful to indicate fatigue damage at its early stage. Since it is the subject of several associated studies, it has not been covered here.

The possibility of using nuclear phenomena can also be considered. The use of the Mössbauer effect for the measurement of residual stresses has been considered by Gonser and Martin (1963), and Gonser (1968) suggests that plastic deformation would affect nearest neighbor interactions. However, for practical purposes, the use of the Mössbauer effect is limited to ferrous alloys.

CONCLUSIONS

Fatigue damage can be correlated with the changes of a number of physical properties. The physical properties which have been investigated have their own merits as well as drawbacks. Magnetic hysteresis losses are limited to ferrous materials. Internal stresses are the principal factor that causes magnetic hysteresis and eddy current losses, but fatigue process is not mainly dependent upon internal stresses. The electric impedance method is better to indicate crack formation and propagation leading to specimen failure than to detect earlier fatigue damage. The changes of correlation intensity of a

coherent system in a fatigue process might offer an indication to earlier fatigue damage. More information is needed. Internal friction is a bulk-type physical property, but early fatigue damage concentrates in the surface layer. Their correlation is therefore poor. Propagation of ultrasonic waves is a promising method to detect fatigue damage. Surface waves instead of longitudinal or shear waves should be utilized to interrogate only the surface layer. There is very likely a relation between fatigue damage and exeoelectron emission because both belong to surface phenomena.

BLANK PAGE

SECTION IV

EXPERIMENTAL EQUIPMENT

FATIGUE TEST UNIT

To investigate the various nondestructive test approaches under dynamic conditions and appropriate environmental control, it was necessary to construct a small, portable fatigue test unit. This unit consists of a pumping, timing, and metering unit which feeds hydraulic fluid into a double-acting piston and cylinder arrangement connected directly to one end of the specimen (figure 1). The piston and cylinder unit is rigidly attached to a loading frame, which also supports the other end of the specimen. A microswitch attached to the loading frame stops all circuits on specimen failure. A plate inserted between the piston and cylinder unit and the specimen serves as a base for mounting a ring carrying a glass chamber, which can be evacuated and which contains necessary instrumentation. Figure 2 shows the ring, the microswitch, and a specimen in the loading frame. The unit is designed for loads up to 5,000 pounds and for cycling rates varying from a steady pull to 120 cycles per minute. The rate for the tests planned is standardized at the upper limit. Actual loads are measured by four strain gages mounted on the connecting link between the piston and the lower end of the specimen. Connecting the lower specimen grip and the base plate is a metal bellows, which gives a flexible vacuum seal. The number of cycles is counted by a counter installed on and electrically connected to the control box of the hydraulic system. Variation of the load during test is displayed on a recorder connected to a carrier amplifier into which the output of the strain gages is fed. A calibration curve relates the load to hydraulic pressure.

The vacuum system (figure 3) consists of a mechanical pump, an oil diffusion pump, two liquid nitrogen cold traps, gages necessary for measuring pressure, and a glass chamber in which the loading frame is housed. The use of a second cold trap is to prevent backstreaming of oil from the diffusion pump and contamination of the instruments in the glass chamber. The ring on which the glass chamber is mounted is pierced by a 2-inch-diameter vacuum suction tube, a 5/16-inch air inlet hole, and electric vacuum leadthroughs. Altogether, provision is made for a high-voltage leadthrough, an RF leadthrough, a seven-pin milliampere leadthrough, and an eight-pin leadthrough for larger currents. The load strain gage leads for load calibration are on the atmosphere side of the bellows.

EXOELECTRON EMISSION

Two approaches to detect and measure exoelectron emission were tried. The first consisted of attempts to detect exoelectrons by means of phosphors. A number of cathode ray phosphors were available. Attempts at detection were

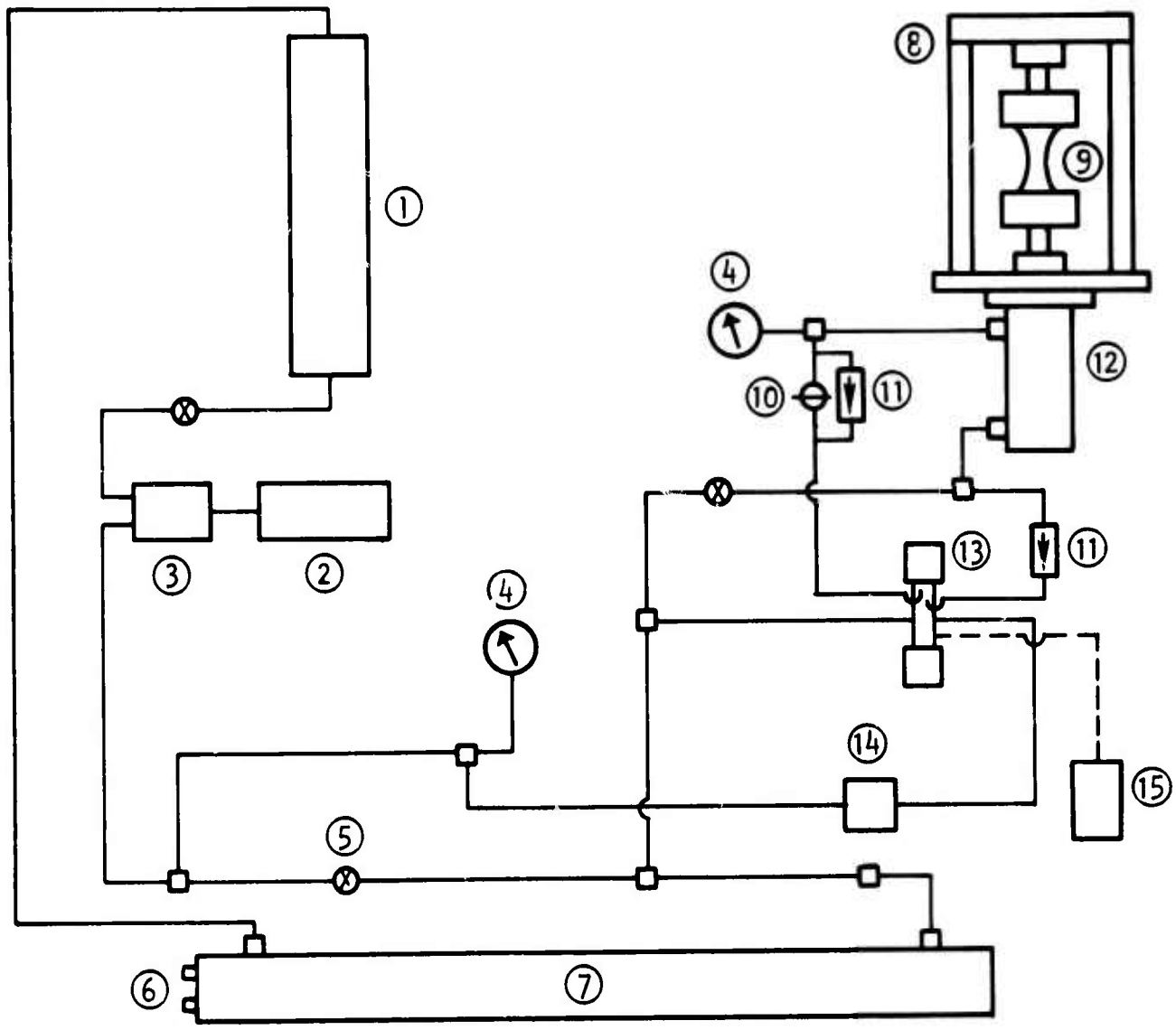

——— HYDRAULIC LINE - - - - ELECTRICAL LINE

1	RESERVOIR	10	NEEDLE VALVE
2	MOTOR	11	CHECK VALVE
3	PUMP	12	HYDRAULIC CYLINDER
4	HYDRAULIC PRESSURE GAUGE	13	FOUR-WAY SOLENOID VALVE
5	BY-PASS VALVE	14	PRESSURE RELIEF VALVE
6	WATER INLET AND OUTLET	15	CONTROL
7	HEAT EXCHANGER		
8	LOADING FRAME		
9	SPECIMEN		

Figure 1. Hydraulic System

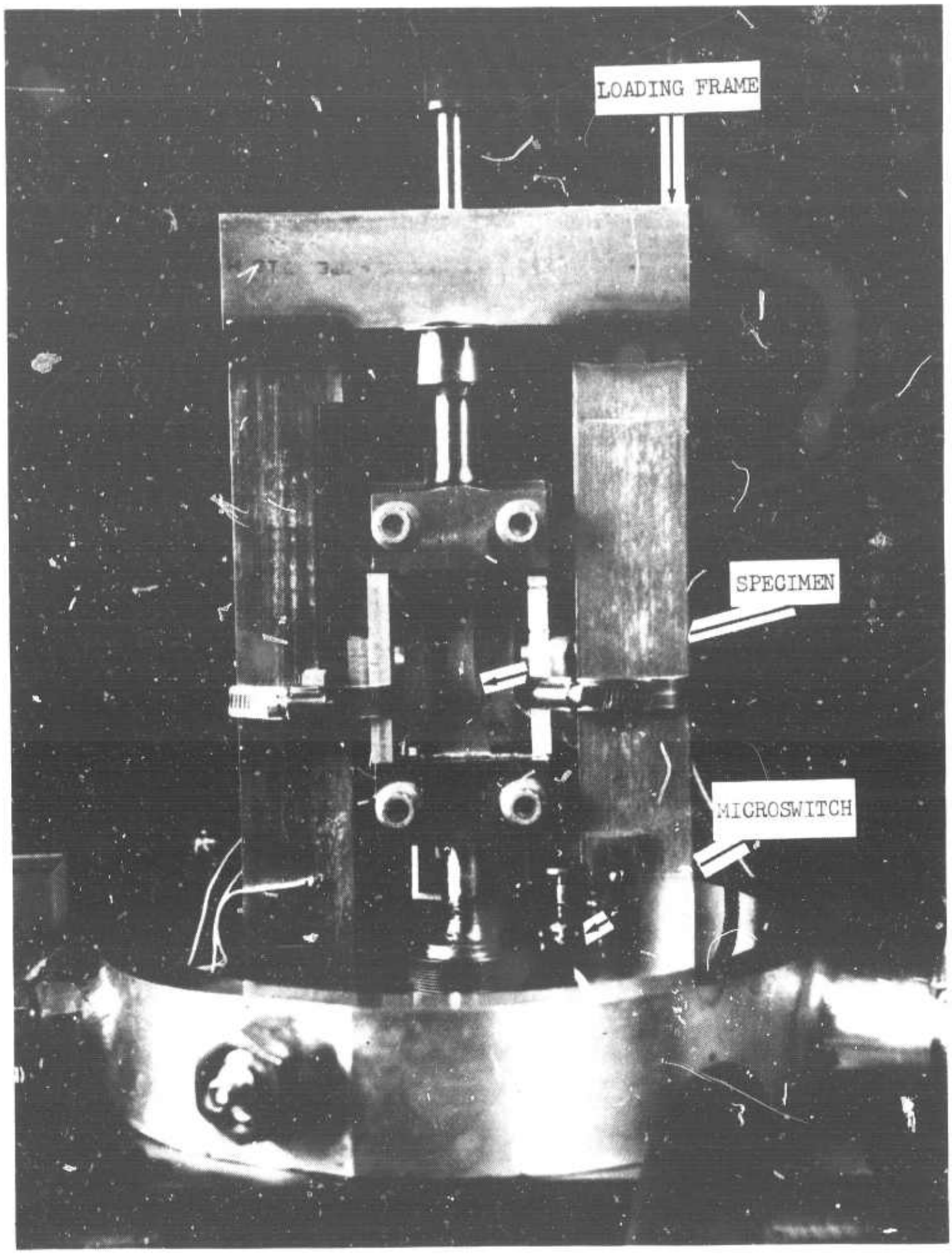

Figure 2. Specimen and Loading Frame

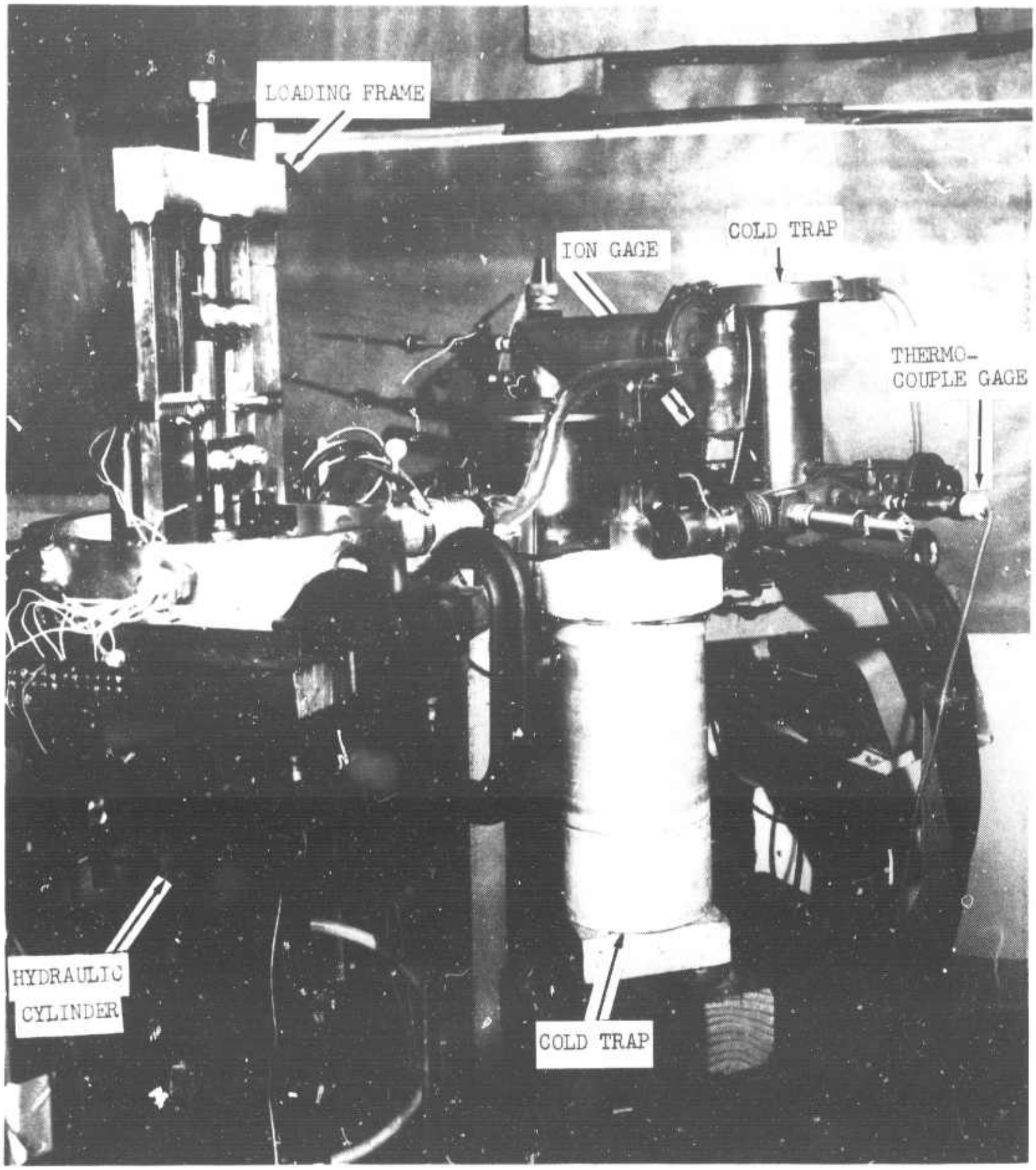

Figure 3. Vacuum System

both visual with the unaided eye and by means of an image intensifier. The instrument used was an Army Night Vision Sight AN/PVS-2 Starlight Scope with about 4X image magnification and approximately 40,000X intensity magnification. The use of this instrument required a completely blacked-out room in which the entire fatigue and vacuum equipment was placed.

The other approach utilized a Bendix type 4039 Channeltron electron multiplier, connected as shown in figure 4. The semiconductor-type multiplier is helical in shape and has a horn of 10 mm diameter at one end. The horn faces the middle portion of the specimen about 3/8 inch away through a hole at one side of a shield box. The shield box is charged at the same positive potential as the bias voltage to the electron multiplier so that only the electrons emitted from the specimen surface facing the horn enter the electron multiplier. The multiplier has a gain of about 10^8 with the application of 3,000 volts dc. The pulses from the electron multiplier are amplified and stretched before they are counted. The number of counts in either 1 or 10 seconds is finally printed on a tape by a digital printer. Figure 5 shows the Channeltron electron multiplier with the shield off and mounted on the loading frame.

After completion of several tests, the type 4039 Channeltron electron multiplier started to behave erratically. It was therefore replaced with a type 4013 electron multiplier which is circular shaped and has a horn with 3 mm diameter. Owing to this change of multiplier configuration as well as the space available in the glass chamber, the type 4013 Channeltron electron multiplier was placed about 2 inches away from the specimen. To compensate for the longer path for electron travel and the smaller horn, the shield box in which the electron multiplier was mounted was not at bias potential but was grounded to collect as many electrons as possible from the specimen surface.

PROPAGATION OF ULTRASONIC SURFACE WAVES

Two methods of surface waves testing were considered: The variable-angle acrylic wedges and an angulated water-column tube. The water-column method does not have flexibility for changing the incident angle but does permit evaluation of a wide range of standard commercial ultrasonic transducers in terms of crystal diameter, test frequency, focusing effects on beam control, etc.

Acrylic wedges were designed for adapting existing 2.25 MHz crystals of lithium sulphate for the mode conversion to surface wave mode. The crystals ranged in sizes from 1/2 to 3/16, 1/4, and 5/16 inch diameter and were encapsulated in an acrylic cylinder, with the crystal axis normal to the principal axis of the cylinder. The crystal assembly was fitted to the acrylic wedge, as shown in figure 6, with provisions for rotating the crystal to vary the incident angle and for locking in a fixed angle.

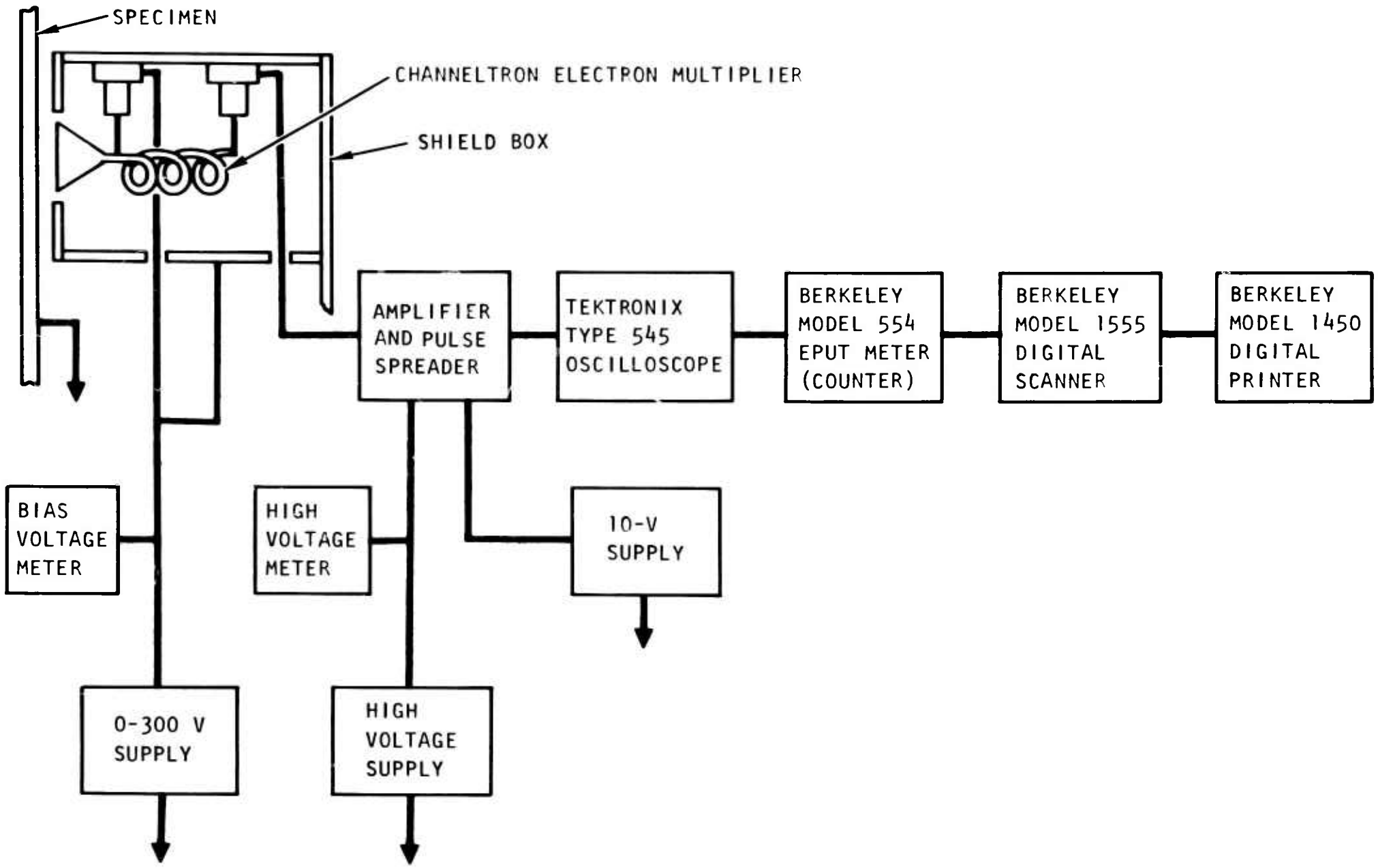

Figure 4. Block Diagram for Measuring Exo-electron Emission

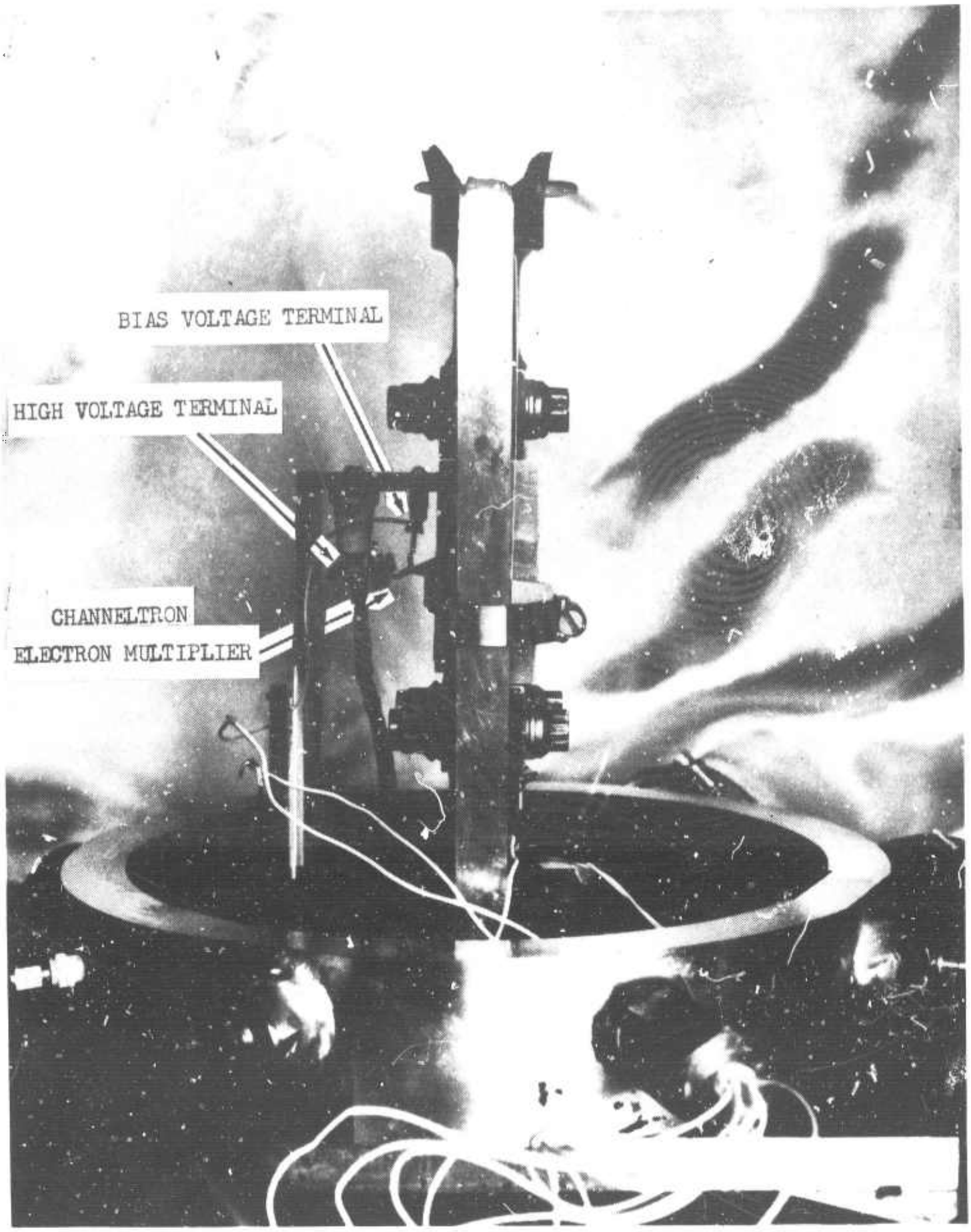

Figure 5. Channeltron Electron Multiplier and Loading Frame

TOP VIEW

3/8 IN. DIA. 1/4 IN. DIA. 1/8 IN. DIA.

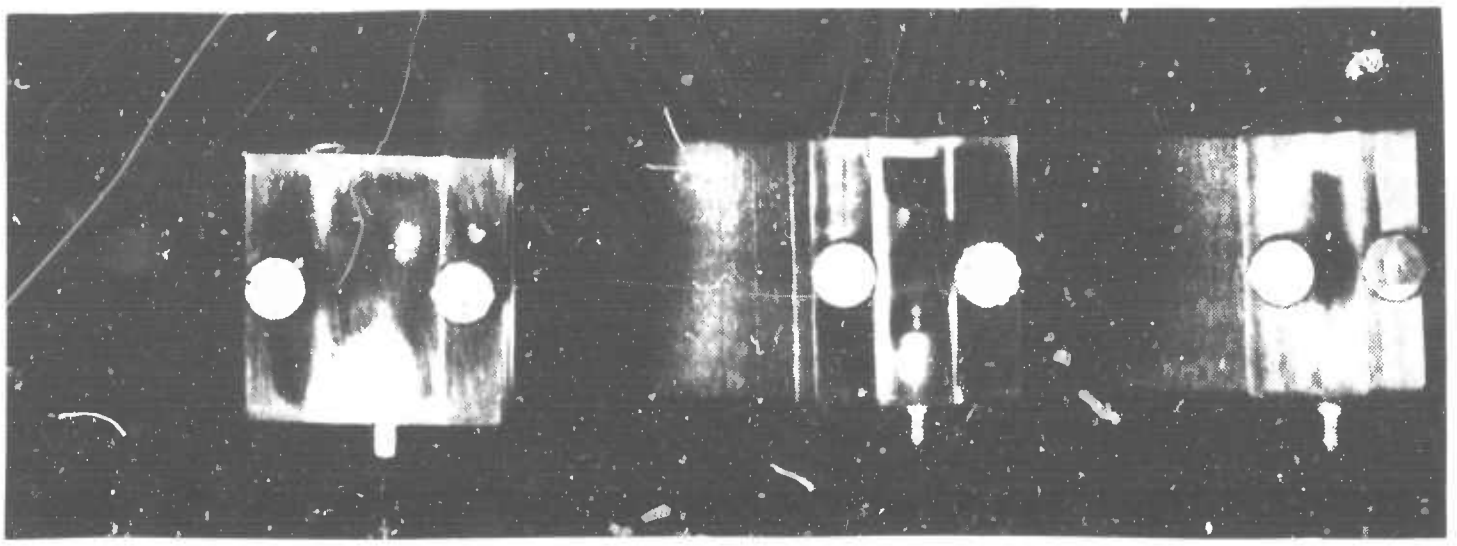

SIDE VIEW

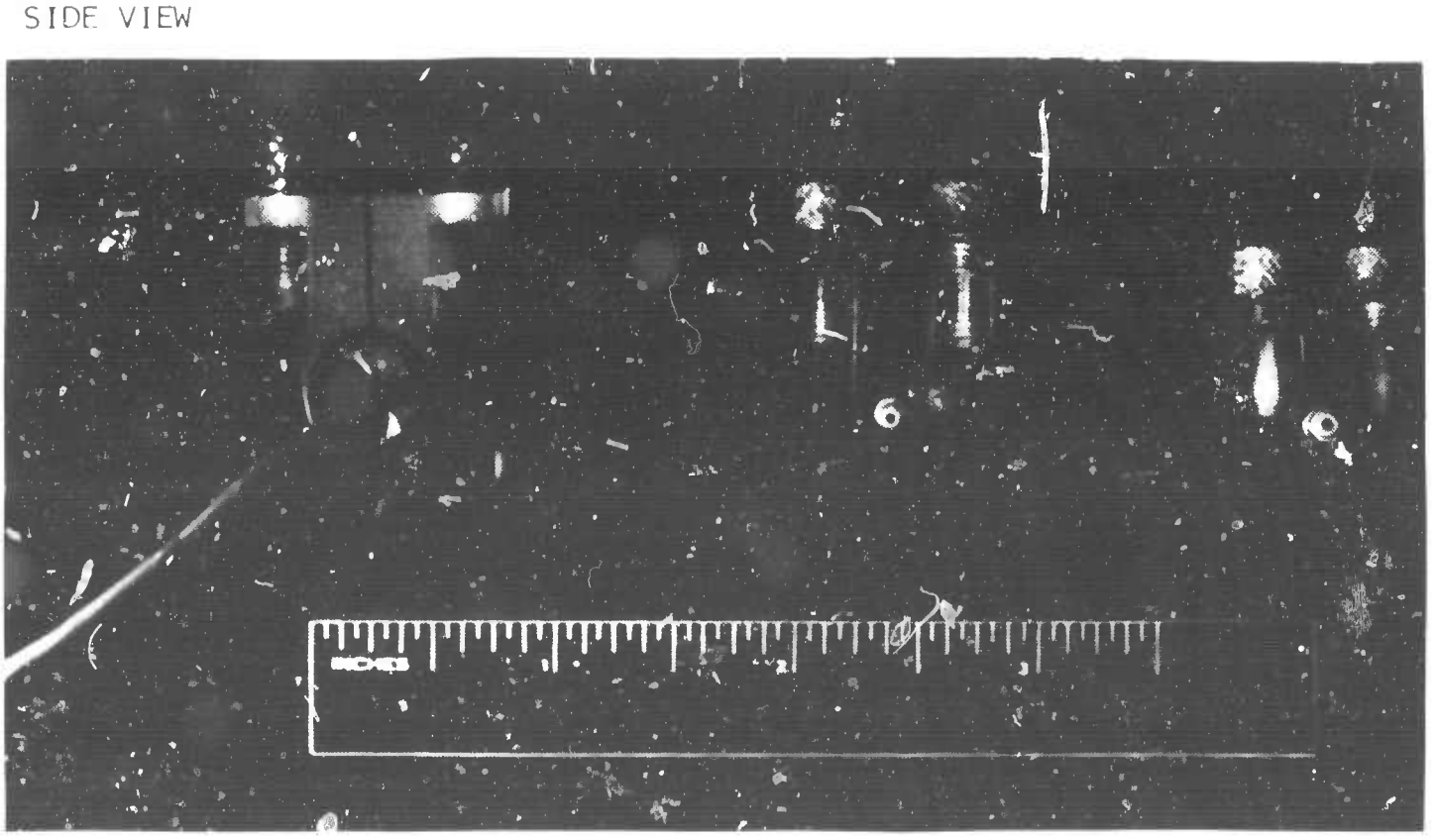

Figure 6. Surface Wave Transducers, 2.25 MHz, Acrylic Wedges

The incident angles for surface wave mode can be estimated from the following equation:

$$\Theta_i = \sin^{-1}\left(\frac{V_L}{V_R}\right)$$

where Θ_i is the incidence angle, V_L is longitudinal velocity in the acrylic wedge material, and V_R is the surface wave velocity in the test material. When the ratio of V_L/V_R equals or exceeds unity, surface waves cannot be generated since the incidence angle is 90 degrees or greater.

However, since the longitudinal acoustic beam from the crystal diverges, the practical optimum angle of incidence is larger and must be determined empirically. The acrylic wedges permitting rotation of the crystal were used for the purpose. As the crystals were rotated, the conditions for pure surface wave generation in the material were determined by touching the surface and noting when the reflected energy could be cancelled. The optimum angle was then determined by increasing the incident angle from a value less than the theoretical value until pure surface wave propagation was obtained.

The water column transducer shown in figure 7 was developed for surface wave propagation using the water-specimen interface for the mode conversion. The column angle was calculated as for the acrylic wedges except that the value was for water. The length of the column (Yo) is calculated using the near field equation:

$$Yo = \frac{0.25\ D^2 f}{V_L} - \frac{0.25\ V_L}{f}$$

where D is the diameter of the crystal, f is the frequency, and V_L is the longitudinal velocity in water. The calculation for 0.5-inch diameter crystal operating at 2.25 MHz in water gives a near field length of 3.6 cm or 1.42 inches.

Evaluation of surface wave transducers was carried out in terms of standardized coupling techniques, velocity determination, and simulated crack detection. The acrylic wedge transducers yielded better results than did the water column transducer. Of the acrylic wedge transducers, the 1/2-inch transducer proved capable of detecting all simulated cracks within a beam spread of approximately 4 degrees.

A 1/2-inch-type SMZ surface wave transducer operating at 2.25 MHz (manufactured by Automation Industries) was used in both velocity and attenuation measurements. Two systems were employed to measure the surface wave velocity. A conventional system (figure 8) consists of a Sperry UW reflectoscope, a Tektronix type 544 oscilloscope, and a Hewlett Packard Model 410B ac voltmeter. A precision ultrasonic velocity measurement system (figure 9) utilizes pulse

TOP VIEW

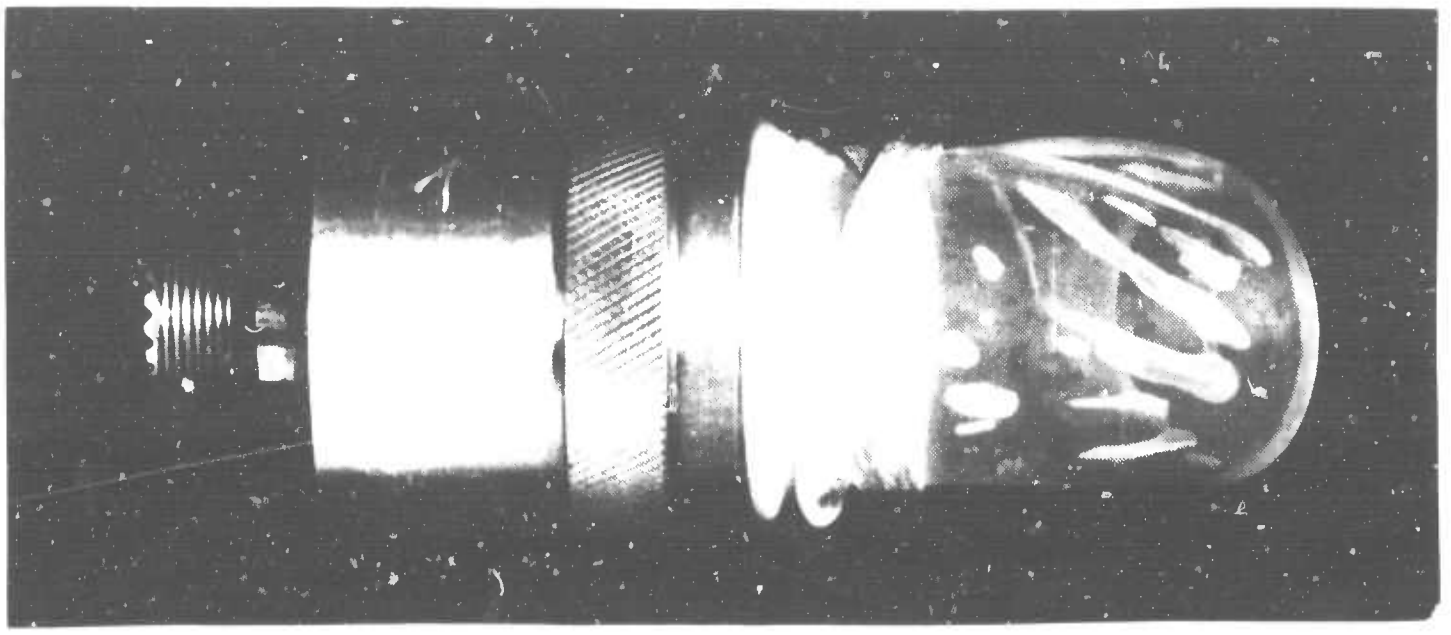

SIDE VIEW

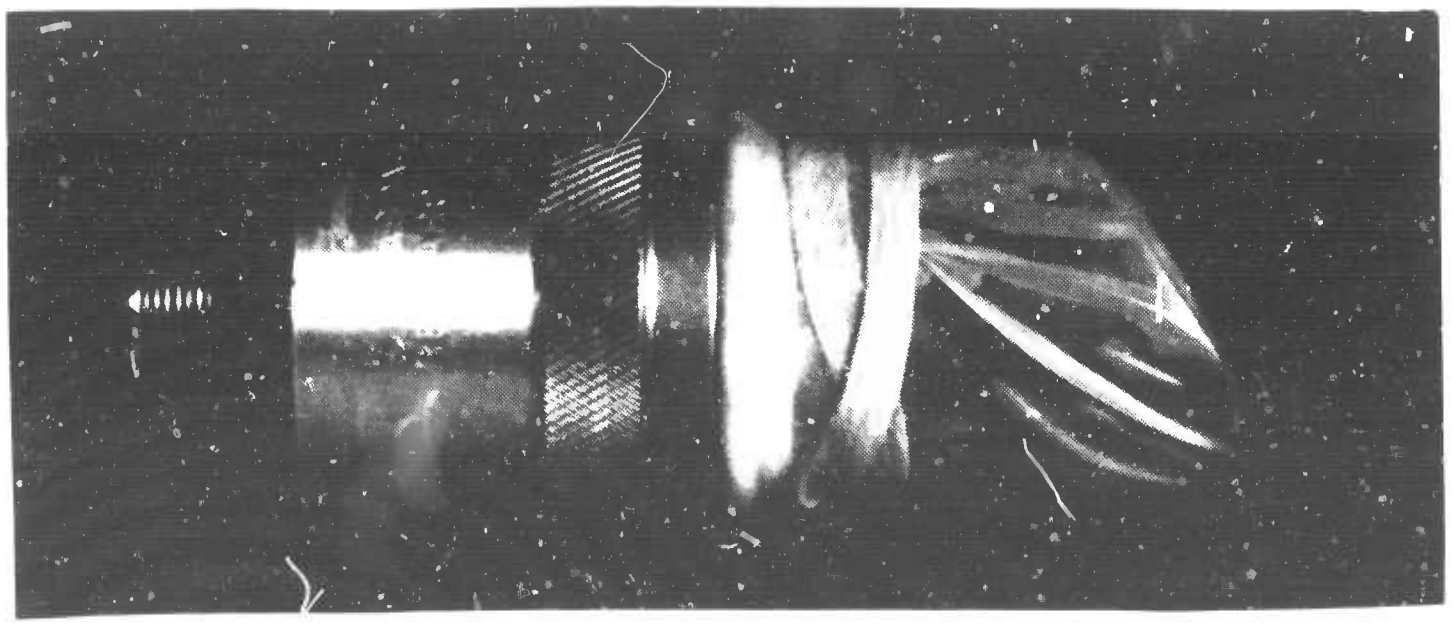

Figure 7. Surface Wave Transducer with Water Column Coupler

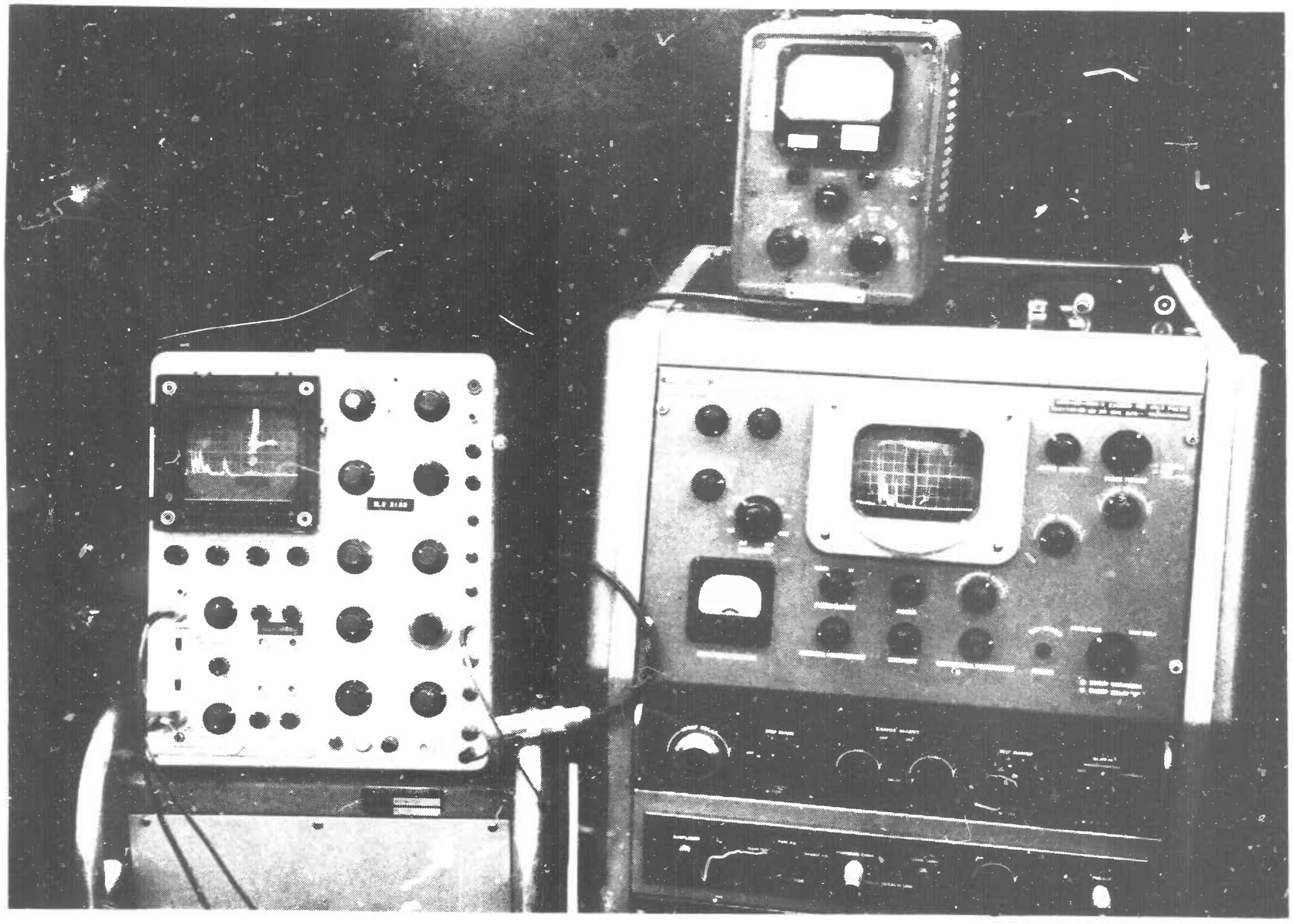

Figure 8. Conventional System for Ultrasonic Wave Velocity Measurement

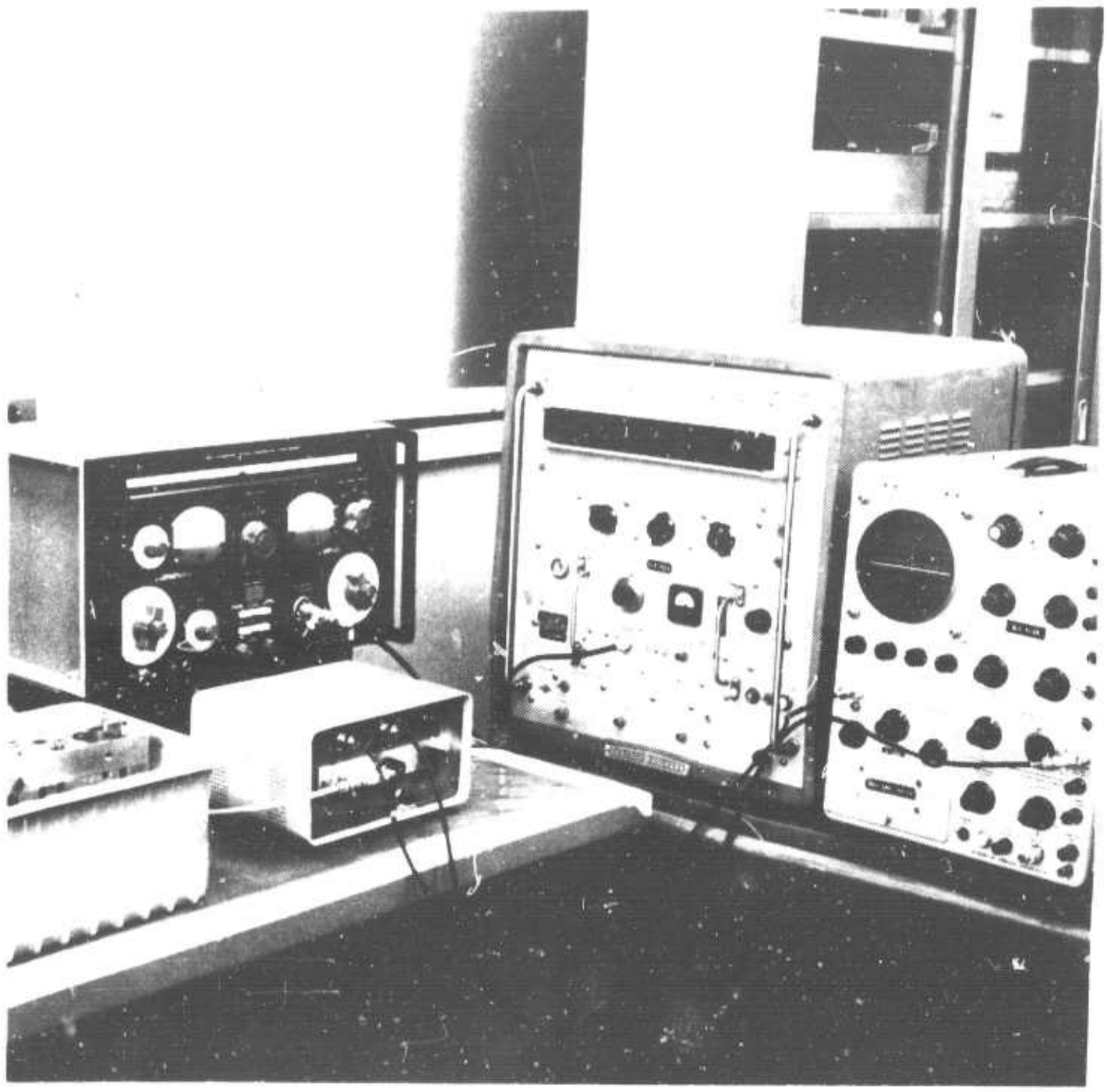

Figure 9. Precision Ultrasonic Wave Velocity Measurement System

superposition technique, i.e., adjustment of the pulse repetition rate to produce superposition of the desired pulse echoes. A block diagram is illustrated in figure 10. The system utilizes a variable, high-stability, sine-wave generator as the pulse rate source. Its output frequency is accurately measured by a digital frequency counter. The generator output is converted by a digital frequency divider to a pulse signal at 1/100 the frequency of the input signal. THis pulse is processed by a pulse-gating circuits to produce a trigger for the high-power pulse generator, an oscilloscope sync signal, and receiver gating signals. The high-power pulse generator produces a nominal 250-volt pulse with a rise time of 3 to 6 nanoseconds (and an exponential decay) which is used to excite the ultrasonic excitation transducer. The conventional system was also used to measure the attenuation of surface waves.

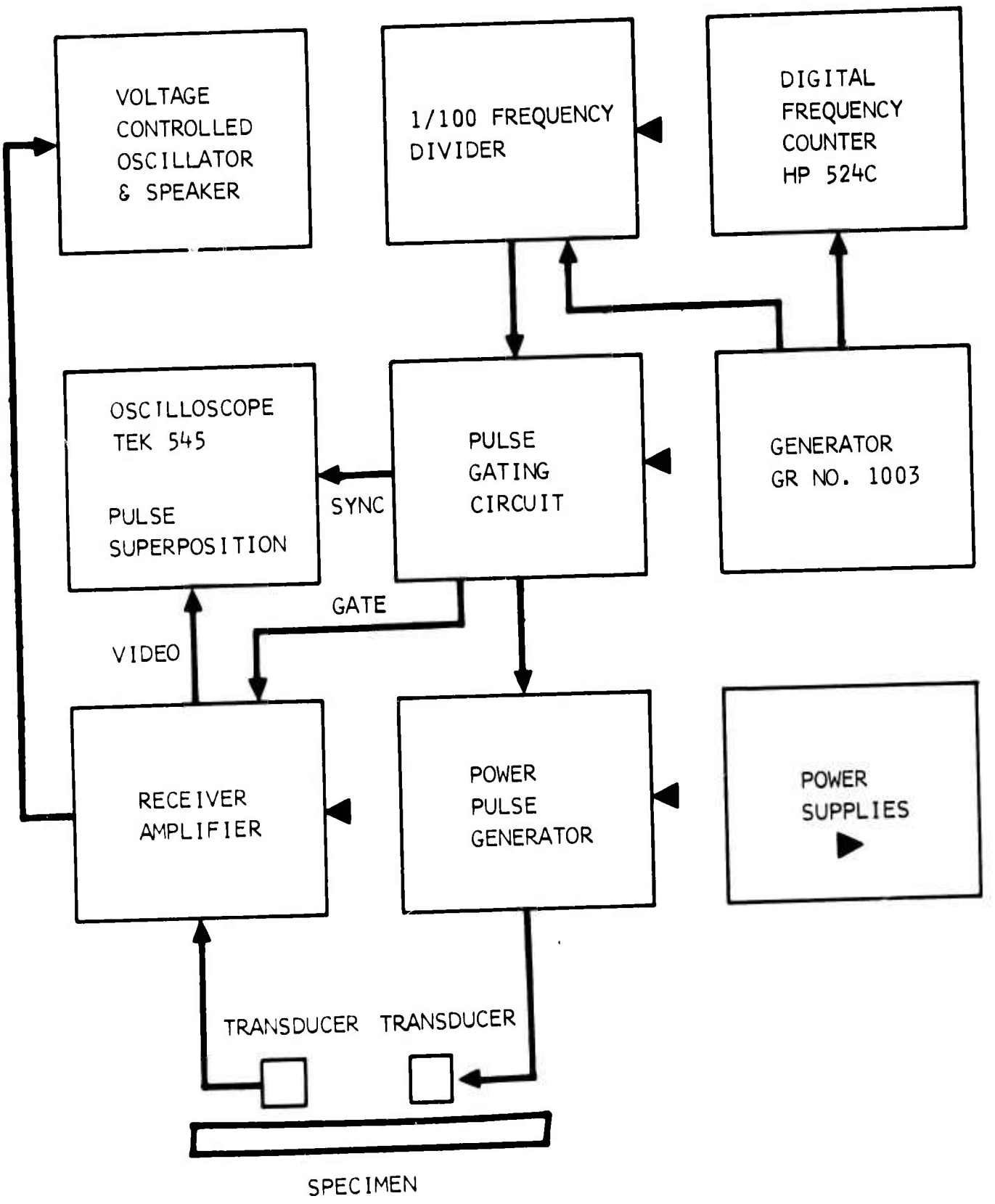

Figure 10. Block Diagram of the Precision Ultrasonic Wave Velocity System

SECTION V

MATERIALS AND SPECIMENS

MATERIALS

Initially, Armco iron was selected on the basis of wide industrial interest, ready availability, and as typical of body-centered cubic material. Preliminary fatigue tests indicated that specimens loaded to 95.7 and 98.2 percent of the ultimate strength failed after 9,000 and 15,000 cycles, respectively, with indications of considerable necking; whereas a specimen loaded to 88.5 percent of the ultimate strength did not fail after 3.6×10^6 cycles. These results indicated an extremely flat fatigue curve, which would have made accurate control of life to failure very difficult. It was, therefore, decided to store the Armco iron for possible future use and, for initial studies, to use a grade 1100-0 aluminum alloy. The material gave the following mechanical properties:

	Supplier Data	Own Data
Ultimate tensile strength, ksi	13.5/13.8	12.76
Tensile yield strength	6.7/618	6.53
Elongation to failure, % in 2 inches	33/34	31.80

Commercial purity titanium and AZ31B-H24 magnesium alloy were also used, but only a few preliminary tests were conducted.

SPECIMENS

Standard fatigue test specimens 7 inches long were cut from the 0.09-inch-thick 1100-0 aluminum sheet stock. Each side of the test section has a 6-inch radius. The widths at the center and at the end of the test section are 1/2 inch and 1-1/8 inch, respectively. After machining they were electropolished in a bath containing 25 percent nitric acid and 75 percent methanol. After electropolish, they were rinsed with water and then with isopropyl alcohol. In addition, several specimens were not electropolished but chemical polished with a solution similar to Keller's etch for aluminum but containing twice the usual amount of hydrofluoric acid. The surfaces of both electropolished and chemical polished specimens exhibit the same grain structure when examined under a microscope.

Shapes of the titanium and magnesium alloy specimens are identical to the aluminum specimen. Titanium specimens were chemical polished with a solution of hydrofluoric acid, hydrogen peroxide, and water; magnesium alloy specimens were chemical polished with a solution of fuming nitric acid and water.

SECTION VI

EXOELECTRON EMISSION TESTS

FATIGUE TEST

As a basis for future work on 1100-0 aluminum, a reliable fatigue curve had to be determined for this test material. The specimens were tested in tention-tension loading at stress levels varying from a minimum stress equal to 3 percent of the maximum stress to maximum stress levels between 11,160 and 11,800 psi or about 92.5 percent of the ultimate tensile strength. Three specimens were tested at each stress level. During tests, the specimen surfaces were continually watched through a telescope to search for the appearance of a visible crack. Tests were also interrupted at intervals to check for the appearance of cracks by means of flourescent penetrant technique. Two specimens at a maximum stress level of 11,800 psi and one specimen at a maximum stress level of 11,640 psi did not develop cracks even at more than their 94 percent of fatigue life. However, their failure was sudden, and ample stretching as well as narrowing at and near the minimum test section observed in the test indicate that tensile fracture by necking was the cause of failure. The upper fatigue loading limit was consequently set at 11,640 psi. The lower limit was roughly established at 10,540 psi because a specimen did not exhibit a crack at this stress level after being stressed to more than 5.3×10^6 cycles.

The S-N curve showing the relationship between maximum stress and number of cycles for 1100-0 aluminum is presented in figure 11. The solid and dotted lines represent, respectively, fatigue failure and the first appearance of cracks.

The fatigue limit is 10,540 psi, i.e., about 82 percent of the ultimate tensile strength (12,760 psi). Relatively high fatigue limits (about 70 and 75 percent of the ultimate tensile strength, respectively, for pure aluminum and low carbon steel) have been obtained also by other investigators (Hempel et al, 1964). These figures are higher than the values for the same materials determined by symmetrical alternate loading with zero mean stress. Such different fatigue behavior is probably due to the characteristics of cyclic loading because the dislocation structure and density in a specimen deformed by repeated tensile stresses (nonzero mean stress) are quite different from a specimen in reverse bending test with zero mean stress (Feltner, 1963).

From the fatigue curve, it appears that necking could occur at a stress level of 11,640 psi, but does not occur at a stress level of 11,500 psi. The corresponding average fatigue life is 400,000 cycles, which is convenient from a test-time point of view. A total of 15 specimens were therefore prepared as noted and cycled, in lots of three, at this stress level to fractions of the total estimated life of 30, 50, 70, 80, and 90 percent. These specimens were used for metallographic evaluation of the fatigue-affected zone and for ultrasonic surface wave tests.

BLANK PAGE

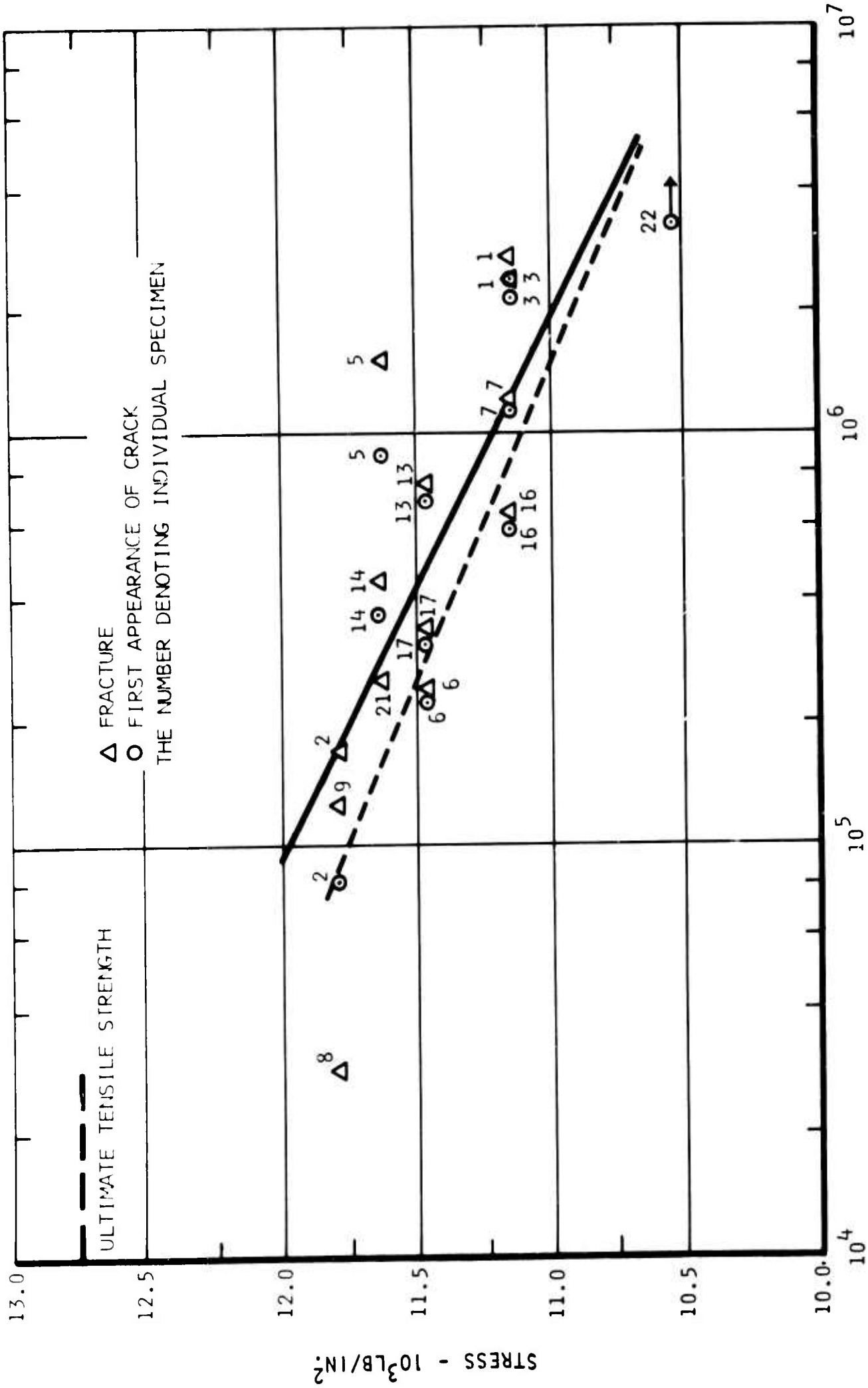

Figure 11. Fatigue Curve for 1100-0 Aluminum

EXOELECTRON DETECTION BY LUMINESCENCE

Several types of luminescent coatings were tried. In one, a ZnO phosphor (lot T 962) developed specially for low-energy electron excitation and supplied by Dr. R. Schraeder of the RCA Laboratories was mixed with distilled water and air sprayed onto a silver film vapor-deposited on a glass substrate. This glass slide was connected to the positive terminal of an electric circuit and hung on the loading frame at an approximate 60-degree angle to the specimen. The Army Night Vision Sight AN/PVS-2 Starlight Scope was aimed at the phosphor-coated glass slide. The phosphor plate was charged with a potential of 5 volts relative to the specimen. Loading tests of the test specimens were carried out in complete darkness, with the specimen in air at atmospheric pressure and under a vacuum in the 10^{-5} torr range. In both tests, the stress was increased from 4,000 to 12,500 psi at an increment of 500 psi. Time at each increment was 2 minutes. No phosphorescence could be seen through the image intensifier at any time during either test.

To settle the problem of the usefulness of phosphor for direct observation of exoelectron emission, two thermal electron sources were used in a vacuum in the 10^{-5} torr range to simulate the emitter. The ZnO-coated glass slide and a cathode luminescent screen from an electron microscope acted as receivers. Circuiting was designed to allow charging of the receivers relatively to the emitters and measurement of the current between receivers and emitters. No electron-generated luminescence was observed with potentials up to 270 volts dc, though currents up to 10 microamperes were measured. Both luminescent receivers, however, responded readily to irradiation by ultraviolet light.

EXOELECTRON EMISSION MEASURED BY CHANNELTRON ELECTRON MULTIPLIER

All tests involving exoelectron emission by Channeltron electron multiplier were conducted at room temperature and in a vacuum in the 10^{-5} torr range. The bias voltage and the high voltage at the electron multiplier were 10 and 3,100 volts, respectively. Test results of aluminum specimens are summarized in table I.

Specimen 42 was subjected to static tensile loading at 10,650 psi under daylight for 20 seconds before the load was released. It is seen in figure 12 that the intensity of emission, expressed in number of counts per 10-second interval, rose rapidly from a background level of 100 to more than 3,250 in about 50 seconds, and decayed subsequently. To prove that the emission phenomenon was in fact associated with deformation of the specimen, the same tensile stress (10,650 psi) was applied again for 15 seconds at about 630 seconds after the peak emission had occurred. The intensity responded by increasing from 1,450 counts to about 4,300 counts in 34 seconds. Subsequent decay appeared to take place fairly slowly with the intensity still about 1,100 counts after the elapse of 22 minutes since the second peak emission.

Table I

SUMMARY OF EXOELECTRON EMISSION TESTS ON 1100-0 ALUMINUM

Specimen No.	Maximum Stress (psi)	Number of Cycles		Strongest Emission (No. of Counts in 10 Sec)	Remarks
		Strongest Emission	End of Emission		
42	10,650	See figure 12.			(1),(3),(4),(7)
45	12,600	See figure 13.			(2),(3),(4),(7)
34	11,450	790	45,000	1,830	(2),(3),(4),(7)
46	11,450	740	31,600	3,430	(2),(3),(4),(6),(7)
66	11,450	630	34,300	2,600	(2),(3),(5),(7)
52	11,450	780	14,740	1,090	(2),(3),(5),(7)
43	11,450			0	(2),(4),(7), tested in darkness
44	11,450	See figure 18.			(2),(4),(8), tested in ultraviolet light
35	11,000	650	10,500	600	(2),(3),(4),(7)
37	11,000	460	28,800	700	(2),(3),(4),(7)
65	11,000	940	32,500	570	(2),(3),(5),(7)
56	10,540	1,080	8,500	100	(2),(3),(5),(7)
57	10,540	830	6,100	110	(2),(3),(5),(7)
36	10,540			0	(2),(3),(4),(8)
61	10,000	950	3,200	70	(2),(3),(5),(7)

NOTE: (1) The specimen was subject to tensile loading.
(2) The specimen was subject to fatigue loading.
(3) The specimen was tested under daylight.
(4) The specimen was electropolished prior to testing.
(5) The specimen was chemical polished prior to testing.
(6) The glass chamber was purged with argon prior to testing.
(7) Type 4039 Channeltron electron multiplier was used in the test.
(8) Type 4013 Channeltron electron multiplier was used in the test.

22A

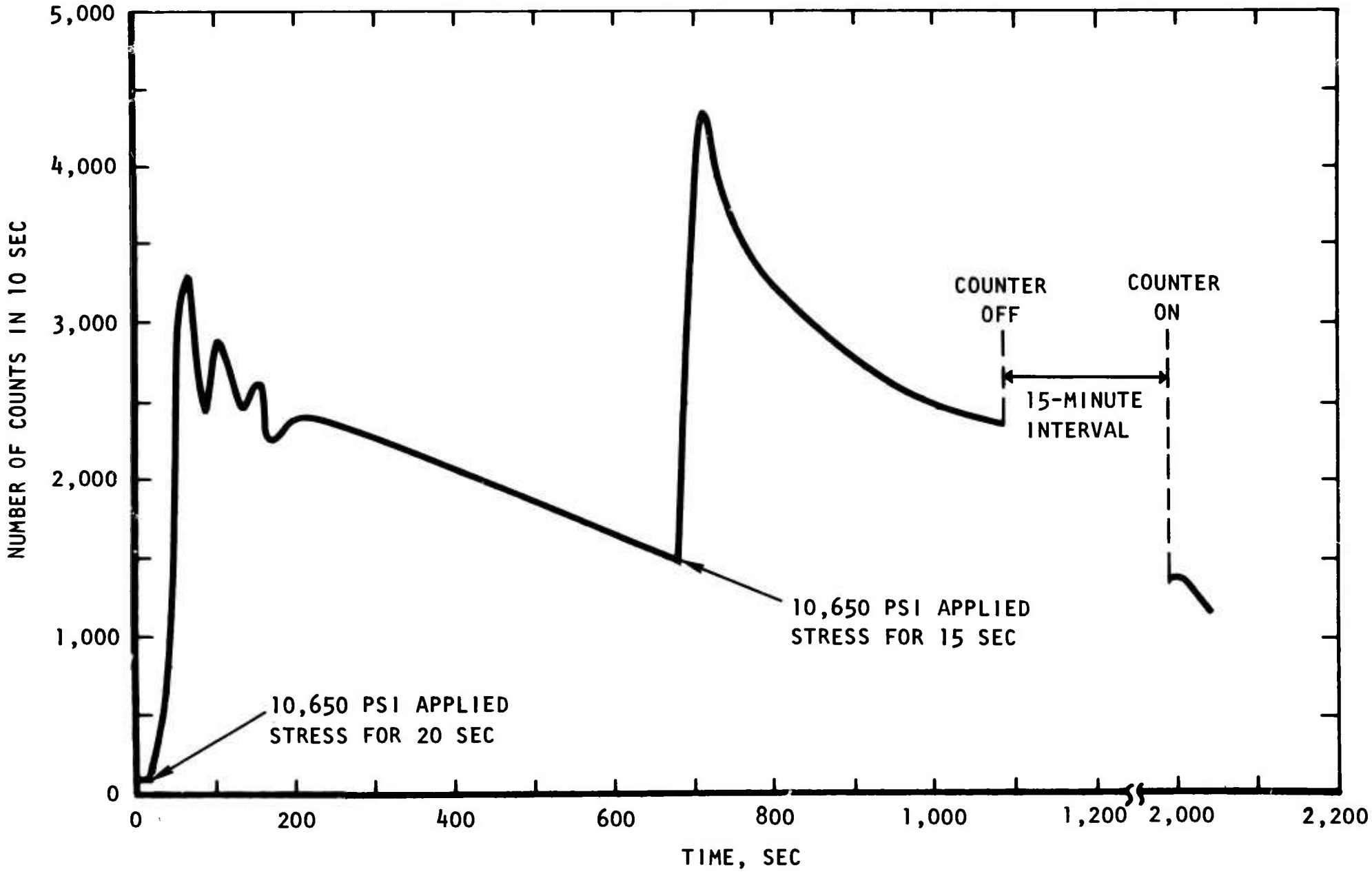

Figure 12. Exoelectron Emission of 1100-0 Aluminum at Tensile Stress 10,650 lb/in.^{2}

Specimen 45 was subjected to a high fatigue load, with a maximum stress of 12,600 psi under daylight. The intensity of emission was measured by the number of counts in 1 second. Figure 13 shows that an emission peak occurred about 3.5 seconds of 7 cycles after start of the test. The emission then appeared to die out quickly, falling to the background level as cycling proceeded. At this point the midsection of the specimen started to fail by necking. The emission rose again during fracturing. The number of cycles to failure was about 120, so the first peak emission occurred at 5 to 6 percent of fatigue life.

To avoid failure by necking, the maximum fatigue stress on specimen 34 was reduced to 11,450 psi. Exoelectron emission started at about 100 cycles. Afterwards, the emission appeared to take place in bursts, as evidenced by a number of peaks shown in figure 14. The strongest intensity occurred at around 800 cycles. However, the emission intensity exhibited a decreasing trend as cycling proceeded, and it fell to the background level after 4.5×10^4 cycles. Upon further cycling, the measured intensity was maintained at the background level until about 6.69×10^5 cycles had elapsed. A number of emission peaks then happened again while a visible fatigue crack propagated during the continuation of fatigue loading. Finally the intensity rose rapidly as the crack traversed the specimen at the point of final failure. The highest intensity near failure was much weaker than most of the peaks observed at the beginning of the test, possibly because the cracks appeared to initiate at the specimen surface that did not face the Channeltron electron multiplier. Indeed, minute cracks were seen to link before the intensity of emission rose from the background level. Furthermore, the intensity did not rise rapidly until close to the end of the test when the crack penetrated through the specimen thickness. The number of cycles to failure was 6.74×10^5. Initial exoelectron emission ceased at 4.5×10^4 cycles; it occupied thus only 6.7 percent of fatigue life.

The same test conditions were repeated on specimen 66. Exoelectron emission started at less than 100 cycles, and there also appeared a number of peak emissions as cycling proceeded. The emission phenomenon again showed a downward trend and disappeared after about 3.4×10^4 cycles (table I). Since the test on specimen 34 reveals that after cessation of emission, no further emission would take place until fatigue cracks developed near the end of the test, and since this earlier emission period is of prime interest for correlating with early fatigue danger, testing of specimen 66 was discontinued after 3.55×10^4 cycles.

Though specimen 52 was also subjected to a maximum fatigue stress of 11,450 psi, exoelectrons were emitted continuously in the test, which ended when the specimen failed after 14,740 cycles. It is seen in figure 15 that, like specimens 34 and 66, the emission displayed a decreasing trend with an increasing number of cycles. However, after the elapse of 1.2×10^4 cycles, the intensity of emission rose again. According to the emission behavior of specimens 34 and 66, the initial emission period with decreasing intensity

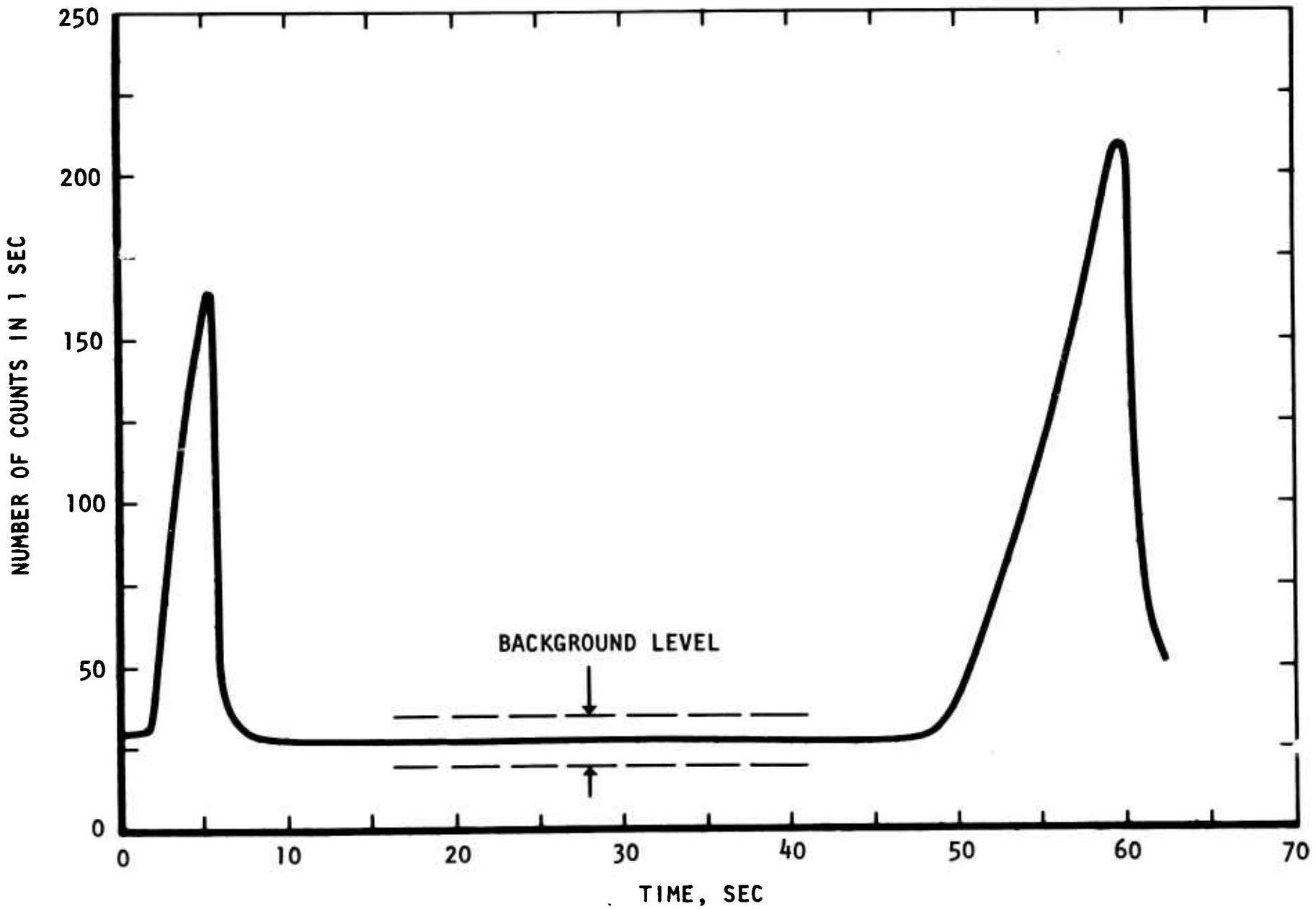

Figure 13. Exoelectron Emission of 1100-0 Aluminum in Fatigue Test at 12,600 lb/in.^{2}

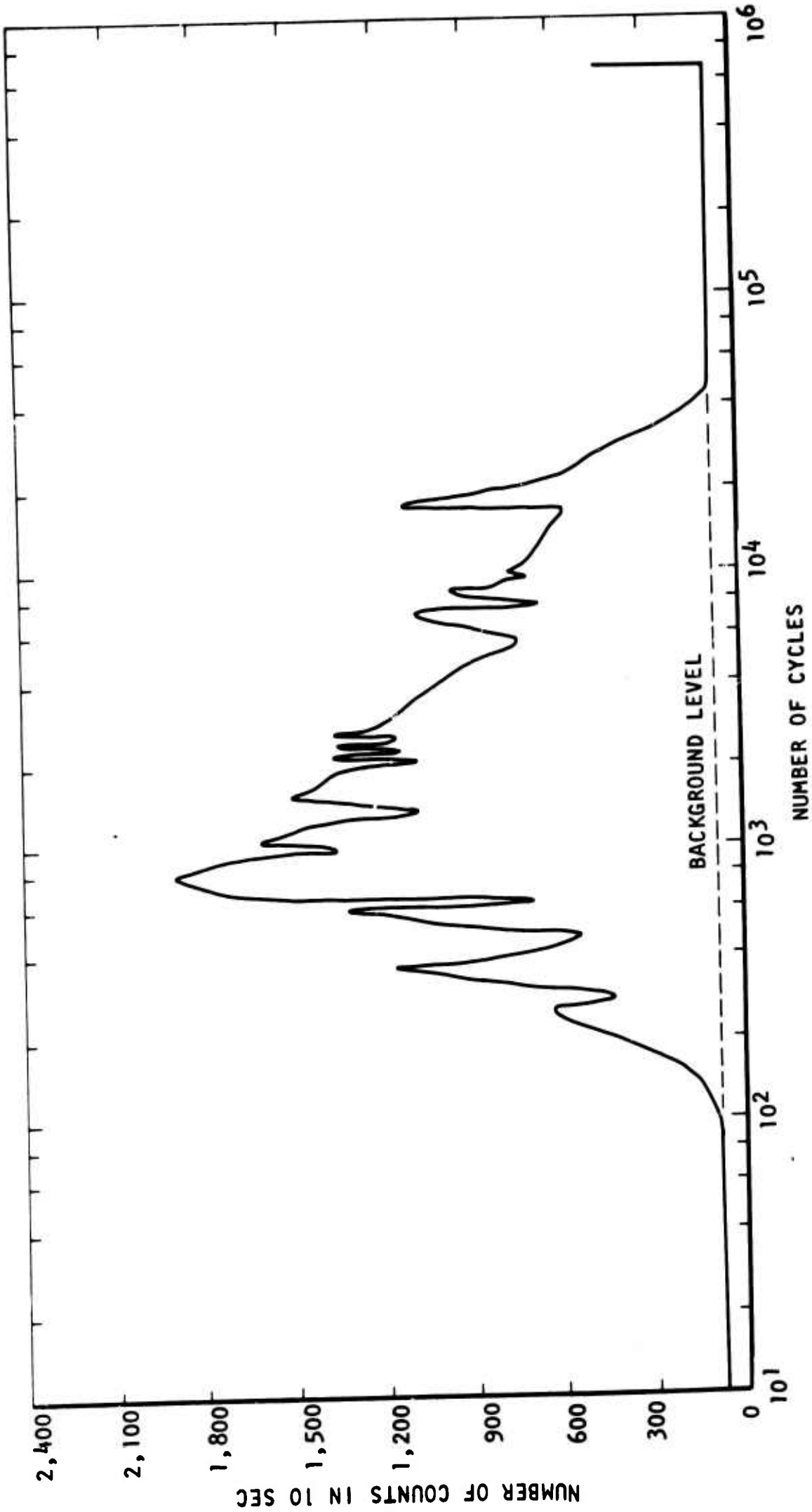

Figure 14. Exoelectron Emission of 1100-0 Aluminum in Fatigue Test at 11,450 lb/in.^{2}

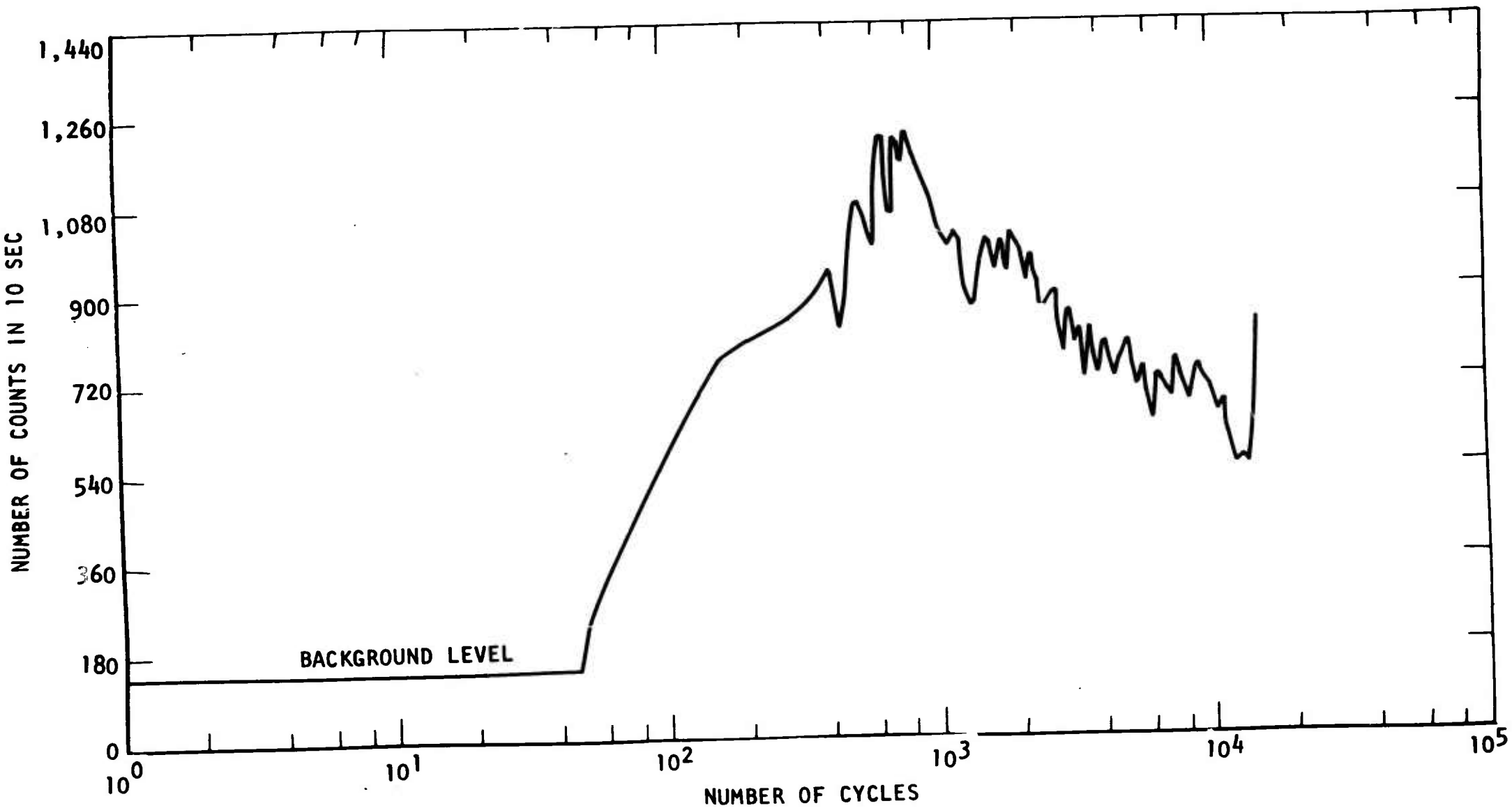

Figure 15. Exoelectron Emission of 1100-0 Aluminum in Fatigue Test at 11,450 lb/in.^{2}

should last at least 3×10^4 cycles. Apparently the earlier rise of emission intensity was associated with formation and propagation of fatigue cracks. The premature failure of the specimen after 14,740 cycles substantiates this reasoning.

Prior to testing specimen 46 at the conditions for specimens 34, 52, and 60, the glass chamber was purged with argon so that, after the vacuum pressure was in the 10^{-5} torr range, the residual gas would be argon instead of oxygen. The purpose of the purge was to find whether the exoelectron emission intensity would be influenced by the residual gas because argon offers less attenuation to electron motion in vacuum. Though the strongest emission from specimen 46 under fatigue deformation was more intense than the other specimens tested without purging with argon, the difference in emission intensity, expressed in number of counts in 10 seconds, was not large, being about three times as high as the recorded lowest value from specimen 52 (table I). Furthermore, the shape and trend of the emission curve for specimen 46 are quite similar to those of curves for other specimens. The test was discontinued soon after the end of emission.

Some sources in the literature cite that electrons do not emit from deformed aluminum in darkness. Some light must be provided as a stimulator. Specimen 43 was therefore subjected to fatigue loading at a maximum stress of 11,450 psi in complete darkness. The recorded intensity in number of counts in 10 seconds did not rise above the background level, indicating no exoelectron emission. The test was discontinued after 3.9×10^4 cycles.

To investigate the effect of fatigue stress level on exoelectron emission, specimens 35, 37, and 65 were each tested under daylight at a maximum fatigue stress of 11,000 psi. Like the specimens subjected to higher fatigue stressing, exoelectron emission started at less than 100 cycles, and the emission generally tended to become weaker as cycling proceeded. The emission curve also had a number of peaks, but magnitude of the strongest emission was much lower and cessation of emission occurred earlier. Figure 16 shows a typical emission curve for the specimens subjected to a maximum stress of 11,000 psi. The tests for specimens 35, 37, and 65 were discontinued shortly after the emission stopped. Later, however, specimen 35 was further tested at the same stress level in air. It did not fail after undergoing an additional 1.79×10^7 cycles.

Specimens 36, 56, and 57 were each tested under daylight at an even lower maximum stress, 10,540 psi, the tentatively determined fatigue limited based on 6×10^6 cycles. Like the previous tests at higher stress levels, the type 4039 Channeltron electron multiplier was used for the tests on speciments 56 and 57. The test on specimen 36, however, was carried out using the type 4013 Channeltron electron multiplier because at that time type 4039 behaved erratically. Though exoelectrons started to emit from specimens 56 and 57 after a little more than 100 cycles, the intensity was quite weak, the strongest emission being only about two and a half times the background level. As cycling proceeded, the emission intensity varied between one and a half and two times

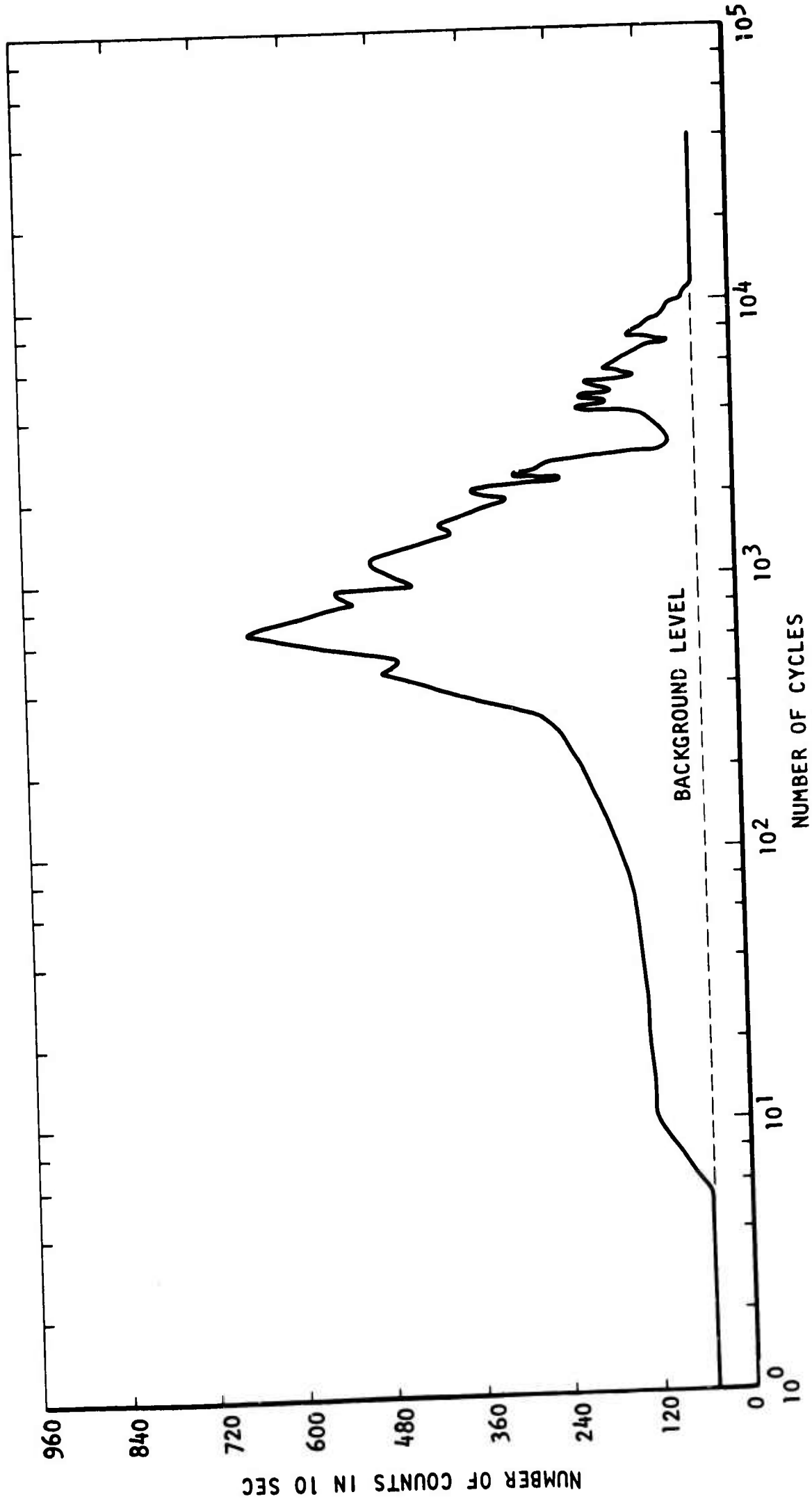

Figure 16. Exoelectron Emission of 1100-0 Aluminum in Fatigue Test at 11,000 lb/in.^{2}

the background level, as indicated in figure 17. During the test, the room in which the test was being conducted was made completely dark several times by lowering blackout curtains. The emission immediately dropped to background level but rose again when the curtains were raised. Therefore, it proved that the emission, however weak, was associated with fatigue deformation of the specimen. Shape of the emission curve, however, is not quite similar to curves for the specimens tested at higher fatigue stresses because the downward trend is not apparent until near the end of emission. The strongest emission occurred later, and the end of emission occurred earlier (table I). As for specimen 36, using the type 4013 Channeltron electron multiplier, no emission above the background level was observed during test. The test was discontinued after 3×10^4 cycles.

To explore the effect of stress further, specimen 61 was tested at a maximum stress of 10,000 psi. Emission did not start until after the elapse of more than 400 cycles. The strongest emission was only about twice as intense as the background level. With an increasing number of cycles, the intensity fluctuated a little above the background level and below the strongest emission. The period of emission lasted 3,200 cycles, but the test was continued until after 7,500 cycles. During emission, the intensity dropped to background level if the test room was made completely dark. This indicates that exoelectrons still were emitted from the 1100-0 aluminum specimen under cyclic stressing below the fatigue limit based on 6×10^6 cycles.

To investigate the effect of light on exoelectron emission of 1100-0 aluminum in fatigue, specimen 44 was subjected to a maximum stress of 11,450 psi. During the test, the specimen was irradiated alternately in a 15-minute period with daylight and long-wave ultraviolet light. The source of the latter was a 15-watt ultraviolet tube housed in a metal tube, throwing a half-inch diameter beam directly to the middle portion of the specimen. The angle of incidence was approximately 45 degrees. Type 4013 Channeltron electron multiplier was used in the test. The emission curve is shown in figure 18. A considerable increase in emission during ultraviolet illumination was observed though the actual levels of emission were much lower than recorded on other specimens using the type 4039 Channeltron electron multiplier. The emission could not be measured after about 6,000 cycles, but the test was continued to 5×10^4 cycles. This specimen was later tested in air; it failed after additional 1.69×10^6 cycles.

Commercial purity titanium and AZ31B-H24 magnesium alloy were tested for exoelectron emission by fatigue deformation. The type 4039 Channeltron electron multiplier was used for all the tests.

Titanium specimen 3 was subject to a maximum stress of 37,800 psi under daylight. No emission above background level was noticed after 3,000 cycles. The stress level was next raised to 43,500 psi, but there was still no emission after an additional 2,000 cycles. The stress was then raised in three steps: 48,500, 51,700, and 55,000 psi with each step lasting 2,000 cycles. Again no

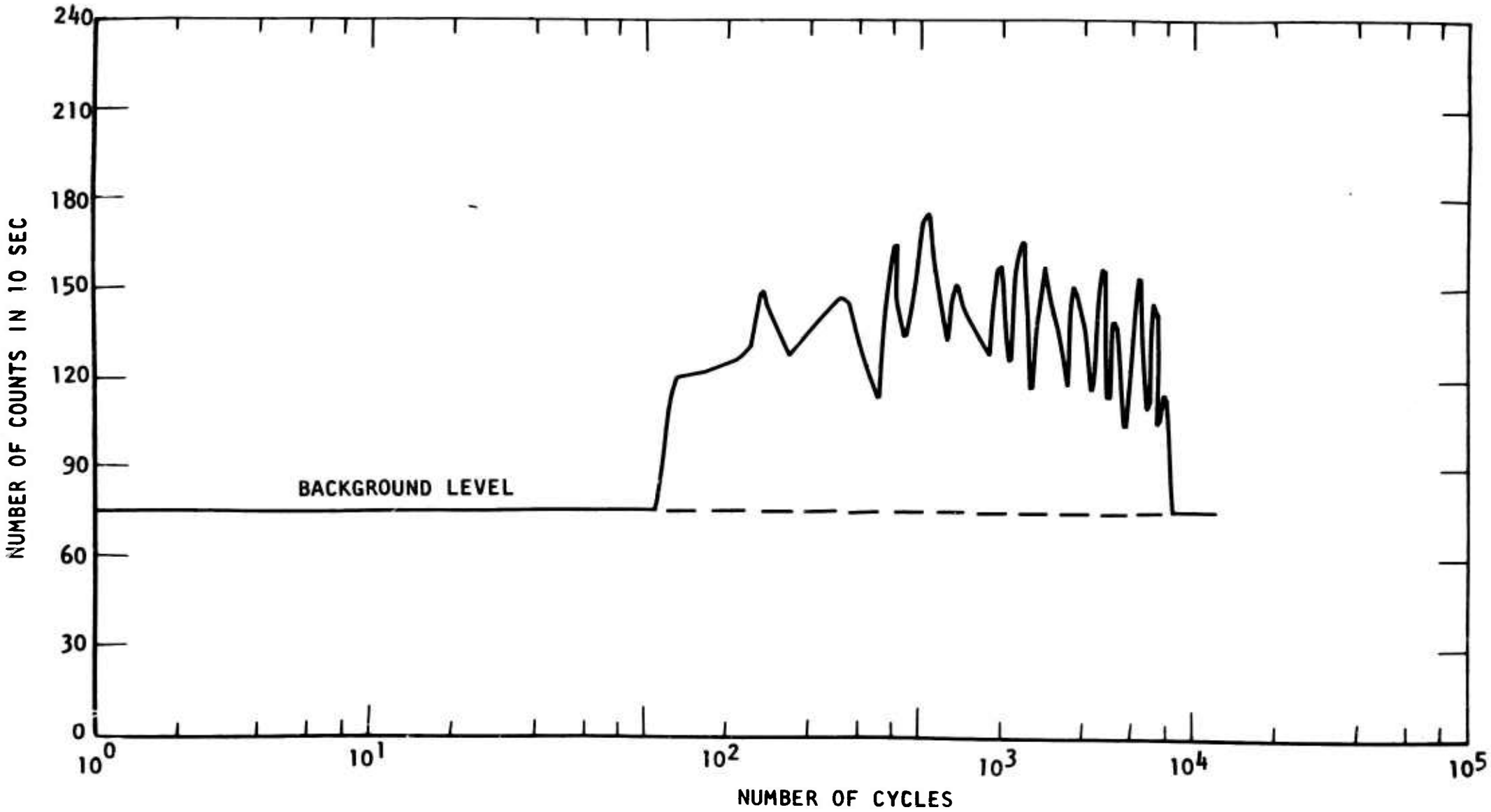

Figure 17. Exoelectron Emission of 1100-0 Aluminum in Fatigue Test at 10,540 lb/in.^{2}

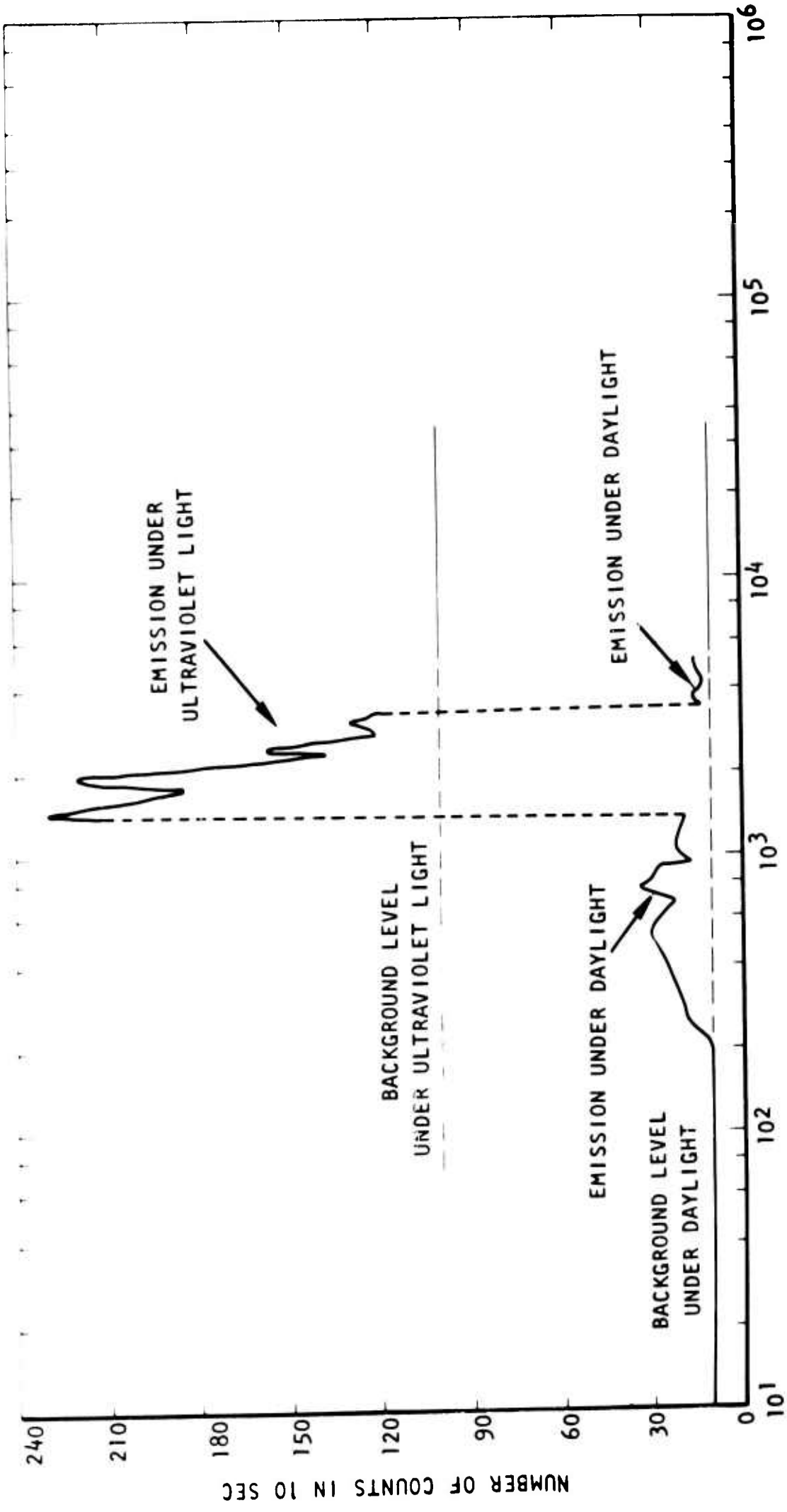

Figure 18. Exoelectron Emission of 1100-0 Aluminum in Fatigue Test at 11,450 lb/in.^{2} and Under Various Light Conditions

emission could be detected in these 6,000 cycles. Finally the stress was increased to 58,200 psi, and the test was continued until the specimen failed. No emission was observed even near the end of the test when propagation of fatigue cracks caused complete fracture of the specimen.

Titanium specimen 5 was tested at a maximum stress of 50,600 psi under long-wave ultraviolet light. No emission occurred after 1,400 cycles. The stress was then increased to 55,600 psi but there was still no emission. The test was stopped after an additional 16,000 cycles.

Magnesium alloy specimen 4 was subject to a maximum stress of 305,000 psi. No emission was observed after 1,200 cycles. The stress was next increased in six steps: 34,600, 37,000, 39,000, 40,000, 41,000, and 42,000 psi, with each step lasting 2,000 cycles. The emission did not rise above the background level in these 1.2×10^4 cycles. The stress was then increased to 43,000 psi. The specimen failed at this stress level in 380 cycles. Neither in this duration nor at the end of the test could emission be observed.

DISCUSSION

Exoelectron emission occurs from both statically and dynamically deformed 1100-0 aluminum. Emission from metal deformed statically in tension has previously been demonstrated, using a Geiger-Müller counter or electron multiplier. However, some additional information on emission behavior has been obtained. For example, the peak emission is reported to occur during (Hempel et al, 1964) or after (von Voss and Brotzen, 1959) deformation, depending on the loading time. As shown in figure 12, emission peak occurs only after the maximum stress is reached. The time to reach peak emission is about twice the time to reach maximum tensile load. Figure 12 further shows that, if a load is released and applied again before the emission decays to the background level, the total emission on the second loading is about the same as the emission on the first loading. It would appear from this test that a relationship might exist between total emission during a loading cycle and the stress time of that cycle.

Exoelectron emission by fatigue deformation has been reported (Grosskreutz and Benson, 1963; Hempel et al, 1964; Krogstad and Moss, 1965; Bogachev et al, 1966; Mints and Kortov, 1967; Mints et al, 1968). The intensity generally increases with the number of cycles. After it reaches a saturated value, the emission decreases slowly until specimen failure. A rapid rise of intensity shortly before failure has also been observed. This rise is attributed to the formation of fatigue cracks. Results of the exoelectron emission tests on 1100-0 aluminum, however, are not in complete agreement with this general description. Emission appears to occur at two stages of the fatigue cycle: an emission period in the early stage of fatigue process and another emission period near the end when developing cracks lead to failure; there is practically no emission between the two stages. The two-stage emission phenomena are clearly indicated in figures 13 and 14. However, the two stages can merge,

resulting in continuous emission during the whole fatigue process, if the second stage starts before the first stage ends (figure 15). Hence, so far as the emission behavior of 1100-0 aluminum by tension-tension fatigue deformation, studied using an electron multiplier, is concerned, the general description in the literature is merely a special case.

The preliminary fatigue tests on commercial purity titanium and AZ31B-H24 magnesium alloy did not indicate emission of electrons. However, emission from titanium by torsional fatigue has been detected by using a 13-stage photomultiplier (Krogstad and Moss, 1965). There are no specific details of emission from titanium, but they observed that the emission from gold, iron, nickel, and titanium in general started after a few hundred cycles, followed by a series of emission events. Frequency with which the emission occurred increased to a maximum (at about one-third of fatigue life) and then decreased slowly until the specimen failed. Emission from magnesium by abrading has also been observed by Lohff (1956) using an electron multiplier, and by Ku and Primbley (1961) using a Geiger-Müller counter. In contrast with these results, the present finding of lack of emission suggests that probably the emission behavior of titanium and magnesium might be influenced by the mode of deformation, the type of detection equipment, the test environment including stimulation, and other factors.

The emission behavior of 1100-0 aluminum by fatigue deformation depends primarily on the maximum stress level. Figure 19 shows that the higher the stress, the stronger the emission (after the deduction of the background level) becomes. The time in reaching the strongest emission is delayed if the stress is reduced (figure 20). The duration of the first stage of emission is also shortened at lower stress (figure 21). Surface preparation by electropolish and chemical polish yields undistinguishable results (table I).

Emission decreases rapidly as the applied stress approaches the fatigue limit, and it becomes even weaker below the fatigue limit. However, a correlation of exoelectron emission and fatigue limit of aluminum is not apparent. Unlike ferrous metals, the fatigue curve for a nonferrous metal, like aluminum, does not exhibit a "knee," the horizontal portion of the curve. The fatigue limit of a nonferrous metal is generally defined at a certain number of cycles. In the present tests, for example, the fatigue limit of 1100-0 aluminum was tentatively determined to be 10,540 psi at 6×10^6 cycles.

Regardless of fatigue limit, however, the test results reveal a marked influence of stress level on emission. When the stress is lowered, duration of the first stage of emission becomes shorter. Since lower stress increases fatigue life, the first stage occurs relatively earlier and occupies a smaller percentage of the fatigue life. For example, the first stage of emission occupies about six percent for specimens subjected to fatigue stressing at 11,450 psi and less than one percent at a stress of 11,000 psi. At a stress of 10,000 psi or lower, the percentage would be negligible.

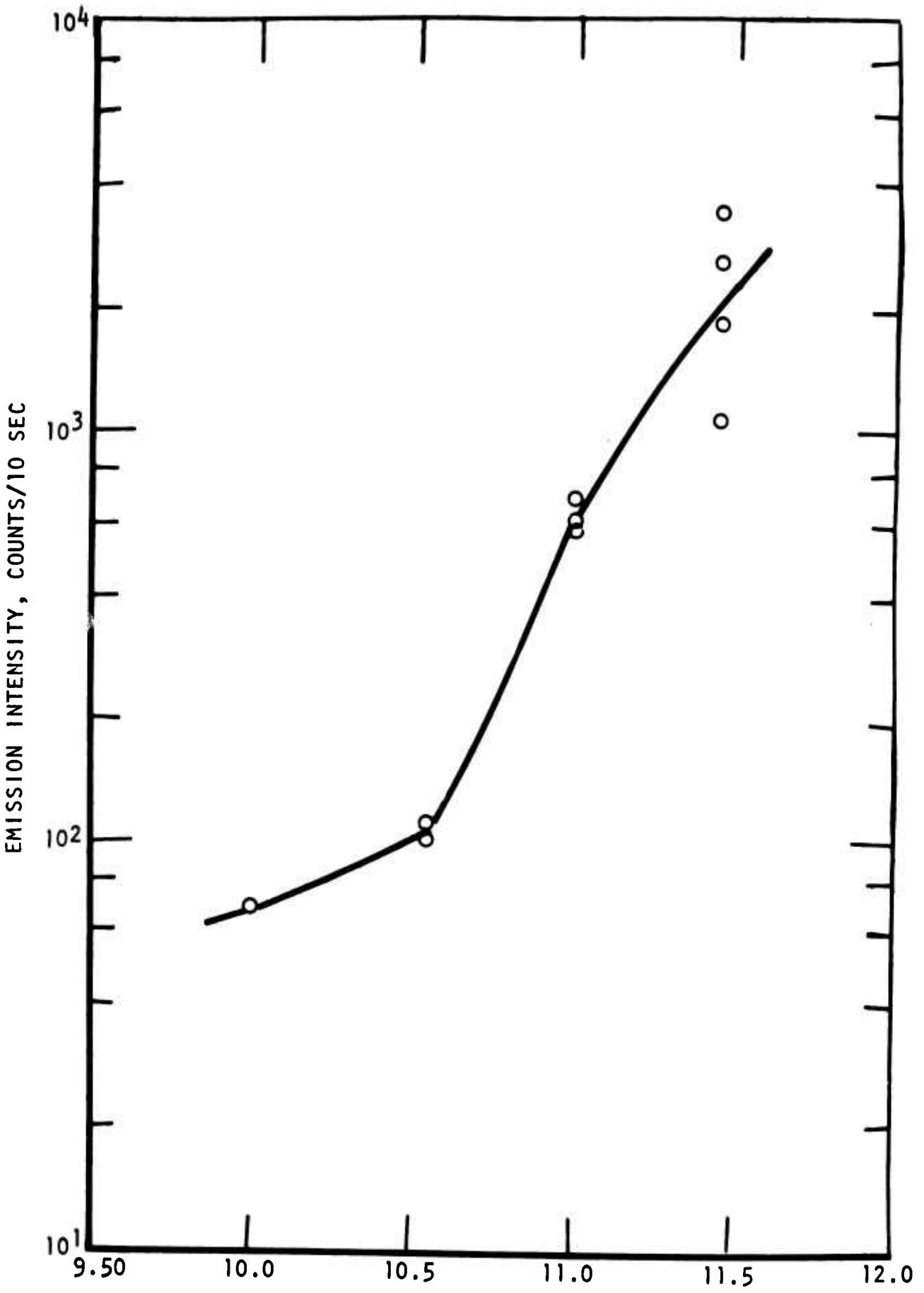

Figure 19. Relation of the Strongest Emission Intensity and Fatigue Stress for 1100-0 Aluminum

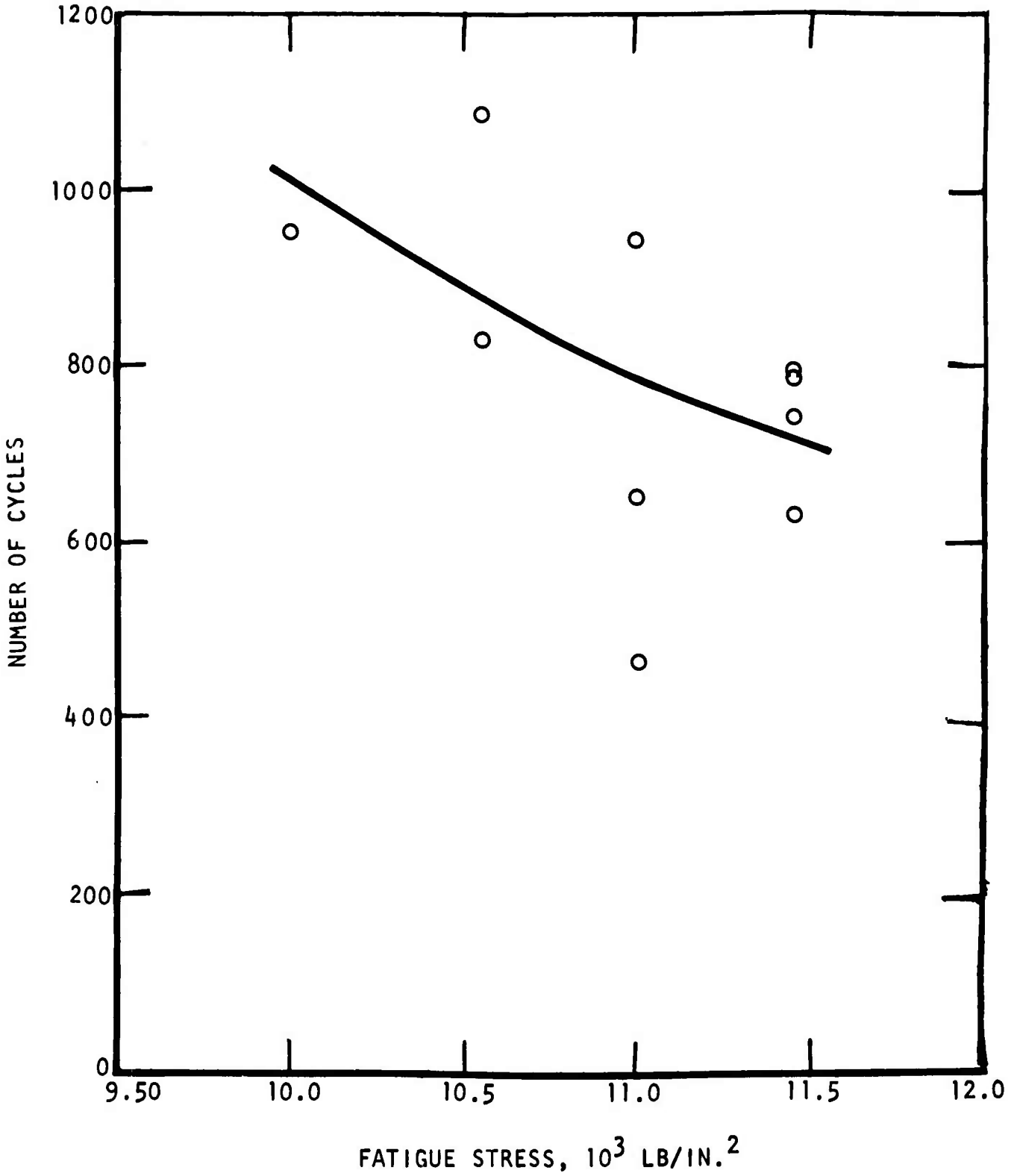

Figure 20. Relation of the Time at Which the Strongest Emission Occurs and Fatigue Stress for 1100-0 Aluminum

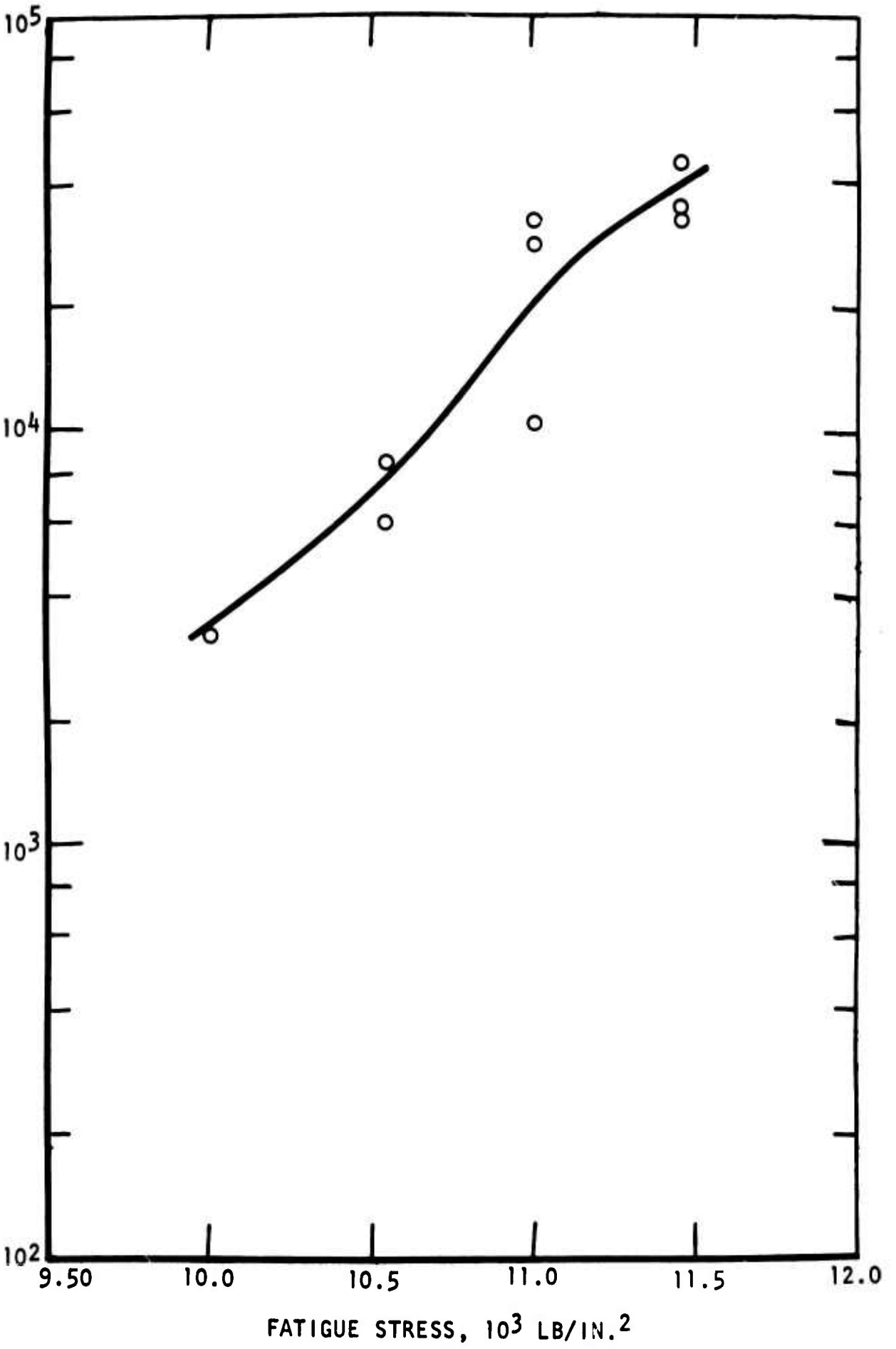

Figure 21. Relation of Duration of Initial Emission and Fatigue Stress for 1100-0 Aluminum

Transmission electron micrography reveals that the disclocation structure in regions near the surface of iron after as little as 10 cycles differs from that in the interior (Wei and Baker, 1965). After 10^3 cycles, the dislocation loop arrays near the surface are often associated with the intense deformation bands in which fatigue cracks eventually form. Since the fatigue life of the specimen is between 10^5 and 10^6 cycles, the intense deformation bands develop at one to 10 percent of fatigue life. Though it is not known whether aluminum would behave like iron, it could be possible that the first stage of emission, which lasts less than 10 percent of fatigue life, might be an indication of early fatigue damage. Metallographic examination of the fatigued aluminum specimens will test this speculation.

There is considerable evidence of a relationship between exoelectron emission and incident light energies. Emission from abraded and deformed metal surfaces, such as Al, Cu, Ni, Sn, and Zn, in complete darkness is not detectable (Conrad and Levy, 1961). The present tests also indicate no emission from 1100-0 aluminum undergoing fatigue deformation in complete darkness. Evidently additional energy is required for the electrons to emit from deformed aluminum surface, as suggested by Pimbley and Francis (1961). The increased energy of ultraviolet light compared to daylight should thus cause increased emission. Its effect in comparison with daylight on exoelectron emission is readily seen in figure 18. The purpose of alternating the light condition every 15 minutes was to compare directly two emission curves under varying light energy conditions from one test specimen.

The experiment with different illumination also explains the failure of detecting exoelectron by luminescence of the phosphor because the tests were carried out in darkness.

SECTION VII

METALLOGRAPHY

EXAMINATION OF FATIGUED SPECIMENS

Metallographic examination using an optical microscope and an electron microscope was conducted on a control and five specimens, which had been subject to fatiguing at a maximum stress of 11,500 psi for 1.2, 2.0, 2.8, 3.2, and 3.6 x 10^5 cycles. The results are shown in figures 22 and 23. The control surface shows a relatively smooth grain structure. The fatigued specimen surfaces exhibit considerable evidence of slip and indications of intrusions and extrusions even at the lowest fatigue exposure of 1.2 x 10^5 cycles. Penetrant tests, however, do not reveal any indication of surface cracks.

Electron microscope replicas of regions near the specimen surface in the maximum stress area on sections cut at 20 degrees to the surface were also examined. The micrographs for the control and the specimens which had been cyclically stressed for 1.2 and 3.6 x 10^5 cycles are reproduced in figure 24. Some possible surface microcracks or surface movement with a depth of roughly 0.1 μm is noted.

To gain some idea of the depth affected by the surface slip movement, the surfaces of specimens cut from the center portion of the specimens fatigued for 2.0 and 3.6 x 10^5 cycles were examined by means of the secondary electron emission microscope. During this examination, the surface layer was progressively etched off by means of an argon bombardment until all traces of slip line structure had disappeared. Details are shown in figures 25 and 26. The specimens were then removed from the microscope and mounted, so that the cross section could be polished across the area exposed to the argon ions. The depth of attack was then measured by means of a reticule microscope objective. The depth of attack after exposure for 2.0 x 10^5 cycles was approximately 10 μm. Lengthening the exposure about two times at the same stress level changed the depth only to about 13 μm.

Table I shows that under fatigue loading to a maximum stress of 11,450 psi, the first stage of exoelectron emission during fatigue deformation ceases between 3.0 x 10^4 and 4.5 x 10^4 cycles. The strongest emission occurs between 600 and 800 cycles. Two specimens were then cyclically stressed at a maximum stress of 11,450 psi for 800 and 3.0 x 10^4 cycles, respectively. Replicas of the surface at the center section of the specimens were made before and after fatigue test. The resulting micrographs are shown in figures 27 and 28. It is seen in figure 27 that slip bands are evident at as low as 800 cycles. As cycling progressed, slip bands appeared in more grains and the bands tended to become wider (figure 28).

Control, 0 Cycle

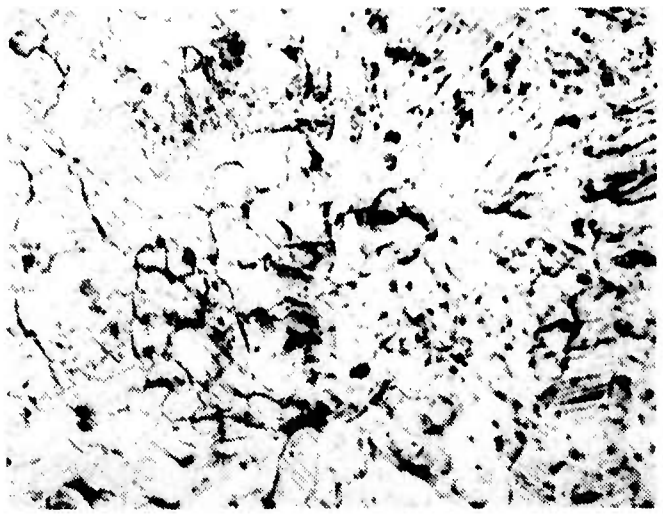

2.8 x 10^5 Cycles

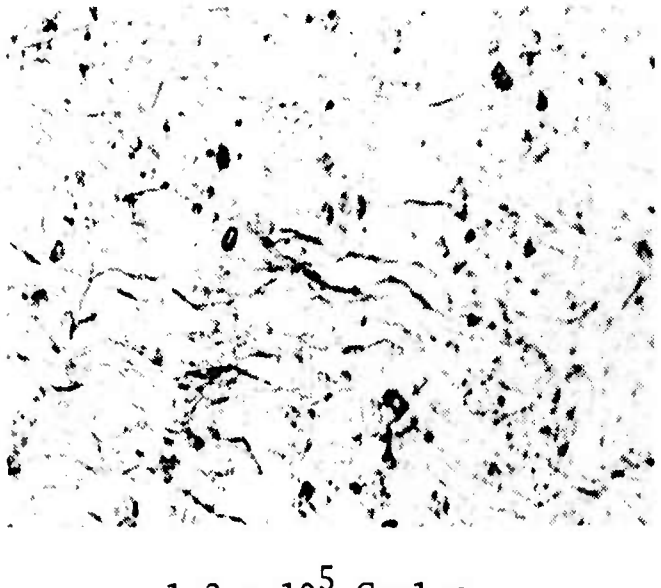

1.2 x 10^5 Cycles

3.2 x 10^5 Cycles

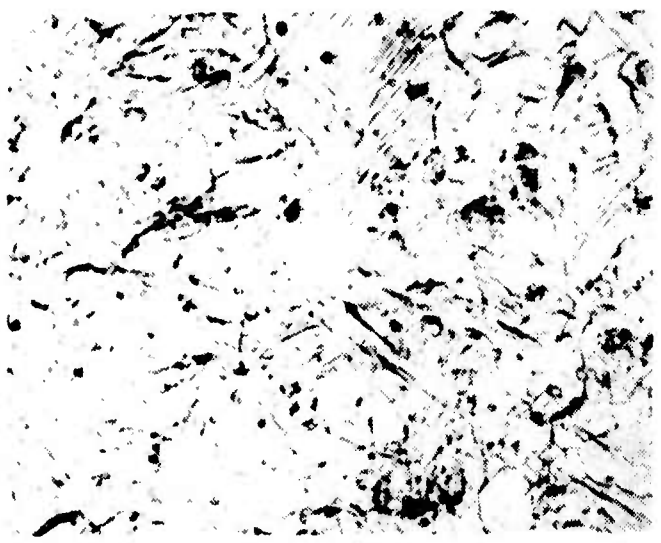

2.0 x 10^5 Cycles

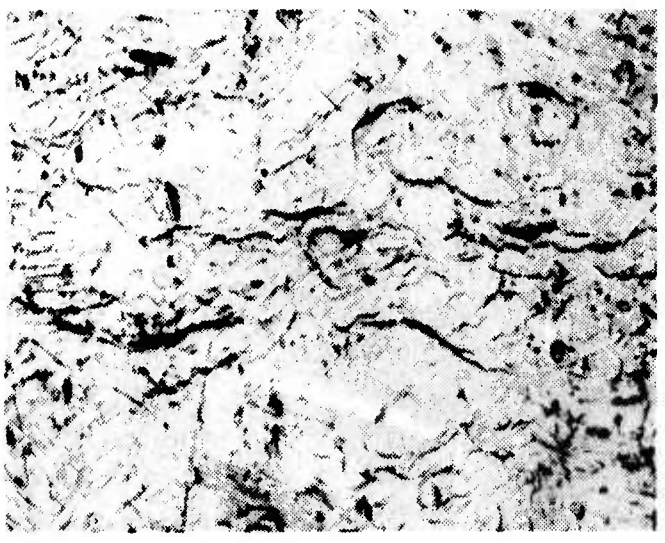

3.6 x 10^5 Cycles

Figure 22. Optical Micrographs of Fatigued 1100-0 Aluminum Specimens (250X)

Control, 0 Cycle

2.8×10^5 Cycles

1.2×10^5 Cycles

3.2×10^5 Cycles

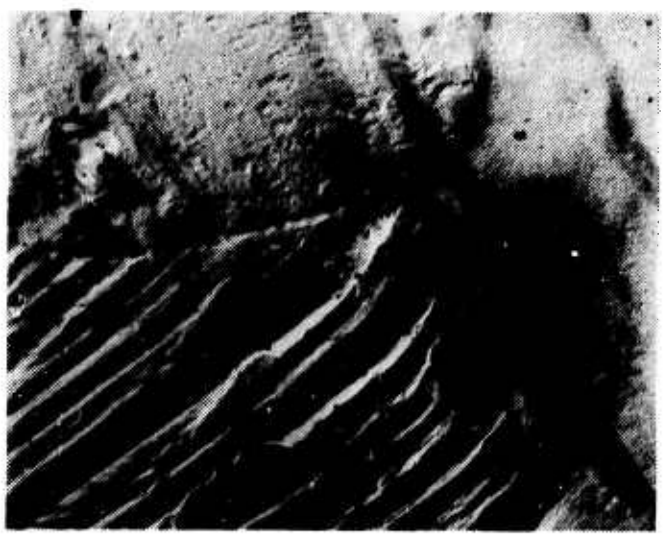

2.0×10^5 Cycles

3.6×10^5 Cycles

Figure 23. Electron Micrographs of Fatigued 1100-0 Aluminum Specimens (2,500X)

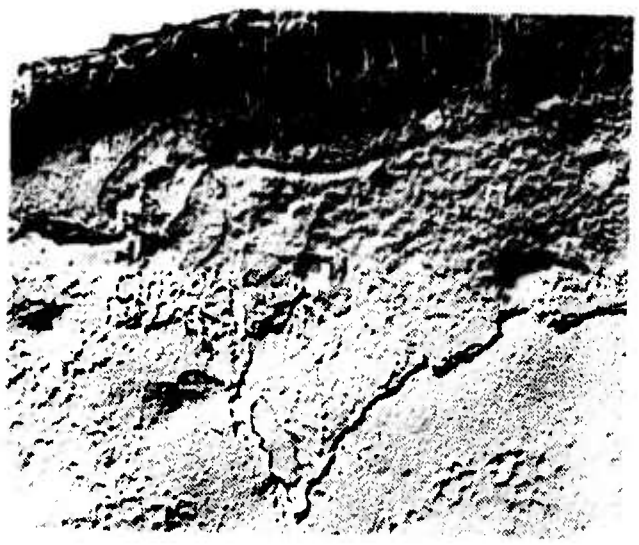

Control, 0 Cycle

1.2×10^5 Cycles

3.6×10^5 Cycles

Figure 24. Replicas of Sections Through Fatigued 1100-0 Aluminum Specimens at 20 Degrees to Surface (6,500X)

As Fatigued

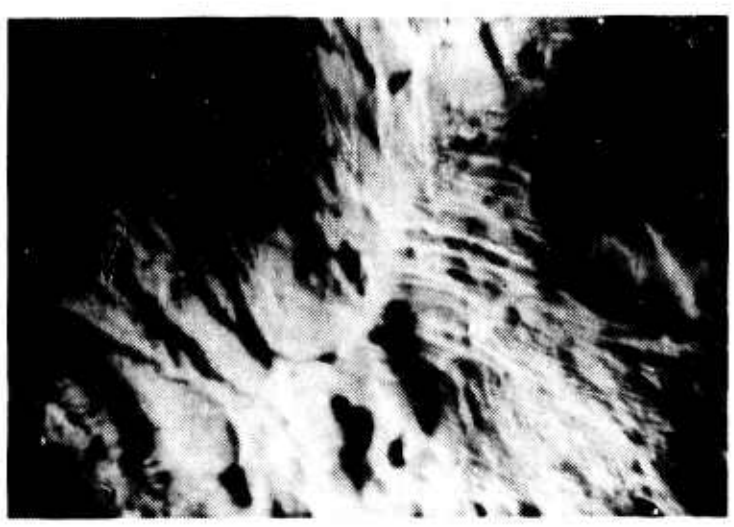

Argon Etch for 30 Minutes

Argon Etch for 4 Hours 35 Minutes

Figure 25. Secondary Electron Emission Photographs at 500X of Surface of 1100-0 Aluminum Specimen After 2.0×10^5 Cycles

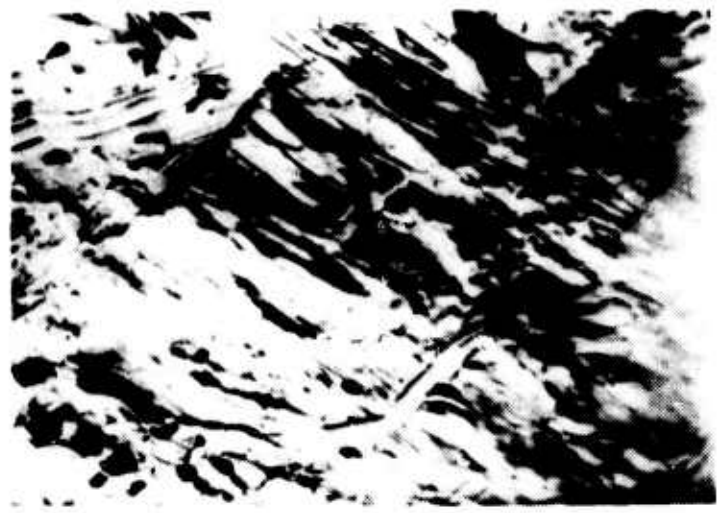

As Fatigued

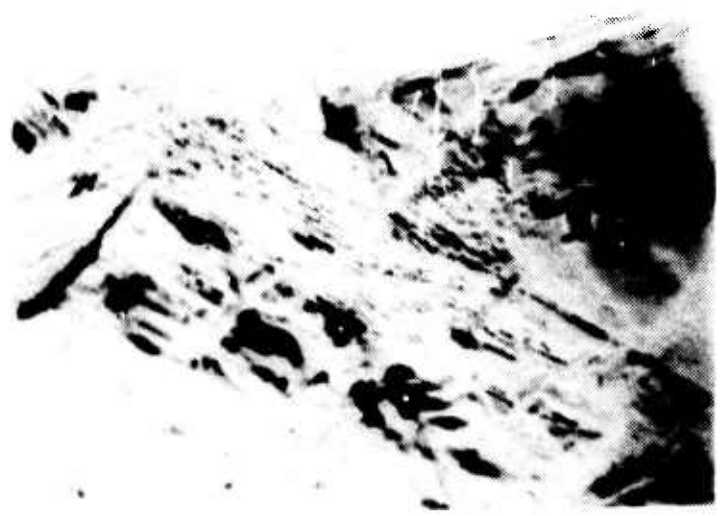

Argon Etch for 57 Minutes

Argon Etch for 3 Hours 27 Minutes

Figure 26. Secondary Electron Emission Photographs at 500X of Surface of 1100-0 Aluminum Specimen After 3.6×10^5 Cycles

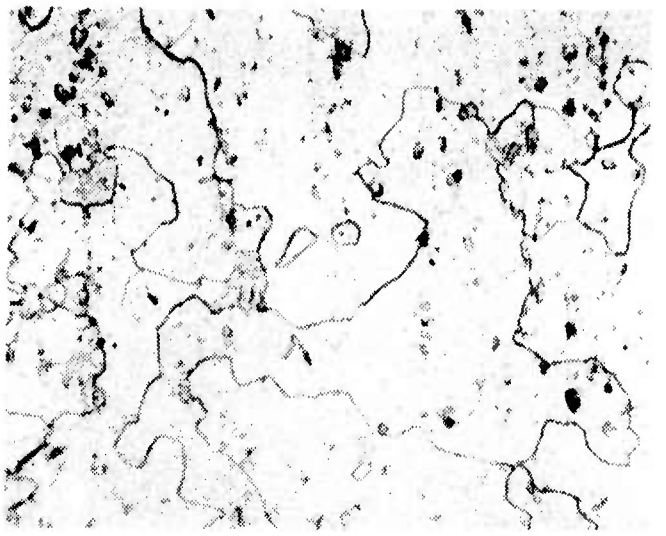

Optical 250X

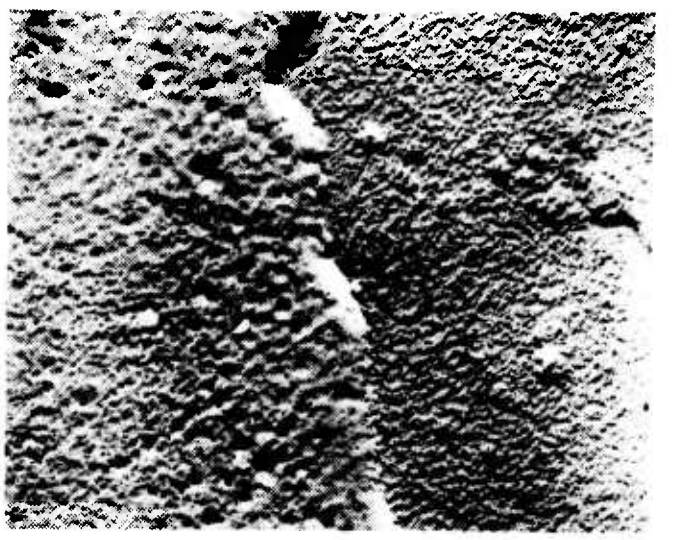

Replica 2,500X

Before Fatigue Test

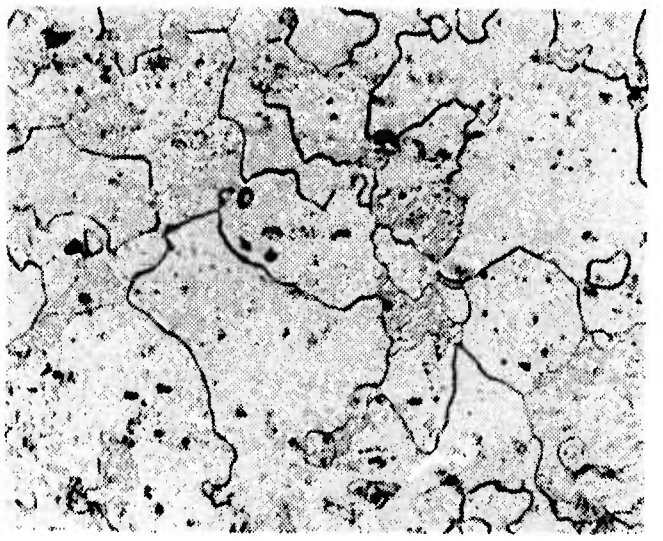

Optical 250X

Replica 2,500X

After Fatigue Test

Figure 2.7. Micrographs of 1100-0 Aluminum Specimen After 800 Cycles

Optical 250X

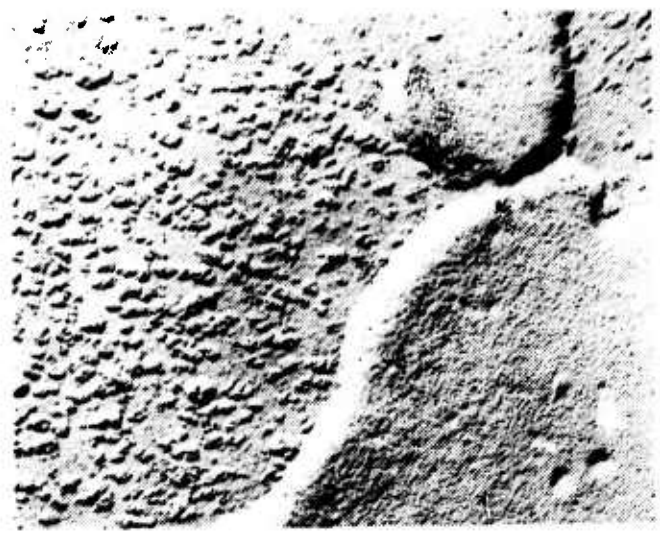

Replica

Before Fatigue Test

Optical 250X

Replica 2,500X

After Fatigue Test

Figure 28. Micrographs of 1100-0 Aluminum Specimen After 3.0×10^4 Cycles

Center sections of the two fatigue specimens were also examined by a secondary electron emission microscope. Argon etch was used to remove the slip line structure, as had been done on the specimens previously fatigued for 2.0 and 3.6 x 10^5 cycles. Details of the changing surface appearance are shown in figures 29 and 30. The depth of attack for the specimen subject to fatigue stressing for 800 cycles was too shallow to measure accurately, while that for the specimen which had undergone 3.0 x 10^4 cycles was roughly 10 μm.

DISCUSSION

Metallographic studies of 1100-0 aluminum reveal that slip striations appear very early on the surface if the material is subject to relatively high stress fatigue. The depth of the disturbed surface layer, even at the earliest observation of surface disturbance, is of the same order of magnitude as the grain size, in this case less than 10 μm. Increasing fatiguing cycles increases the depth of the affected layer only very slightly. These observations agree with those of other investigators. These generally report that micropores (or the intrusion extension by means of tubular hole growth) and zones of abnormal distortion within grains are produced between 1/1000 and 1/200 specimen life (Wood et al, 1963). They do not grow but their number increases upon continued cycling. The micropores are not actual cavities but regions of high internal strain (Grosskreutz et al, 1966). Presence of micropores or zones of abnormal distortion can also be deduced from ultrasonic measurement because both ultrasound velocity and attenuation undergo a change at 1/1000 to 1/100 specimen life (Truell et al, 1959 and 1961). Microcracks eventually develop in these centers which can be called fatigue damage centers.

The investigations here, additionally, confirm that increasing fatigue damage is confined to a surface layer and does not, until a much later crack growth stage, penetrate beyond this layer.

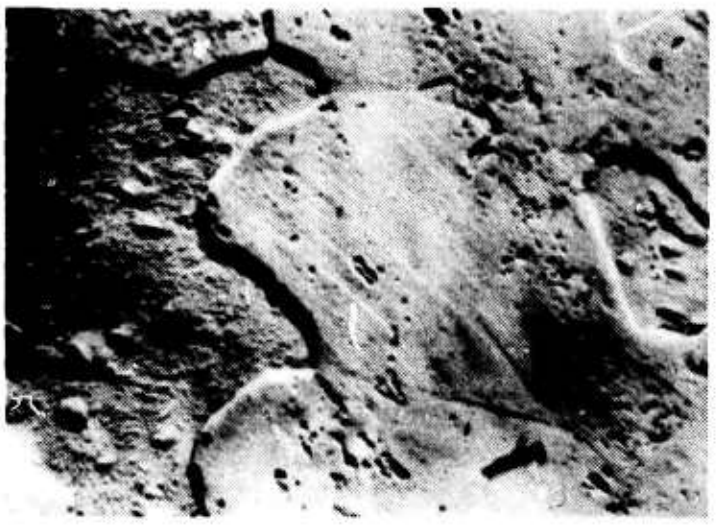

As Fatigued

Argon Etch for 50 Minutes

Argon Etch for 2 Hours 35 Minutes

Figure 29. Secondary Electron Emission Photographs at 550X of Surface of 1100-0 Aluminum Specimen After 800 Cycles

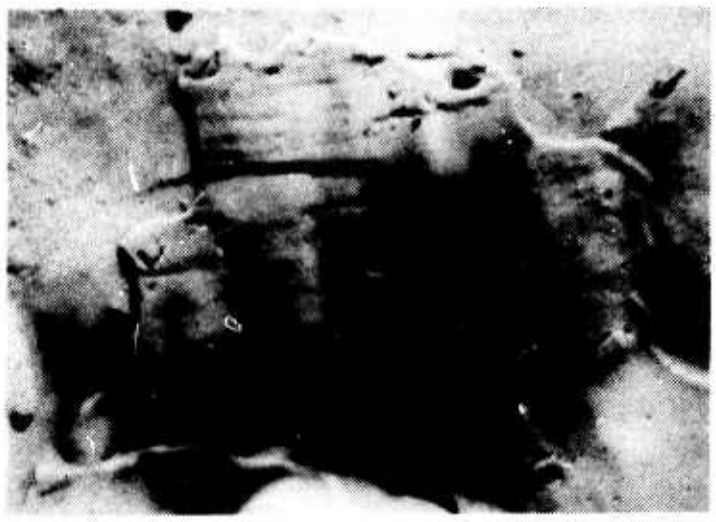

As Fatigued

Argon Etch for 50 Minutes

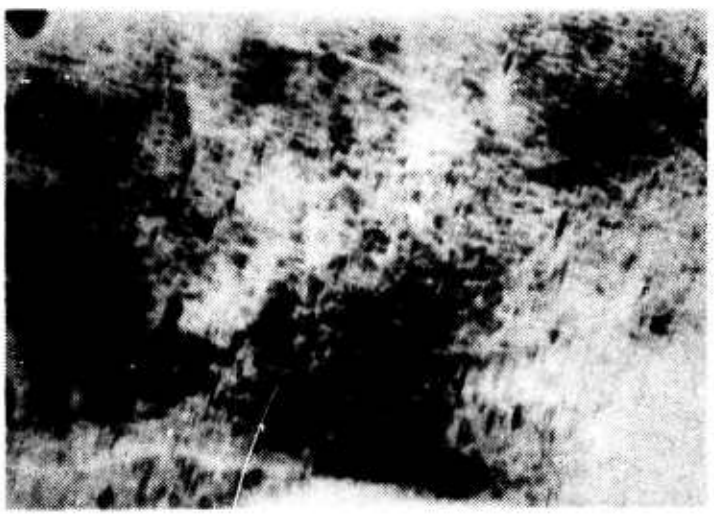

Argon Etch for 3 Hours 58 Minutes

Figure 30. Secondary Electron Emission Photographs at 550X of Surface of 1100-0 Aluminum Specimen After 3.0×10^4 Cycles

SECTION VIII

ULTRASONIC SURFACE WAVE MEASUREMENTS

TECHNIQUES

The pulse-echo method was employed to measure surface wave velocity by means of the conventional system (figure 8). One transducer was placed on the surface about 1 inch from the specimen center, and the interval between the first pulse and the echo was measured. The transducer was then moved 1 inch farther away from the specimen center, and using the same time base as before, the distance between the first pulse and the echo again was measured. In the precision system, (figure 9) surface wave velocity was measured by the through-transmission method using one transmitter and one receiver placed on the same specimen surface. The signals are amplified by the receiver to a level adequate for oscilloscope presentation. The receiver utilizes gating signals to control receiver gain to prevent blocking caused by the high generator pulses. By using the oscilloscope in the main sweep delay mode, it is possible to display the desired signal and observe pulse superposition. When superposition is achieved (by adjusting the sine-wave generator frequency), the actual frequency is monitered on the counter. Based on this accurate frequency data, it is possible to calculate ultrasonic surface velocity with high precision.

For attenuation measurement using the conventional system, the transducer was moved in a manner similar to the velocity measurement. A portion of the signal displayed on the reflectoscope was gated and amplified to an ac voltmeter. Difference between voltmeter readings at the two transducer locations was an indication of attenuation. Measurements were made at 1 and 5 MHz frequencies.

RESULTS AND DISCUSSION

Surface velocity measurements were carried out on a control specimen and five specimens which had undergone fatigue deformation for 1.2, 2.0, 2.8, 3.2, and 3.6 x 10^5 cycles or, respectively, 30, 50, 70, 80, and 90 percent specimen life (based on 4.0 x 10^5 cycles) at a maximum stress of 11,500 psi. Results obtained from both the conventional system and the precision measurement system at 2.25 MHz fall in the ranges illustrated in figure 31. A comparison of the change in attenuation in the family of these specimens is shown in figure 32. The ordinate is the ratio of the voltage difference at 5 to 1 MHz. The scatter in figures 31 and 32 was mainly due to the use of SAE 30 oil as couplant. Heavyweight oil couplant is reliable for detecting cracks. For velocity or attenuation measurement, however, one no longer looks for the presnce or absence of a responding signal, but one must resolve and define the waveform and cycles of that signal. Any minute variation in coupling pressure or

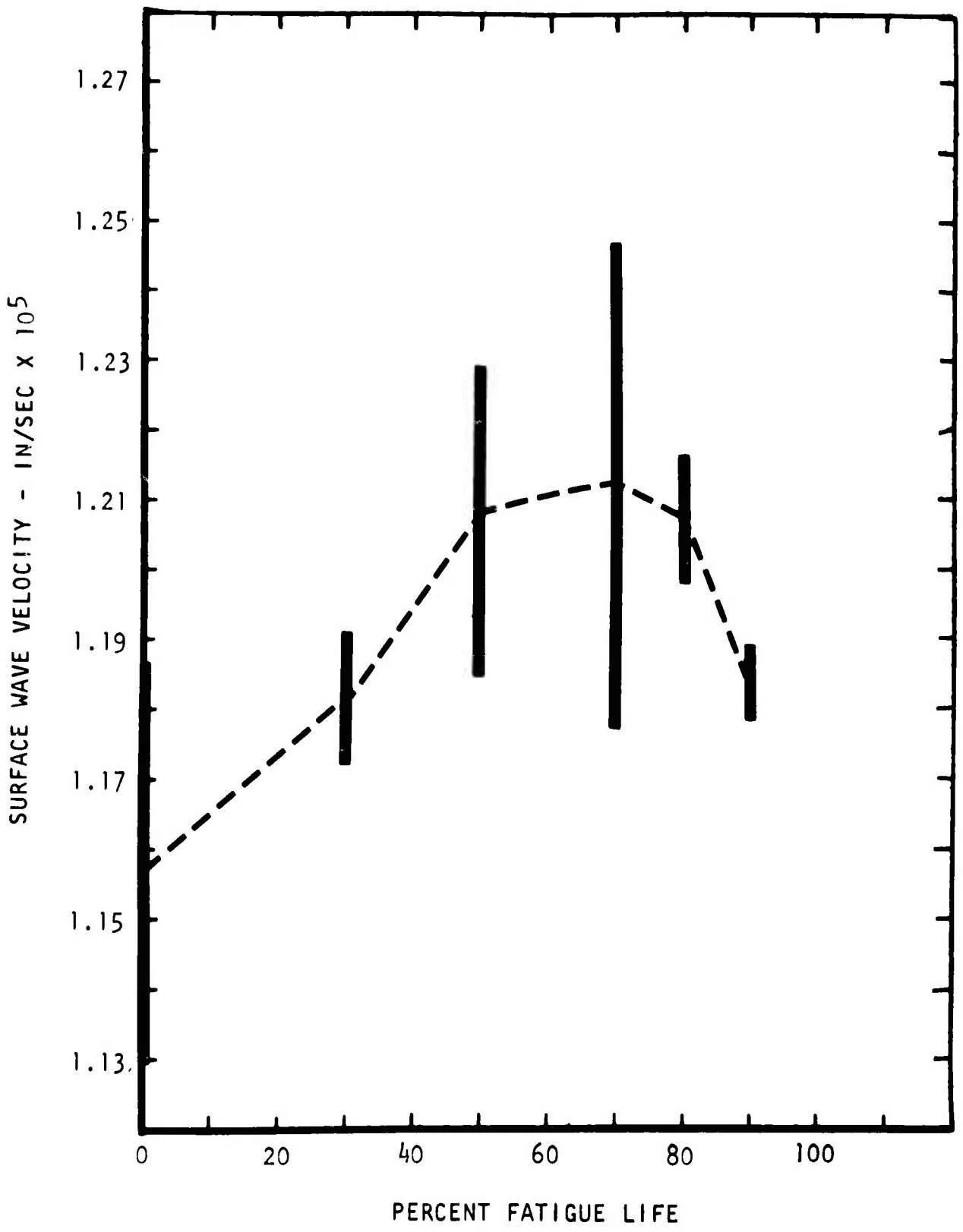

Figure 31. Relationship Between Surface Wave Velocity and Fatigue Life of 1100-0 Aluminum

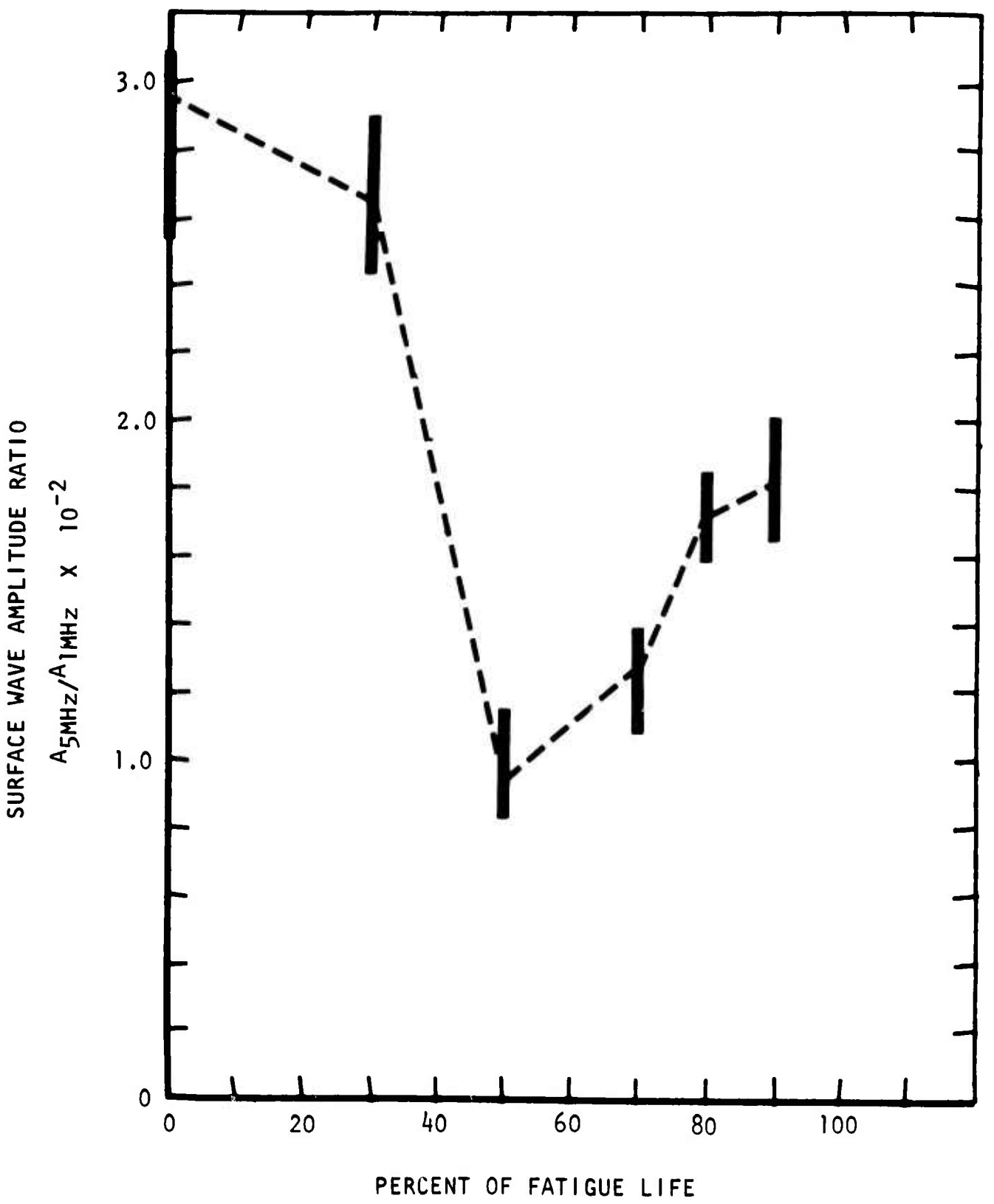

Figure 32. Relationship Between Surface Wave Attenuation and Fatigue Life of 1100-0 Aluminum

thickness has a marked effect on the waveform. It is necessary to use a coupling medium to eliminate air from the transducer-specimen interface with compatible acoustic impedance and yet to be sufficiently fluid to insure removal of all air bubbles. Furthermore, any changes in the couplant thickness affect both the acoustic pulse transit time and the amount of energy transferred to the specimen. Late in the present investigation, a coupling medium under the trade name Aroclor 1260, manufactured by Monsanto Chemical Co, was found more suitable than SAE 30 oil. Its use yielded more reproducible results on attenuation. The trend of the curve shown in figure 32 was confirmed.

Both figures 31 and 32 indicate a gradual reversal of fatigue life to surface wave velocity and fatigue life to attenuation ratio trend at about 50-percent specimen life. However, owing to the wide scatter of the experimental data, it is not certain whether there is a perceptible change in velocity or attenuation between the control specimen and the specimen which had spent 20 percent of its fatigue life based on 4.0×10^5 cycles.

The frequencies (1 to 5 MHz) chosen were dictated by the availability of suitable transducers. The depth of penetration of surface waves is about one wavelength, which in the present case is about 0.05 inch, much larger than the depth of the fatigue-affected zone determined by metallography. The present results, however, are somewhat similar to those observed by Herlescu and coworkers (1967) on steel in bending fatigue.

Several 1/2-inch-diameter, Y-cut quartz crystals operating at 50 MHz were purchased. Use of these crystals would reduce the surface layer to be interrogated by surface waves to about 0.003 inch or 76 μm, a value at the same order of magnitude as the fatigue-affected depth. It would thus be possible to obtain better ultrasonic test results.

SECTION IX

CONCLUSIONS AND RECOMMENDATIONS

Exoelectron emission of 1100-0 aluminum during fatigue stressing takes place in two stages. The initial stage, which occurs very early in the fatigue process, appears to correlate with the initiation of fatigue damage, indicated by the formation of a disturbed layer. The greater the fatigue stress, the longer and the stronger are the initial emissions. Metallographic examination of briefly fatigued specimens reveals that this emission stage coincides with the formation of fatigue-affected surface zone. The final emission stage coincides with the formation and propagation of fatigue cracks leading to failure. At least at room temperature, light simulation is needed for emission because no emission above the background level can be observed under complete darkness. The intensity of emission also increases when the specimen is illuminated with ultraviolet light. There is a long period of lack of emission between the two stages and, apparently, no change in the depth of the fatigue-affected zone. However, preliminary test results of the ultrasonic surface wave measurements indicate that some changes occur in this intermediate quiescent period.

From these observations the following recommendations are suggested for future work:

1. Exoelectron emission tests on 1100-0 aluminum should be continued covering a wider area of enviromental parameters. Tests should be extended to other metals and alloys. Various stimulations should be employed to aid emission.

2. Evaluation of the response of fatigued 1100-0 aluminum and other materials, tested for exoelectron emission, to ultrasonic surface waves should be conducted using transducers operating at high frequencies (about 50 MHz). Tests should be carried out both after or during fatigue deformation.

3. Metallographic evaluation of fatigued specimens should be carried out to correlate the results of exoelectron emission and ultrasonic tests with the fatigue phenomena.

APPENDIX I

BIBLIOGRAPHY RELATING TO EXOELECTRON EMISSION

APPLICATION OF THE METHOD OF EXOELECTRON EMISSION IN METAL SCIENCE

I. N. Bogachev, R. I. Mints, and V. S. Kortov

Metal Science and Heat Treatment, July-August 1966, pp 591-594

MATERIAL

Fe-Ni alloy, Fe-Mn alloy, and 1Kh18N8 stainless steel

SPECIMEN PREPARATION

Cleaning and etching

EXCITING CONDITION

Static pressing with a cone with a 90-degree angle on a 5-ton press
Dynamic loading by impact from a free-falling cone weighing 20 kg from a height of 0.5 m
Microimpact
Microindentation using 100 g load
Cyclic stressing

DETECTION EQUIPMENT

BFL end-window counter with mica window having minimum thickness less than 1 mg/cm^2, operating between 2×10^{-3} and 2×10^{-5} torr
Distance between specimen and nickel grid, which is placed 0.1 mm below the counter = 2.9 mm
Voltage between grid and specimen = 4 kv

RESULT

Variation of emission intensity after static or dynamic loading with time exhibits a maximum; time to reach the peak intensity depends on the specimen material tested.
Dynamic loading produces more intense emission peak than static loading.
Emission from grain may differ from emission from grain boundary.
Emission intensity of ferrite is greater than that of austenite which in turn is greater than that of martensite or epsilon carbide.
In cyclic stressing, 1Kh18N8 steel emission intensity increases with number of cycles and then decreases as cyclic stressing continues. Shape of the emission versus time curve depends on magnitude of the stress.

EXOELECTRONIC EMISSION DURING $\gamma \rightleftharpoons \epsilon$ TRANSFORMATIONS

I. N. Bogachev, V. F. Yegolayev, V. S. Kortov, and R. I. Mints

Physics of Metals and Metallography, Vol 23, 1967, pp 100-104

MATERIAL

Fe-Mn austenite alloy

SPECIMEN PREPARATION

EXCITING CONDITION

Phase transformation ($\gamma \rightleftharpoons \epsilon$)

DETECTION EQUIPMENT

End-window counter, operating at 2×10^{-5} torr with accelerating voltage 4 kv
Electron multiplier

RESULT

In the metastable condition, phase transformation of the alloy is accompanied by electron emission.

Emission intensity depends on the amount of ϵ phase and structural changes (formation of structural imperfections such as increased probability of stacking faults, microdistortions, and block fragmentation) during phase transformation.

Emission intensity varies with number of transformation cycles, the peak occurring after three cycles; subsequent cycles of transformation stabilize the austenite and structural imperfections, which is accompanied by a reduction in emission.

ON THE THEORY OF CHEMIELECTRON EMISSION OF METALS

A. Bohun, J. Sak, and M. Pšeničková

Czechoslavakia Journal of Physics, Vol 15, 1965, pp 667-677

MATERIAL

Li, Na, K, Rb, and Cs

SPECIMEN PREPARATION

Vacuum-deposited metal layer having about 65 cm^2 reacting surface area

EXCITING CONDITION

Reaction with halogens (Cl_2, Br_2, I_2) or oxygen

DETECTION EQUIPMENT

Lutz-Edelman electrometer

RESULT

The highest electron emission yield is measured for the reaction of chlorine with cesium.

The yield decreases from cesium to lithium (for the same halogen) and from chlorine to iodine (for the same alkaline metal).

At the beginning of the measurement, when the metal surface is clean, the yields do not depend on the temperature between 20° and -78° C.

The yield of the reaction of the alkaline metal-oxygen system is at least five orders lower than that of the reaction of chlorine with the corresponding metal.

ELECTRON EMISSION FROM ALUMINUM AFTER LOW-TEMPERATURE DEFORMATION

R. N. Claytor and F. R. Brotzen

Journal of Applied Physics, Vol 36, 1965, pp 3549-3555

MATERIAL

99.993 percent Al

SPECIMEN PREPARATION

0.020-inch-diameter wire annealed for 2 hours at 550° C

EXCITING CONDITION

Tensile loading at -140° C to a strain 7.5 of 12 percent, then allowed to warm up (0.27° C/sec) while measurement being taken

DETECTION EQUIPMENT

Open-window Geiger-Müller counter containing 99 percent He and 1 percent methane at 0.5 atmospheric pressure
Distance between window and specimen = 5 mm
Potential between counter case and specimen = 45 v
300-watt incandescent reflector spotlight placed 18 inches from specimen

RESULT

Variation of emission rate with temperature exhibits a peak in the general temperature range (210°-230° K) same as that for the drop in electrical resistivity and the release of stored energy, suggesting that point defect migration plays an important role in emission by plastic deformation. Migration energy of the point defect involved in emission is about 0.44 ev, which coincides closely with the energies for annealing of defects introduced in aluminum by quenching from elevated temperatures and by electron bombardment.

ELECTRON EMISSION FROM ALUMINUM AFTER QUENCHING
R. N. Claytor, J. E. Gragg, and F. R. Brotzen
Journal of Applied Physics, Vol 37, 1966, pp 149-152

MATERIAL
99.993 percent Al

SPECIMEN PREPARATION
0.020-inch-diameter wire
3/4 inch square x 0.020 inch thick

EXCITING CONDITION
Heating by alternating current the wire specimen to 300°-400° C at a pressure about 100μm Hg in a chamber containing the Geiger-Müller counter and quenching the specimen by the counter gas to room temperature
Heating the plate specimen in a furnace to 300°-400° C at a less than 50μm Hg pressure and quenching the specimen in ice-brine solution.

DETECTION EQUIPMENT
Open-window Geiger-Müller counter containing 99 percent He and 1 percent methane

RESULT
Only little or no emission is observed without illumination of the specimen.
Except for the initial portion, the emission decay curve for the quenched wire is almost identical to the curve for the quenched plate.
Emission occurs after quenching because of the creation and diffusion of point defects toward the surface.

PHOTOEMISSION FROM METAL SURFACES MEASURED WITH GEIGER COUNTERS
M. A. Conrad and S. Levy
Nature, Vol 189, 1961, pp 887-889

MATERIAL
Commercial purity Al, Cu, Ni, Sn, and Zn

SPECIMEN PREPARATION
1 inch diameter x 1/4 inch thickness

EXCITING CONDITION
Abrasion, filing, polishing, or compression
A grating monochromator and an incandescent ribbon lamp as the light source

DETECTION EQUIPMENT
Windowless Geiger-flow counter containing 98.5 percent He and 1.5 percent isobutane
Specimen forming a part of the cathode
Distance between anode and specimen = 3/4 inch

RESULT
No detectable emission from abraded or deformed metal surfaces in complete darkness suggests that the mechanism of the Russell effect cannot be explained by the action of delayed electrons detectable in a Geiger counter.
Photoelectric wavelength thresholds of the metals are in the near ultraviolet region of the light spectrum; they differ slightly for the different metals.
X-ray irradiation of metals does not induce delayed electron emission but strongly deactivates the materials with respect to photoemission.

EXOELECTRON EMISSION DURING OXYGEN CHEMISORPTION AT CLEAN NICKEL SURFACES

T. A. Delchar

Journal of Applied Physics, Vol 38, 1967, pp 2403-2404

MATERIAL

Ni

SPECIMEN PREPARATION

Evaporated film deposited on walls of a cell having a very low electrical capacity (0.1 $\mu\mu$ F)

EXCITING CONDITION

Addition of spectroscopically pure oxygen to 10^{-10} torr vacuum

DETECTION EQUIPMENT

Dc amplifier connected to the ionization gage grid in the cell

RESULT

Each oxygen addition at 77° K is accompanied by a burst of electrons with the yield about 10^{-9} electron per adsorbed molecule.

Number of electrons ejected at room temperature depends on the time allowed to elapse between oxygen additions: higher yield at increased dose interval because time is required for incorporation of oxygen in the nickel lattice which does not occur significantly at 77° K.

Oxygen chemisorption causes electron emission from nickel surfaces.

INVESTIGATION OF EXOELECTRONIC EMISSION DUE TO SLIDING FRICTION

V. D. Evdokimov

Soviet Physics - Doklady, Vol 12, 1968, pp 732-734

MATERIAL

Steel 25, steel 45, cast iron SCH-32, and aluminum

SPECIMEN PREPARATION

Specimen in the form of a ring 60 x 50 x 15 mm

EXCITING CONDITION

Specimen subject to dry one-directional or reversing friction against a bar of steel 40 with a 90.5 m/min sliding velocity under a normal load of 13.2 kg in a duration of 10 minutes.

Ultraviolet lamp OJ-18 with filter UFS-1 for steel and cast iron and with an additional BS-12 filter for aluminum

DETECTION EQUIPMENT

Open surface counter

RESULT

Emission of electrons from the metal surface after reversing friction is greater than emission after one-directional friction. The process of rubbing reduces the work of electron escape by locally increasing the lattice energy. Reversing friction, by increasing the surface of metal and the number of its various defects, should reduce the work function to a greater degree than does one-directional friction. Hence, exoemission after reversing friction is more intense than after one-directional friction.

Both emission decay curves for aluminum conform to hyperbolic law and show a sharp fall of the emission with time.

Emission of electrons for steel 25 also decreases with time.

Exoemission for steel 45 and cast iron increases initially and latter decreases steeply with time.

The tendency for inflections on the decay curve to appear increasing with decreasing plasticity of the material.

Chemisorption of oxygen and the influence of the oxide film on the work function play a significant role in shaping the decay curve.

INVESTIGATION OF EXOELECTRONIC EMISSION OF SURFACE LAYERS DURING SLIDING FRICTION

V. D. Evdokimov

Soviet Physics - Doklady, Vol 13, 1968, pp 475-477

MATERIAL

Steel 25 and steel 45

SPECIMEN PREPARATION

Flat specimen (20 x 20 x 50 mm) and annular specimen (60 x 50 x 15 mm)

EXCITING CONDITION

Sliding friction at various normal loads but with a constant sliding rate of 90.5 m/min

Ultraviolet light

DETECTION EQUIPMENT

Open-type transducer

RESULT

The intensity of exoelectron emission during sliding friction increases steadily with time, reaching a stabilized state in a few minutes.

The intensity increases with increase of normal load at the start of friction, but later it slows down and finally it even diminishes.

Under a steady-state sliding condition, the least load corresponds to the highest exoelectron emission.

There is a relationship between exoelectron emission and microhardness: the higher the microhardness, the higher the intensity of emission.

Variation of exoelectron emission and microhardness with normal load and time is attributed to the formation of structural defects in the surface layers of metals during friction. In the course of plastic deformation, the generation of dislocation gradually diminishes and steady state sets in. Both working hardening and relaxation occur simultaneously in this state. Further increase in the normal load raises the temperature of the friction surface, thus intensifying relaxation and reducing work hardening and the density of defects in the deformed lattice, giving a corresponding reduction in the level of exoelectron emission as well as the microhardness.

AUTORADIOGRAPHY OF FATIGUE FRACTURE IN ALUMINUM

J. C. Grosskreutz

Journal of Applied Physics, Vol 33, 1962, pp 2653-2654

MATERIAL

99.99 percent Al

SPECIMEN PREPARATION

EXCITING CONDITION

Push-pull fatigue loading at constant strain (±0.002) for 50,000 cycles (approximately 10 percent of expected life)

DETECTION EQUIPMENT

Stripping emulsion on specimen surface and 18-hour exposure time in total darkness

RESULT

Photographic image is a faithful replica of the slip band and crack structure induced by fatigue loading.

THE EMISSION OF EXOELECTRONS FROM ALUMINUM DURING FATIGUE

J. C. Grosskreutz and D. K. Benson
NASA CR-57918, 1963

MATERIAL

Pure Al and 2S alloy

SPECIMEN PREPARATION

EXCITING CONDITION

Constant stress fatigue loading at 400 cps and a pressure of 2-5 x 10^{-5} torr in complete darkness

Unidirectional tensile straining at 10^{-6} to 10^{-9} torr

DETECTION EQUIPMENT

Snooper-scope image converter tube

AR.10 stripping emulsion, Kodak SWR vacuum ultraviolet film, and Tri-X film placed over zinc sulphide phosphor

14-stage electron multiplier having a current gain about 10^6

RESULT

There is no detectable image using AR.10 stripping emulsion and Kodak SWR film after fatiguing 3.5 x 10^6 cycles and between 10^5 and 2 x 10^6 cycles, respectively; negative result is also obtained from Tri-X film with zinc sulphide phosphor.

When the electron multiplier is used, emission is observed 5 minutes after start of the fatigue test; the emission rate varies widely with increasing number of cycles but tends to rise near end of the test (about 4.36 x 10^5 cycles in 18 minutes) due to formation of macrocracks; failure of the specimen occurs after 8 x 10^5 cycles.

No emission from aluminum with oxide coating subject to unidirectional tensile straining at 10^{-6} or 10^{-9} torr even when the specimen is illuminated during test; emission rate after 10 percent strain is about 10^2 electrons/cm^2-sec, a very low figure.

UNTERSUCHUNGEN ÜBER DIE EXOELEKTRONEN-EMISSION MECHANISCH BEANSPRUCHTER METALLE

M. Hempel, A. Kochendörfer, and A. Tietze

Archiv für das Eisenhüttenwesen, Vol 35, 1964, pp 465-474

MATERIAL

99.989 percent Al and 0.09 percent C steel

SPECIMEN PREPARATION

Al specimens: 7 mm thick, annealed in air for 1/2 hour at 350° C

Steel specimens: 15 mm thick, annealed in vacuum (10^{-2} torr) for 1/2 hour at 930° C

Electropolishing before test

EXCITING CONDITION

Tensile-tensile fatigue loading with lower stress at 0.5 kg/mm^2

Static tensile loading to 4 kg/mm^2 corresponding at 5.25 percent strain

Illuminated with unfiltered incandescent lamp at 250, 275, or 300 ma with wavelengths longer than 0.33 μm but shorter than 0.5 μm

DETECTION EQUIPMENT

17-stage electron multiplier operating at 10^{-4} torr

Distance between specimen and multiplier end facing first dynode = 2 cm

RESULT

For Al:

Emission intensity reaches a plateau in 0.5-5.1 kg/mm^2 fatigure loading 10 to 15 minutes after start of test (test duration = 35 minutes) and decreases after test but is still way above the background level in 1 hour.

Emission intensity increases with increase of fatigue stress range but the intensity is more or less independent of stress range in the first 1.3×10^5 cycles; no emission is observed at a stress range of 2 kg/mm^2.

Emission starts after static loading to 1.25 percent strain with illumination using 275 or 300 ma, but the emission intensity at 300 ma is much greater than that at 275 ma.

Little emission is observed in the absence of illumination even at 10 percent strain in static loading.

Emission in static loading starts at a stress of 2 kg/mm^2, increases rapidly until end of the test at 4 kg/mm^2, and decreases slowly thereafter.

Surface treatment affects the rate of emission: Emission rate of electropolished specimen is greater than the rate of electropolished and anodized (in 0.1 N NaOH) specimen which in turn is greater than the rate of electropolished and heated (350° C in air for 1/2 hour or 500° C in vacuum for 1/2 hour) specimen.

Emission intensity increases with increase of temperature (18 to 100° C).

For steel:

No emission intensity above the background level is observed in both fatigue test and tensile test using illumination with wavelengths longer than 0.33 μm, regardless of different heat treatments.

EXOELECTRONIC EMISSION AS A METHOD OF STUDYING THE DEFORMED SURFACE OF METALS

V. S. Kortov and R. I. Mints

Physics of Metals and Metallography, Vol 19, 1965, pp 72-76

MATERIAL

Al, 1Kh18N8 steel, and bronze

SPECIMEN PREPARATION

Cleaning and etching

EXCITING CONDITION

Abrading Al surface with emery paper
Hydraulic shock for 40 minutes on steel
Diamond pyramid (200 g load) indentation on bronze

DETECTION EQUIPMENT

BFL end-window counter with mica window having minimum thickness not less than 1 mg/cm^2, operating between 2 x 10^{-3} and 2 x 10^{-5} torr
Distance between specimen and Ni grid, which is placed 0.1 mm below the counter, = 2.9 mm
Voltage between grid and specimen = 4 kv

RESULT

Emission intensity of Al increases with increase of accelerating voltage between grid and specimen.
Emission curve for 1Kh18N8 steel exhibits a maximum, but no such peak is observed in the curve for bronze.
Emission intensity of ferrite is greater than the intensity of austenite which in turn is greater than that of martensite.

ELECTRON EMISSION DURING METAL FATIGUE

R. S. Krogstad and R. W. Moss

Proceedings of the Symposium on Physics and Nondestructive Testing
September 28-30, 1965, Dayton, Ohio, pp 9-21

MATERIAL

Al, Au, Fe, Ni, and Ti

SPECIMEN PREPARATION

Electropolish

EXCITING CONDITION

Torsional fatigue

DETECTION EQUIPMENT

Phosphor film deposited on transparent stannous oxide conducting film, which is lined over the inner surface of a glass cylinder containing the specimen

13-stage photomultiplier

RESULT

Except for Al, emission from other metals tested starts after a few hundred cycles, followed by a series of emission events.

Frequency with which the emission events occur increases to a maximum (at about one-third of fatigue life) and then decreases slowly until specimen fails.

Duration of an emission event (less than 5×10^{-6} sec) is several orders of magnitude too short to ascribe to chemisorption.

The observed emission from gold which has no stable oxide coating is incompatible with the concept of emission by thermal dissociation of deformation-induced electron levels.

Since a large number of electrons (about 10^4) are involved in emission, it is difficult to assume vacancy annihilation as the mechanism of electron ejection from metal surface.

Tentative mechanism of emission: Energy associated with the stress fields around dislocations in the slip process. Emission occurs if this energy exceeds work function, and it is also transferred to an electron.

Based on this mechanism, calculation shows that there is no emission from Al.

EXOEMISSION FROM GROUND SURFACES OF GERMANIUM AND SILICON

V. I. Kryuk, R. I. Mints, and V. S. Kortov

Soviet Physics - Solid State, Vol 8, 1966, pp 1295-1296

MATERIAL

Single-crystal Ge, single-crystal Si, and polycrystalline Si

SPECIMEN PREPARATION

Area of etched specimen = 3.5 cm^2

EXCITING CONDITION

Grinding with emery cloth for 1 minute

Soft ultraviolet light which does not cause photoelectric emission

DETECTION EQUIPMENT

Electron multiplier operating at 10^{-5} torr and 3.2 kv

RESULTS

No emission is observed from undeformed metal surfaces.

Emission intensity varies with accelerating voltage and wavelength of the illumination, but nature of the decay curve remains practically the same.

Ge shows more intense and more rapid emission decay than Si.

Kinetic characteristics of emission are closely associated with the diffusion of vacancies to the surface; the lower mobility of vacancies in Si is indicated by the activation energy Q for self-diffusion in Si and Ge, which proceeds by a vacancy mechanism (Q = 86-100 kcal/mol and 54 kcal/mol for Si and Ge, respectively).

EFFECT OF TEMPERATURE ON THE EMISSION OF ELECTRONS FROM ABRADED SURFACES OF BERYLLIUM, CALCIUM, ALUMINUM, AND MAGNESIUM

T. C. Ku and W. T. Pimbley

Journal of Applied Physics, Vol 32, 1961, pp 124-125

MATERIAL

Al, Be, Ca, and Mg

SPECIMEN PREPARATION

EXCITING CONDITION

Abrading and then placed in counter

Abrading, placed in counter to start counting, and then withdrawing from counter to store in liquid nitrogen for 2,260 seconds before placing back into counter

Abrading, placed in counter to start counting, and then withdrawing from counter to store at 550° C for 120 seconds before placing back into counter

White light or zirconium arc lamp as the light source

DETECTION EQUIPMENT

Open-window Geiger-Müller counter containing 98.7 percent He and 1.3 percent butane

Specimen at a negative potential of 50 v with respect to the grid at aperture of the counter

RESULT

Under identical experimental conditions, the rate of emission from Be is approximately one-third the rate from Al, and the rate of emission from Ca is about twice that from Al.

There is no measurable emission when the light is shut off.

Emission rate decreases or increases respectively with decrease or increase of temperature.

Emission is thought to be influenced by diffusion of vacancy so that the condition of emission is that the sum of potential energy released by vacancy and photon energy is equal to or greater than photoelectric work function.

EXOELECTRON EMISSION DUE TO ULTRASONIC IRRADIATION

J. A. M. Langenecker and D. B. Ray

Journal of Applied Physics, Vol 35, 1964, pp 2586-2588

MATERIAL

99.999 percent Al, 2024 and 6061 Al alloys

SPECIMEN PREPARATION

12 mm diameter specimen annealed for 4 hours at 450° C and oven-cooled under inert atmosphere (96 percent N and 4 percent H)

Standard cleaning, no effort to restrict oxide formation

EXCITING CONDITION

Filing, abrading with steel brush (2 seconds) or carborundum paper

Ultrasonic irradiation using transducer with intensity 0-100 W/cm^2 and frequency 20 KHz

DETECTION EQUIPMENT

Windowless flow counter containing 98.5 percent He, 1 percent isobutane and 0.5 percent butadiene

RESULT

Abrading with steel brush yields good reproducibility

Ultrasound causes increase in emission rate for 6061 Al alloy; the higher the ultrasound intensity (20-45 W/cm^2), the higher is the emission rate

Without light stimulation, emission from pure Al is at the background level; a very small increase of emission is observed during the application of ultrasound (intensity not greater than 45 W/cm^2). 2024 Al alloy shows no emission intensity above the background level.

6061 Al alloy has to be heated to 320° K to produce the same emission intensity as produced at 297° K with the application of ultrasound of 45 W/cm^2 intensity.

EFFECT OF TEMPERATURE AND AIR HUMIDITY ON THE PHOTOSTIMULATED EXOELECTRON EMISSION FROM OXIDE FILMS ON ALUMINUM

T. Lewowski

Journal of Applied Physics, Vol 33, 1962, pp 2393-2394

MATERIAL

Al

SPECIMEN PREPARATION

EXCITING CONDITION

Abrading

(6 v, 20 w) tungsten bulb

DETECTION EQUIPMENT

Open Geiger counter operating at atmospheric pressure

Both counter and specimen in a closed chamber

RESULT

Emission intensity is maximum while the temperature of the abraded specimen is increased to about 400° C.

If the specimen at 400° C falls rapidly to room temperature, the emission intensity decreases, passes through a minimum, afterwards a maximum, and decays again.

The rate of this decay varies with air humidity; it is much faster in the moist than in the dry atmosphere.

Emission is associated with the presence of an oxide layer. Because of the very higroscopic properties of alumina, the electrical character of the oxide layer might be changed with the humidity of air.

DIE ELEKTRONENEMISSION BEARBEITETER METALLOBERFLÄCHEN

J. Lohff

Die Naturwissenschaften, Vol 44, 1957, pp 228

MATERIAL

Al

SPECIMEN PREPARATION

EXCITING CONDITION

Abrading with steel brush at 5×10^{-4} torr oxygen pressure

DETECTION EQUIPMENT

Electron multiplier

RESULT

When the system is suddenly evacuated after the emission decay proceeds for a period, the emission drops rapidly. Later when the original oxygen pressure is restored, the emission rises to a level substantially lower than the level at the time of evacuation.

The processes, such as changes of defect structure in the oxide layer and the metal, taking place in the specimen during evacuation are thought to affect the subsequent emission rate.

DIE ELEKTRONENEMISSION BEI DER OXYDATION MECHANISCH BEARBEITETER METALLOBERFLÄCHEN

J. Lohff

Zeitschrift für Physik, Vol 146, 1956, pp 436-446

MATERIAL

Ag, Al, Au, Be, Cu, Fe, Mg, Pb, Pt, and Zn

SPECIMEN PREPARATION

EXCITING CONDITION

Abrading with steel brush at 22° C in oxygen pressure of 1×10^{-4} to 7×10^{-6} torr

DETECTION EQUIPMENT

Electron multiplier

RESULT

In the case of abraded Al, emission intensity at oxygen pressure of 10^{-4} torr is much greater than that at oxygen pressure of 7×10^{-6} torr.

Emission current from abraded Be, Mg, Pb, and Zn also depends on oxygen pressure.

Less than 2 electrons/cm^2-sec emit from Ag, Au, Cu, Fe, and Pt at 10^{-5} and 5×10^{-4} torr 10 seconds after abrading.

In the case of abraded Zn, the emission reaches a maximum at various pressures before decay sets in; the higher the oxygen pressure, the higher is the emission peak and the shorter is the time to reach that peak.

Emission intensity of Zn at 22° C is greater than that at 100° C at various pressures; the same trend is noted for Al and Pb.

DIE ELEKTRONENEMISSION BEI DER PLASTISCHEN VERFORMUNG VON ZINKKRISTALLEN

J. Lohff

Zeitschrift für Physik, Vol 145, 1956, pp 504-507

MATERIAL

99.9 percent Zn

SPECIMEN PREPARATION

3-3.5 mm diameter single crystal

EXCITING CONDITION

Tensile loading to maximum elongation 50 percent of original length at 2×10^{-5} torr or at oxygen pressure 10^{-4} torr

DETECTION EQUIPMENT

Electron multiplier

RESULTS

Emission rate at 2×10^{-5} torr increases with increase of strain; under steady straining, emission rate increases and then decreases with time.

There is practically no difference in emission for a given amount of straining (0.5 percent) at 2×10^{-5} torr or oxygen pressure 10^{-4} torr, suggesting that emission by tensile straining is independent of oxygen.

DIE ENERGIEVERTEILUNG DER ELEKTRONENEMISSION MECHANISCH BEARBEITETER METALLOBERFLÄCHEN

J. Lohff

Zeitschift für Naturforschung, Vol 12a, 1957, pp 267-268

MATERIAL

Al, Li, Mg, and Zn

SPECIMEN PREPARATION

Specimen surface area = 0.4 cm^2

EXCITING CONDITION

Abrading with steel brush at 1-5 x 10^{-4} torr oxygen pressure or 5-7 x 10^{-6} torr residual gas pressure

DETECTION EQUIPMENT

Electron multiplier

RESULT

The average energy of exoelelectron emission is determined by the number of electrons per second versus grid potential curve. The average energy of emission for Al and Zn is independent of oxygen pressure and is 0.20 and 0.15 ev, respectively.

The average energy of emission for Li and Mg is slightly dependent upon pressure, but the value is in the neighborhood of 0.2 ev.

A POSSIBLE ORIGIN OF EXOELECTRON EMISSION IN PLASTICALLY DEFORMED METALS

A. H. Meleka and W. Barr

Nature, Vol 187, 1960, pp 232-233

MATERIAL

High purity Zn

SPECIMEN PREPARATION

Single crystal rod

Electropolished and thoroughly cleaned

EXCITING CONDITION

Static tensile straining

DETECTION EQUIPMENT

Kodak AR 10 stripping emulsion

Exposure time = 1 hour if commencing exposure within a few minutes of straining

RESULT

Black lines on emulsion correspond exactly to slip lines on the crystal surface.

Rows of individual spots resemble dislocation etch pits along slip lines.

It is suggested that the centers of emission are the points where dislocations terminate at the surface of the crystal.

THE TIME REQUIRED TO REACH MAXIMUM ELECTRON EMISSION FROM DEFORMED METALS

R. I. Mints and V. S. Kortov

Russian Metallurgy and Fuels (Mining), No. 2, 1967, pp 90-96

MATERIAL

High purity (99.93 percent) Al, Au, and Cu; Fe-Ni alloy; Fe-Mn alloy; and 1Kh18N8 stainless steel

SPECIMEN PREPARATION

Annealing, grinding, and electropolishing

EXCITING CONDITION

Grinding
Local static loading with a diamond pyramid using 100 g load
Microimpact loading
Cyclic loading

DETECTION EQUIPMENT

Electron multiplier

RESULT

Admission of air into the apparatus changes pressure from 2×10^{-5} to 2×10^{-4} torr, but emission current from ground Au and 1Kh18N8 steel is affected very little.

When air is admitted into the apparatus containing ground Al or Cu, a jump in emission current is noted, the effect on Al being more pronounced.

Emission from ground metal surface is therefore not entirely due to oxidation.

Admission of air during emission decay from locally indented Al surface has no effect on fall of emission, indicating that emission depends on size of the deformed area. This is also true of surfaces deformed by microimpact loading.

For equal amount of microimpact deformation, the time to reach peak emission for Fe-Mn alloy is longer than that for Fe-Ni alloy because high defect mobility in the latter leads to a shorter rise time.

Emission current depends on mobility of vacancy; vacancy mobility for Al is greater than that for Au, so the time reaching peak emission for microimpacted Al surface is shorter than that for the similarly deformed Au surface.

Increase of amount of microimpact deformation generally increases the time reaching peak emission because increasing degree of hardening of surface decreases defect mobility.

During cyclic loading, Al emission intensity increases with number of cycles until microcracks develop. At the moment of microcrack formation, vacancies on the surface flow into the submicrocracks, leading to a decrease in electron emission. Further deformation produces fatigue cracks with a sharp increase in the number of vacancies, which are not dissipated, so there is an increase in electron emission directly prior to fracture.

EXOELECTRONIC EMISSION FROM AUSTENITIC STEELS UNDER ALTERNATING CYCLES OF STRESS

R. I. Mints, V. S. Kortov, V. L. Aleksandrov and V. I. Kryuk

Physics of Metals and Metallography, Vol 26, 1968, pp 681-687

MATERIAL

Austenitic steels 30Kh10G10, 68Kh7N7, 1Kh18AG10, and 1Kh18N8

SPECIMEN PREPARATION

Specimen dimensions: 2 x 5 x 100 mm
Electropolishing in sulphophosphochromic bath

EXCITING CONDITION

Symmetrical bending fatigue at a frequency of 50 cycles/sec

DETECTION EQUIPMENT

Cu-Be electron multiplier operating at 2×10^{-5} torr
Accelerating potential on specimen = -300 v

RESULT

The emission intensity rises with increasing number of cycles, the biggest change in intensity occurring before the elapse of 10^5 cycles. Afterwards, the emission current grows more slowly. There is a tendency to saturation or even reduction at large number of cycles.

The kinetics of exoelectron emission is largely controlled by the applied stress level. The emission rate increases rapidly and its maximum level rises as the stress increases.

The shape of emission curve is explained on the basis of the hypothesis that its intensity is controlled by the number of defects contained in the surface layer of metal and its kinetics by their mobility.

Under the same conditions of stress, alloys 30Kh10G10 and 68Kh7N7, which undergo the greatest strengthening by fatigue deformation, have less emission than alloys 1Kh18N8 and 1Kh18AG10. The considerable strengthening of the former, which is due to phase and structure transformations, has the effect of pinning the defects generated, restricting the total number of active emission centers at the surface, and reducing their size.

There is an interrelation between the dissipation of mechanical energy and exoelectron emission. The internal friction of 35KhGF steel in temper-embrittled state is higher than in ductile state, and the emission intensity in fatigue process for the temper-embrittled state is correspondingly lower.

Exoelectron emission can be regarded as an electrical effect which is the result of the storing of deformation energy. Large dissipation of energy, indicated by internal friction measurement, reduces the fraction of stored energy and lowers the intensity of emission.

EXOELECTRON EMISSION FROM A MECHANICALLY TREATED SILICON SURFACE

R. I. Mints, V. S. Kortov, V. I. Kryuk, A. I. Tatarenkov, and I. A. Petrushkova

Soviet Physics - Semiconductors, Vol 1, 1968, pp 1535-1537

MATERIAL

n-type and p-type Si single crystals

SPECIMEN PREPARATION

30 mm diameter x 0.3 mm thickness cut along (111) plane
Washing specimen in acetone and alcohol after grinding
Exposing ground and washed specimens in air at room temperature for 1 month

EXCITING CONDITION

Grinding with green SiC powder or white electrocorundum which was elutriated in distilled water
Grinding with the same abrasive powders as above and additionally treating the specimens with SAM3 and SAM1 powders deposited on a cloth
Electric current pluse (150 v for 100 μ sec) as the stimulating agent
Negative potential at the specimen surface

DETECTION EQUIPMENT

Electron multiplier at 2 x 10^{-5} torr
Accelerating potential at the grid above the specimen = 250 v

RESULT

No emission occurs at room temperature or 250° C if no current passes through the specimen.
With excitation by current pulse, emission from the surface of p-type Si is roughly two orders of magnitude weaker than emission from n-type Si at room temperature.
All the n-type Si specimens after decay of emission exhibit exoemission peaks when the temperature is increased; the nature of the exoemission depends on the method of surface treatment with various abrasive powders.
Emission is observed if a specimen is excited with a current pulse before it is heated again.
However, the thermally stimulated emission after the passage of a current pulse is not observed when the direction of the exciting current is reversed in the case of n-type Si, for any polarity of the exciting voltage in p-type Si, and in specimens in which the surface layer disturbed by grinding with abrasive powders is removed by etching.

EXOEMISSION FROM ABRADED AND ETCHED ALUMINUM

R. K. Mueller and K. Pontinen

Journal of Applied Physics, Vol 35, 1964, pp 1500-1502

MATERIAL

99.4 percent Al and 2024 Al alloy

SPECIMEN PREPARATION

Annealing

Etched for several minutes in 1 percent HF and carefully washed and dried

EXCITING CONDITION

Abrading with No. 600 emery paper

Successive removal of surface layers by etching with 1/2 or 1 percent HF

Illumination with a fluorescent lamp

DETECTION EQUIPMENT

Geiger-Müller counter containing 93 percent argon and 7 percent ethyl alcohol, operating at 100 torr and 850 v

Specimen at -6 v with respect to the grounded tube cathode

RESULT

Both Al and 2024 alloy yield similar result, suggesting that impurities have no effect on emission.

A 1-second etch in 1 percent HF is sufficient to recover 90 percent of original emission activity.

Compared with a freshly abraded specimen, an abraded specimen oxidized in air for 6 days exhibits a wider maximum of recovered activity, probably due to the added etching time necessary to break up and remove the oxide layer.

Pattern of emission decay with total time of etch for a freshly abraded specimen is similar to that for an abraded specimen after it is stored 8 days in the counter gas mixture.

Emission from a freshly abraded specimen and an abraded specimen stored in air for several days and then etched for 4 seconds in 1 percent HF decays with the same time constant.

Since aging does not affect significantly decay, it is unlikely that the transport of imperfections to the active surface is of importance for emission.

EFFECTS OF TEMPERATURE ON THE EXOEMISSION OF ELECTRONS FROM ABRADED ALUMINUM SURFACES

W. T. Pimbley and E. E. Francis

Journal of Applied Physics, Vol 32, 1961, pp 1729-1733

MATERIAL

99.999 percent Al

SPECIMEN PREPARATION

26 gage thick

Standard cleaning technique without effort to restrict oxide formation

EXCITING CONDITION

Abrasion by four to five passes using 400 or 600 grade SiC paper

Zirconium arc source for illumination at low excitation or at lower temperature (temperature range = 9.9 to 44.4° C)

DETECTION EQUIPMENT

Windlowless, open-end Geiger counter containing 98.7 percent He and 1.3 percent butane

Specimen at a negative potential of 50 v

RESULT

No count above the background count can be obtained from the abraded paper itself nor from the freshly clean, unabraded specimen.

The emission decay curve is composed of two exponential decays according to the expression $I = A \exp(-k_1 t) + B \exp(-k_2 t)$ where I is the emission intensity, t is the time, k_1 and k_2 are decay constants, and A and B are temperature-dependent constants.

The decay constant is related to the temperature according to $k = F \cdot \exp(-E/RT)$ where E, R, T, and F are the activation energy, the universal gas constant, the absolute temperature, and constant, respectively. Both the first and second decay constants have the same activation energy (about 5.6 kcal/mol).

Vacancies are created by abrasion; emission depends on diffusion of vacancies in metal; emission intensity increases with increase of temperature because of increasing diffusion constant.

EXOELECTRON EMISSION FROM ABRADED METAL SURFACES AT HIGH AND ULTRAHIGH VACUUMS

J. A. Ramsey

Journal of Applied Physics, Vol 37, 1966, pp 452-453

MATERIAL

Spectroscopically pure Al and pure Zn

SPECIMEN PREPARATION

EXCITING CONDITION

Abrading with stainless steel brush in vacuo (10^{-6} to 10^{-9} torr) for 2-3 seconds

Lamp

DETECTION EQUIPMENT

Be-Cu particle multiplier and electrometer

RESULT

There is a slight decrease in the intensity of peak emission at lower pressure (0.7 - 50 x 10^{-6} torr); maximum emission current = 10^{-15} amp.

No emission is detected at 10^{-8} torr; subsequent increase of electrometer sensitivity and switching on and off of illumination yield a current about 2.5 x 10^{-18} amp.

At 2.7 x 10^{-9} torr, emission current is about 0.3 to 0.5 x 10^{-18} amp.

Time reaching the emission peak is 10^{3} to 10^{4} x 10^{-18} times greater than the time required to form a monolayer on clean metal surface in the case of Zn and is 10 to 100 times greater in the case of Al.

THE EMISSION OF ELECTRONS FROM ALUMINUM ABRADED IN ATMOSPHERES OF AIR, OXYGEN, NITROGEN, AND WATER VAPOR

J. A. Ramsey

Surface Science, Vol 8, 1967, pp 313-322

MATERIAL
Pure Al

SPECIMEN PREPARATION

EXCITING CONDITION
Abrading with stainless steel brush in air, spectroscopically pure oxygen, spectroscopically pure nitrogen, and water vapor bled at pressure from 10^{-5} to 10^{-8} torr into a bakeable glass ultrahigh vacuum system. Illumination wavelength longer than 3450 Å.

DETECTION EQUIPMENT
Be-Cu particle multiplier and electrometer
Phillip 56002 omegatron for gas analysis

RESULT
Emission is negligible below 10^{-8} torr.
Exposure to air pressure 10^{-5} to 10^{-8} torr: t_{in} (incubation time) increases with decrease of pressure, t_m (time to peak emission) increases with decrease of pressure, and i_m (emission current peak) decreases with decrease of pressure.
Exposure to oxygen pressure 10^{-4} to 10^{-8} torr: Change of t_{in} is similar to that for the exposure to air; change of t_m is about one-fourth of that for the exposure to air; i_m is comparatively independent of pressure and is lower than i_m in air.
Exposure to nitrogen pressure 10^{-5} to 10^{-8} torr: Changes of t_{in} and t_m are longer than those for exposure to air and oxygen; i_m is comparable with i_m for exposure in oxygen.
Exposure to water vapor 10^{-5} to 10^{-8} torr: The initial stage of emission current vs time curve at 4×10^{-6} and 3×10^{-7} torr is comparable respectively to the initial stage of the same curve at 10^{-5} and 10^{-6} torr in air.
Time at onset of emission decay in water vapor becomes shorter when oxygen is admitted to the apparatus; the higher the pressure of admitted oxygen, the shorter is the time at onset of emission decay.
Initial growth stage of emission is thus due to the adsorption of water vapor; the subsequent decay is associated with the establishment of an oxide film.

SENSITIZED PHOTOELECTRIC EMISSION DURING OXIDATION OF ALUMINUM

J. A. Ramsey and G. F. J. Garlick

British Journal of Applied Physics, Vol 15, 1964, pp 1353-1360

MATERIAL

Pure Al and pure Zn

SPECIMEN PREPARATION

1 cm diameter

Degreasing before test

EXCITING CONDITION

Abrading with stainless steel brush at one atmosphere and 0.28×10^{-3} to 10^{-5} torr and at a temperature range from 195° to 500° K

Visible ultraviolet light (wavelength = 3000-4000 Å)

DETECTION EQUIPMENT

Ag-Mg electron multiplier

RESULT

For Al:

Abrasion at room temperature and below and emission at 0.28×10^{-3} and 10^{-5} torr: At 195° K and below, the emission rises rapidly after abrasion but quickly reaches a peak which is followed by a rapid decay; the maximum emission is always much smaller than that at room temperature and is inhibited by some thermal activation barrier; rate of emission at 195° K is very little dependent on pressure between 10^{-3} and 10^{-5} torr.

Abrasion between 343° and 473° K at 0.28×10^{-3} and 10^{-5} torr: The plateau reached after initial rise of emission is prolonged especially at low pressures. Decay is more prominent as the pressure is increased; at higher temperatures, the initial rise is much slower but is markedly pressure dependent.

For Zn:

The pattern of behavior is similar to that of Al, but the effects characteristic of elevated temperatures in Al are observed at room temperature for Zn.

A tentative mode suggests that oxygen vacancies of intenstitial metal atoms in the developing metal oxide layer provide electron levels above the Fermi level of the metal, from which they are ejected by photon absorption.

ELEKTRONENNACHEMISSION UND PHOTOEMISSION VON ALUMINIUMOBERFLÄCHEN

A. Scharmann and G. Seibert

Zeitschrift für Physik, Vol 183, 1965, pp 249-364

MATERIAL

Al

SPECIMEN PREPARATION

EXCITING CONDITION

Milling

5 x 10^{11} Sr-90 β particles

X-ray (10^{-5} R, 29 kv)

Electron bombardment (10^{15} electrons with 3.5 to 4 kev/5 mm^2)

Mercury vapor lamp

DETECTION EQUIPMENT

17-stage electron multipler operating at 10^{-9} torr

RESULT

There is no emission from milled Al surface at 8 x 10^{-9} torr is darkness even if the surface is further bombarded by electrons; there is also no emission in darkness when the Al surface is irradiated with X-ray or intense ultraviolet light from a mercury vapor lamp.

A weak emission in darkness is observed from milled Al surface at 10^{-5} torr. Upon heating, emission peaks occur at 10^{-5} torr in definite temperature ranges whether the Al surface is milled, irradiated by β particles or X-ray, or bombarded by electrons; either visible light or ultraviolet light has no effect on thermoemission.

There is emission from milled Al surface at 10^{-9} torr when it is illuminated by light having 3540 Å wavelength; the emission increases with time, probably attributable to gradual adsorption of gas, which through the creation of a dipole layer, lowers the work function of Al.

Emission, however, decays with time at 10^{-5} torr; emission intensity of milled Al surface decreases with storage time in darkness at 10^{-5} torr; presence or absence of light has no effect on decay of emission.

EXOEMISSION OF ELECTRONS WITHOUT PHOTOSTIMULATION

C. Simoi, I. Hrianca, and P. Crăciun

Physica Status Solidi, Vol 29, 1968, pp 761-766

MATERIAL

Al

SPECIMEN PREPARATION

Specimen dimension: $3 \times 2\ cm^2$

EXCITING CONDITION

Scratching by brush for 30 seconds

Emission under daylight without photostimulation

DETECTION EQUIPMENT

Windowless Geiger-Müller counter filled with argon and butane

Distance between counter and specimen = 1.5 cm

Specimen potential = -250 v

RESULT

After repeated scratching and counting operations on the same specimen, the initial number of counts decreases from 1,370 to 23 electrons per second.

The decay curve is composed of three distinct exponentials:

$$\frac{dN}{dt} = A_1 \exp(-\lambda_1 t) + A_2 \exp(-\lambda_2 t) + A_3 \exp(-\lambda_3 t)$$

where N is number of counts per second, t is second, A_1, A_2, and A_3 are the components of initial counts, and λ_1, λ_2, and λ_3 are decay constants of the components. λ_i may also be the probability for the emission of an electron per unit time at a local condition specific for component i. This probability is related to the energy E_i at the mentioned conditions by the equation $\lambda_i = C \exp(-E_i/kT)$ where k is Boltzmann constant, T is the absolute temperature, and C is a constant.

Impurities and defects in the lattice of metals produce relatively high local energy levels having a reduced work of function of electrons. There is a probability of emission due to internal excitation in the absence of photostimulation.

ELECTRON EMISSION FROM PLASTICALLY STRAINED ALUMINUM
W. D. von Voss and F. R. Brotzen
Journal of Applied Physics, Vol 30, 1959, pp 1639-1645

MATERIAL
99.993 percent Al and 1100-0 Al Alloy

SPECIMEN PREPARATION
16 x 2 x 0.063 inches
Annealing in air at 400° C for 2 hours

EXCITING CONDITION
Continuous tensile loading at 0.063, 0.10, and 0.159 in./min and irradiation with natural light
Tensile loading in steps (loading rate = 0.032 in./min), allowing about 10^3 sec between steps for the decay of emission and irradiation with mercury vapor lamp (with filter to eliminate wavelengths shorter than 3,000 Å)

DETECTION EQUIPMENT
Geiger-Müller flow counter containing 1 percent methane and 99 percent He and operating at about 900 v

RESULT
There is only little emission, difficult to detect above the background level, if the specimen is strained in complete darkness.
Emission starts at about 2 percent strain and increases with further straining; emission rate is higher at higher loading rate.
Emission behavior of pure Al (99.993 percent purity) is about the same as that of 1100-0 Al Alloy.
After plastic straining has stopped, the emission may continue to rise for a while before it begins to decay. This effect may be due to the draining of vacancies from the interior to the metal surface.
Emission rate at end of straining in each step (2 percent strain per step except the first step at 7 percent strain) is higher than that at end of the preceding step. This indicates that the state of deformation strongly affects the emission.

AN INVESTIGATION OF EXOELECTRON EMISSION FROM VARIOUS MATERIALS USING ABRASION AND ULTRASONIC TECHNIQUES

R. A. Williams
RM 630.328-04, Naval Ordnance Systems, Navy Department, 1966

MATERIAL

6061 Al alloy, brass, Cu, stainless steel, cold rolled steel, Nb, Ni, and Pb

SPECIMEN PREPARATION

1-inch-diameter bar having plane cross-sectional surface or cross-hatched, cross-sectional surface (ratio of plane area to cross hatched area = 4.2:1)

EXCITING CONDITION

Filing, grinding with steel brush, or sanding with No. 80 Al_2O_3 paper
Standard cleaning technique without further preparation to restrict or eliminate surface film or oxide films
Ultrasonic irradiation using piezoelectric transducer with a resonant frequency about 19 KHz
28-volt lamp

DETECTION EQUIPMENT

Proportional counter containing 90 percent argon and 10 percent methane
Anode voltage = 1,700 volts

RESULT

There is no emission above the background level from Cu, Nb, Ni, and cold rolled steel; some counts above the background are noted from brass but emission decays very rapidly; emission intensity of Pb is greater than emission intensity of brass probably due to presence of radioactive isotopes in Pb.
The best emission producer is 6061 Al alloy; the emission rate by sanding with Al_2O_3 paper is greater than that by filing, which in turn is greater than the emission rate by grinding with steel brush.
The greater the active surface area (the plane surface), the greater is the emission.
Emission increases at elevated temperature.
Ultrasonic irradiation (intensity = 5 W/cm^2) increases emission intensity.

UNTERSUCHUNGEN ÜBER EXOELEKTRONEN AN METALLISCHEN AUFDAMPFSCHICHTEN UND EINIGEN NICHTMETALLISCHEN OBERFLÄCHEN

J. Wüstenhagen

Zeitschrift fur Naturforschung, Vol 14a, 1959, pp 634-641

MATERIAL

Al

SPECIMEN PREPARATION

Evaporated film having 1.2 cm^2 surface area deposited on various substrates (bright Pt, polished Al, and scratched Al)

Film thickness = 5 - 300 Å

EXCITING CONDITION

Admission of oxygen at 10^{-5} to 10^{-7} torr

DETECTION EQUIPMENT

17-stage electron multiplier

Potential at specimen = -250 v

RESULT

At 2×10^{-5} torr, the emission rate increases with surface roughness of the substrate and increases with decreasing rate of deposition, probably because the finer Al grains in the film which form at lower deposition rates contain more imperfections to react faster with oxygen.

There is no emission at oxygen pressure of 4×10^{-7} torr, but emission rises to 500 counts/second when the pressure changes to 2×10^{-5} torr.

Emission is also noted from Be, Li, and Mg but not from Cu and Fe.

The metal layer-adsorbed oxygen system does not show any spontaneous emission; oxygen molecules must fall on the metal surface to maintain emission.

No emission is observed from Al film at spectroscopically pure nitrogen pressure of 5×10^{-5} torr.

EFFECT OF TEMPERATURE ON PHOTO-EXOEMISSION
J. F. Young and D. J. Williams
Journal of Applied Physics, Vol 35, 1964, pp 2279-2282

MATERIAL
Commercial purity Al

SPECIMEN PREPARATION

EXCITING CONDITION
Abrading with 400 grade SiC paper
Ultraviolet lamp as a light source
Chemical etch using a mixture of chromic acid and sulphuric acid at 60° C

DETECTION EQUIPMENT
Geiger counter with a glass window to permit illumination
Counter gases: 98.7 percent He and 1.3 percent isobutane
No necessity to bias the specimen negative due to the use of an anode loop, resulting in a higher field strength at the specimen

RESULT
There is no emission above the background in the absence of illumination.
Upon heating, the emission intensity vs time curve for abraded surface is the same as that obtained for chemically etched surface.
The count rate at room temperature for an unabraded specimen is no greater than background; however, emission occurs as the temperature increases. The peak emission rate is shifted to a higher temperature than the abraded specimen.
On lowering the temperature during emission, behavior becomes extremely anomalous. The emission rate as a function of temperature depends on past history in the counter, and decrease in temperature can result in an increase in emission rate.
The anomalous results cannot be explained by a vacancy mechanism or by electron traps.
Emission decay appears to depend on adsorption of counter gas. Photo-exoemission can be decreased by adsorption, and its intensity can be increased by desorption.

APPENDIX II

ELECTRON ENERGY SPECTROSCOPY

APPENDIX II

ELECTRON ENERGY SPECTROSCOPY

Estimation of the electron energy is essential for a better understanding of the mechanism of exeoelectron emission. The type of spectrometer to be considered is based on the cylindrical, electrostatic mirror design principle because the accelerating potential does not involve the specimen itself.

The simplest electrostatic analyzer is the parallel-plate electrostatic mirror. However, in past years probably the most popular electrostatic analyzer has been the 127-degree, cylindrical deflection system (Pichanick, 1967). In more recent years, both of these analyzers have been surpassed in performance by the concentric spherical deflection system (Purcell, 1938). More recently, however, investigators have realized that even the concentric spherical system is surpassed in performance by the cylindrical electrostatic mirror (Zashkvara et al, 1966; Sar-el, 1967, Hafner et al, 1968).

The geometry of the cylindrical mirror system is shown in figure A-1. This geometry was used more than 10 years ago by Blauth (1957), but only recently, Zashkvara has shown that it gave the fortunate effect of second-order focusing when $\theta_o = 42.3°$ and when

$$\frac{E_o}{eV} = \frac{1.3}{\ln\left(r_2/r_1\right)}$$

where E_o is the particle kinetic energy and V is the potential difference between the two cylinders. Refocusing occurs at $L_o = 6.1\ r_1$.

The resolution of this device, R_o, for a point source is given simply by

$$R_o = \frac{\Delta E}{E} = 21T^3$$

where T is the percent of solid angle transmission through the slit system. In this case we have

$$T = \sin \theta_o \cdot \alpha$$

where α is the semiangular operative shown in figure A-1a. Due to the second-order focusing and the 2π entrance slit, this spectrometer has very good energy resolution with a relatively large-entrance solid angle.

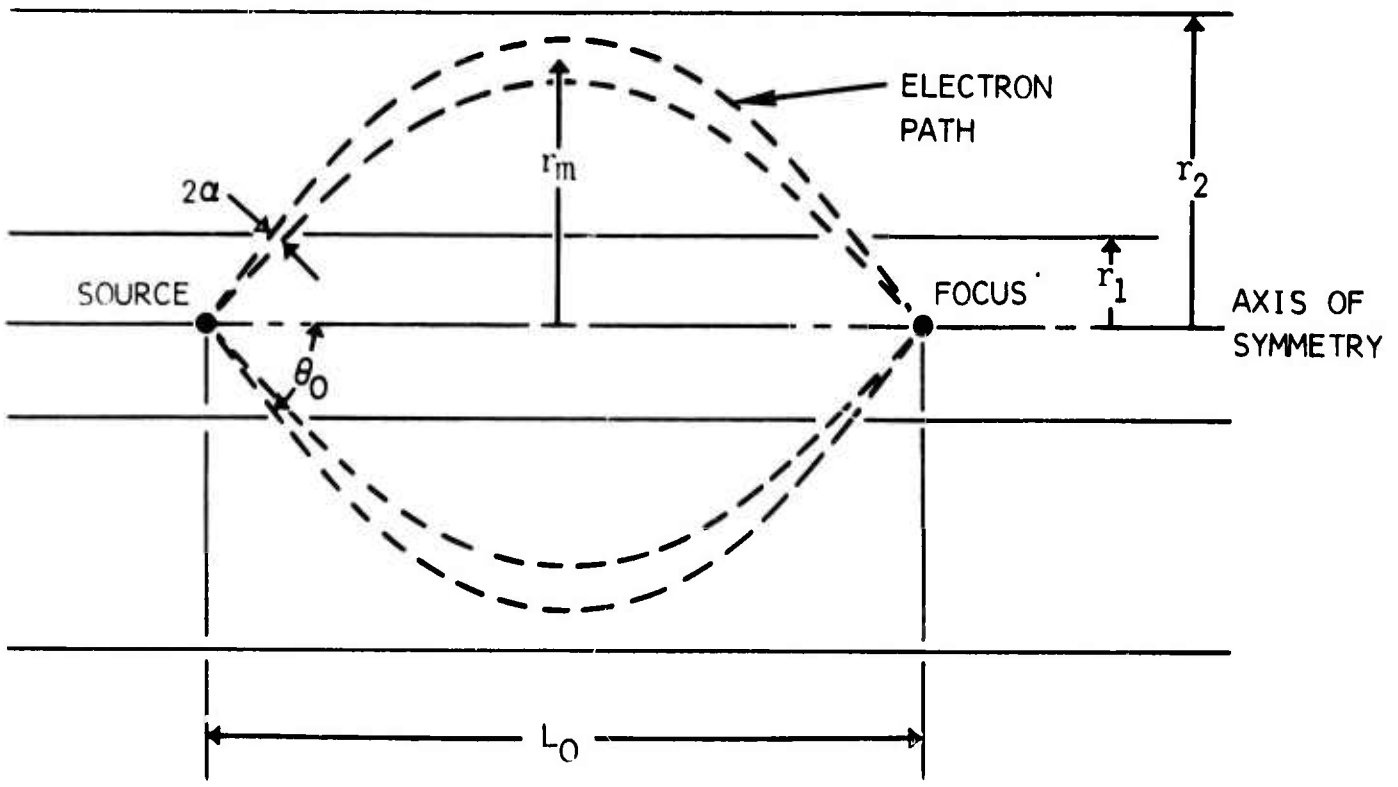

A. SPECTROMETER GEOMETRY

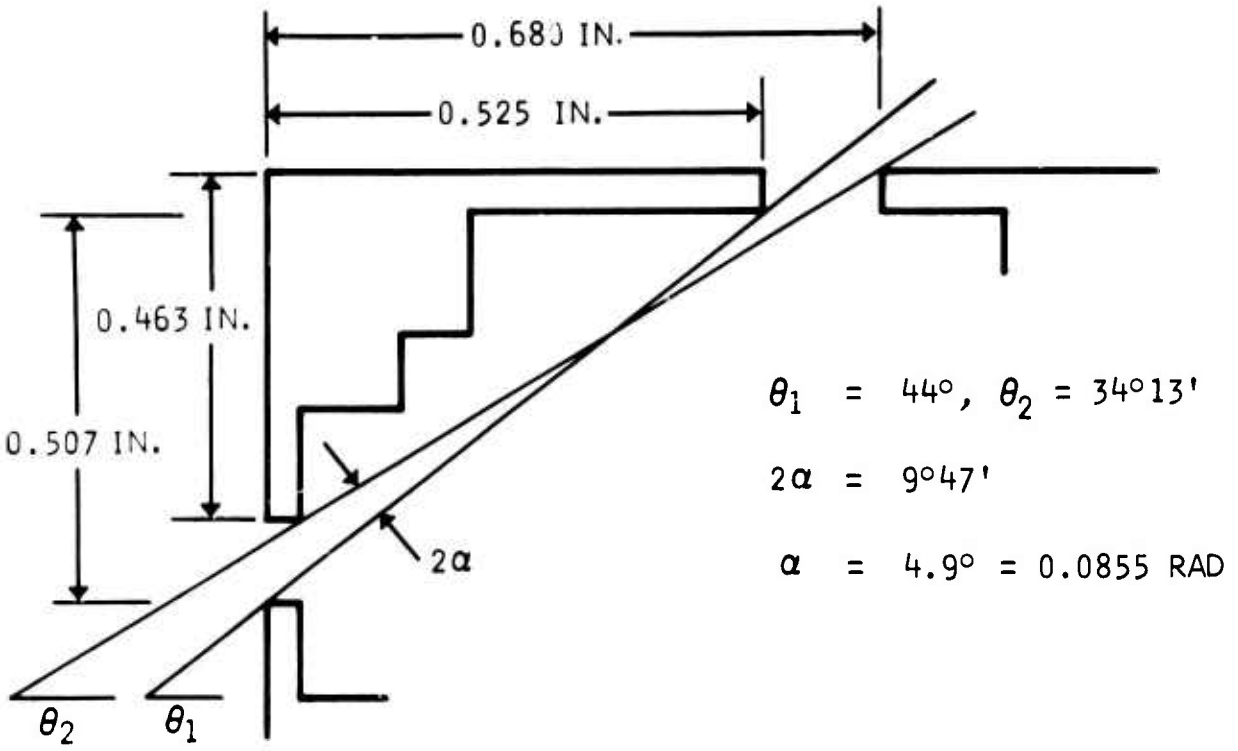

B. SPECTROMETER DIMENSIONS

Figure A1. Electron Energy Spectrometer

The analysis giving the results of the previous section assumes a purely radial electrostatic field between two cylinders. This cannot be obtained in practice by using infinite cylinders or guard rings. Because of large samples to be used at the source and of large detectors near the focus, the spectrometer must terminate at these two points. Metal rings have been mounted on the end support insulators which separate the two cylinders. The proper potentials are placed on these rings to keep the field radial in the region of electron orbits. The potential between concentric, infinite cylinders is given by

$$\varphi - \varphi_1 = A \ln\left(\frac{r}{r_1}\right)$$

where φ is the potential of the inner cylinder which has a radius γ_1, and A is a proportionality constant. The device built has

$$r_1 = 0.50000 \text{ in.} \qquad r_2 = 1.4325 \text{ in.}$$

Thus, if we install four rings between the cylinders at radii such that potential jumps from the inner cylinder to the wires and to the outer cylinder can be in constant increments, we have for the radii:

$$r_{i_a} = 0.6170 \text{ in.} \qquad r_{i_c} = 0.9395 \text{ in.}$$

$$r_{i_b} = 0.7615 \text{ in.} \qquad r_{i_d} = 1.1595 \text{ in.}$$

The design for constant potential jumps simplifies the construction of a potential divider for maintaining the proper potentials.

It is expected that the spectrometer will be exposed repeatedly to air at atmospheric pressure. Also, it is expected that the exoelectron flux will be sufficiently low that individual electrons must be counted. This presents a problem since the usual multistage electron multiplers have dynode surfaces which deteriorate in the presence of air. The more durable dynodes are of beryllium-copper, but even these are adversely affected. Thus the Bendix Channeltron electron multipler is chosen for a detector (Evans, 1965). Although these are sensitive to diffusion pump oils, they are not affected seriously by air. The gain of the Channeltron is about 5×10^7 with the application of about 3,000 volts dc. At this voltage, the output current pulses are in the order of 20 nanoseconds wide.

The energy of the electrons passed by the spectrometer is given by

$$E_o = 1.3 \text{ eV}/\ln\left(\frac{r_2}{r_1}\right)$$

Thus, since r_2 = 1.4325 in. and r_1 = 0.50000 in. we have

$$E_o = 1.23 \cdot eV$$

where V is the potential difference between the cylinders.

The resolution is given approximately by

$$R_o = \frac{\Delta E}{E} = 21 \left(\sin \theta_o \cdot \alpha\right)^3$$

The dimensions of the spectrometer as it is now constructed are shown in figure A-1b.

The spectrometer should be designed to work at θ_o = 42°18.5' where we have $\sin \theta_o$ = 0.673. Thus, resolution is given by

$$R_o = \frac{\Delta E}{E} = 21 \ (0.673 \times .0855)^3$$

$$= 0.004$$

This resolution is achieved with a transmission of

$$T = 0.058$$

This figure neglects the obstruction of the three spacing sleeves.

The instrument constructed consists essentially of two concentric cylinders mounted coaxially and insulated from each other, as shown in figures A-2 and A-3. It will be mounted inside the vacuum glass chamber, facing the specimen under test, together with the amplifier, pulse spreader, and low-impedance-output emitter-follower. A pulse spreader is required to widen the approximately 20-nanosecond pulse width expected from the Channeltron multipler to approximately 1 microsecond to allow standard pulse counters to be used. The emitter-follower permits the use of a long lead between it and the pulse counter. The bias voltage applied to the coaxial cylinders and end guard rings permits the selection of specific energy electrons to pass to the Channeltron electron multipler.

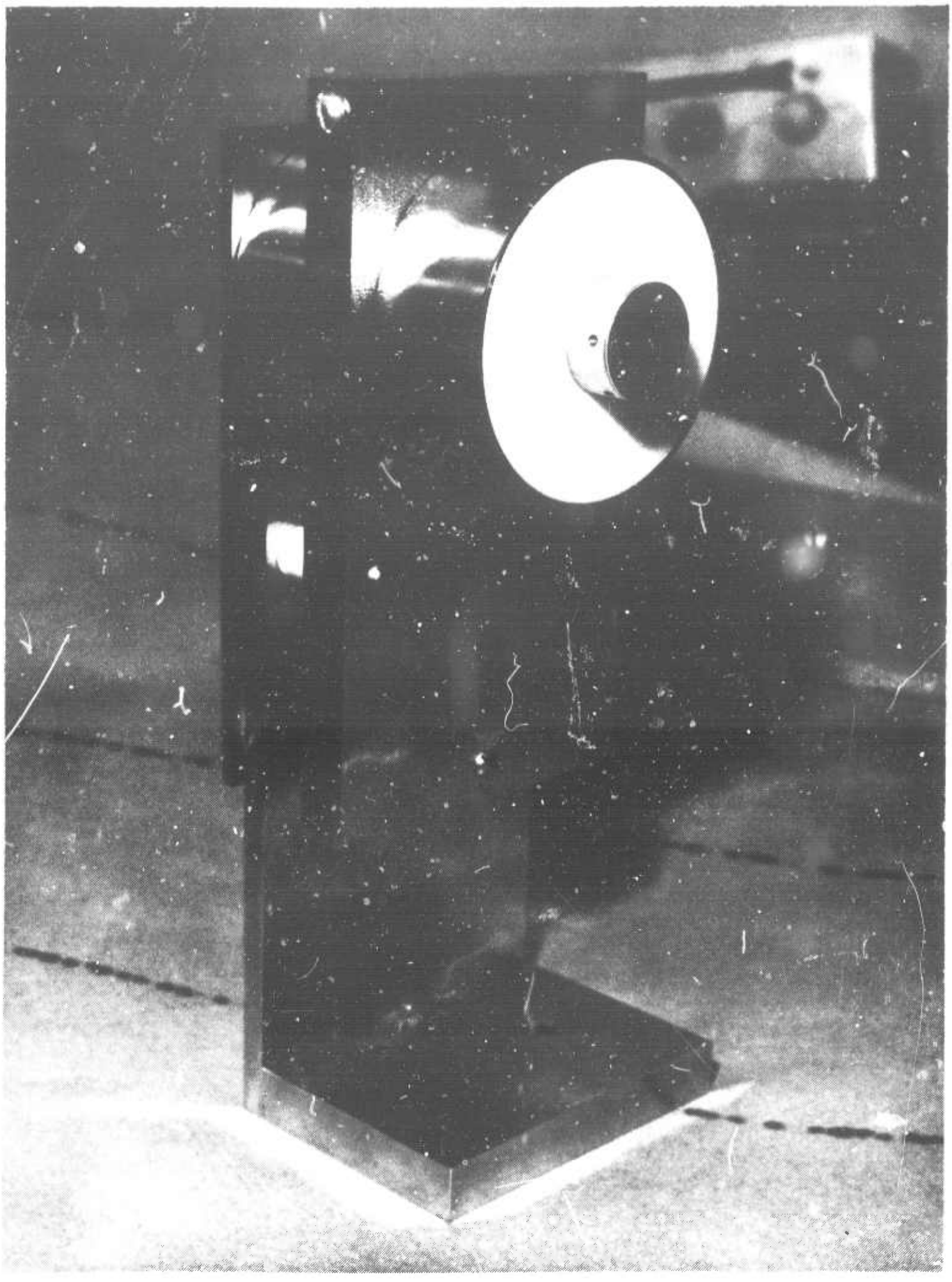

Figure A2. Spectrometer Photograph, Assembled View From Specimen Side

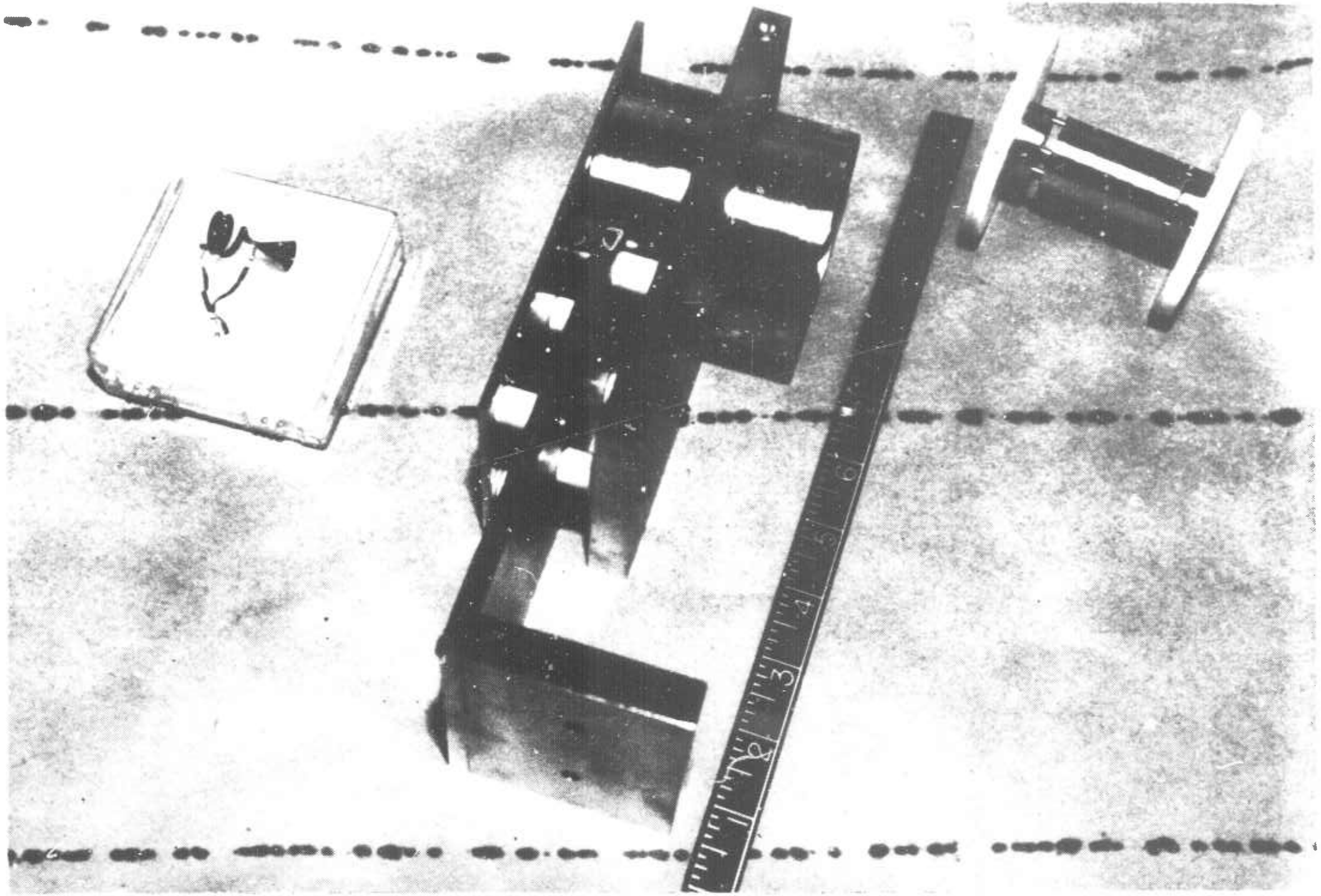

Figure A3. Spectrometer Photograph, Exploded View of Concentric Cylinders and Channeltron Electron Multiplier

BIBLIOGRAPHY

Blauth, E., "Zur Energieverteilung der von Protonen in Gases ausgelösten Sekundärelektronen," Z Physik, Vol 147. 1957, p 228

Evans, D. S., "Low-Energy Charged-Particle Detection Using the Continuous - Channel Electron Multipler," Rev Sci Instr, Vol 36, 1965, p 375

Hafner, H., Simpson, J. A., and Kuyatt, C. E., "Comparison of the Spherical Detector and the Cylindrical Mirror Analyzers," Rev Sci Instr, Vol 39, 1968 p 33

Pichanick, F. M. J., "Ion Spectrometers," Methods of Experimental Physics, Vol 4, Part A, edited by V. W. Hughs and H. L. Schulz, Academic Press, New York, 1967, p 360

Purcell, G. M., "The Focusing of Charged Particles by Spherical Condenser," Phys Rev, Vol 54, 1938, p 818

Sar-el, H. Z., "Cylindrical Capacitor as an Analyzer - I. Nonrealistic Part," Rev Sci Instr, Vol 38, 1967, p 1210

Zashkvara, V. V., Korsunskii, M. I., and Kosmachev, O. S., "Focusing Properties of an Electrostatic Mirror With Cylindrical Field, Soviet Physics - Tech Phys Vol 11, 1966, p 96

BIBLIOGRAPHY

BIBLIOGRAPHY

Andreev, L. A., and Paligé, Ya., "Change of the Electron Work Function of Molybdenum and Tantalum Upon Cold Deformation Under Ultrahigh Vacuum Conditions," Soviet Physics - Doklady, Vol 8, 1964, p 1003

Andreev, L. A., and Paligé, Ya., "The Effect of Deformation on the Work Function of Monocrystalline Molybdenum Filaments," Soviet Physics - Solid State, Vol 3, 1962, p 2238

Bathow, G., "Über die Energie von Exoelektronen," Naturwiss, Vol 45, 1958, p 381

Benson, R. W., and Associates, "Development of Nondestructive Methods for Determining Residual Stress and Fatigue Damage in Metals," Final Report, Contract No. NAS8-20208, Robert W. Benson and Associates, Inc, 1968

Bogachev, I. N., Mints, R. I., and Kortov, V. S., "Application of the Method of Exoelectron Emission in Metal Science," Metal Science and Heat Treatment, July/August, 1966, p 591

Bohun, A., "Exoelektronenemission von Ionenkristallen," Phys Stat Sol, Vol 3, 1963, p 779

Bohun, A., "L'emission Exoélectronique des Corps Solides," J Physique, Vol 26, 1965, p 149

Brotzen, F. R., "Emission of Exoelectrons from Metallic Materials," Phys Stat Sol, Vol 22, 1967, p 9

Claytor, R. N., Gragg, J. E., and Brotzen, F. R., "Electron Emission From Aluminum After Quenching," J Appl Phys, Vol 37, 1966, p 149

Chuang, K. C., "Application of the Optical Correlation Measurement to Detection of Fatigue Damage," Materials Evaluation, Vol 26, No. 6, 1968, p 116

Conrad, M. A., and Levy, S., "Photoemission From Metal Surfaces Measured With Geiger Counters," Nature, Vol 189, p 887

Dover, W. D., and Jones, W. J. D., "The Initiation of Fatigue Cracks in Copper," Brit J Appl Phys, Vol 18, 1967, p 1257

Feltner, C. E., "Dislocation Arrangements in Aluminum Deformed by Repeated Tensile Stresses," Acta Met., Vol 11, 1963, p 817

Forsyth, P. J. E., "Fatigue Damage and Crack Growth in Aluminum Alloys," Acta Met., Vol 11, 1963, p 703

Gieroszynski, A., and Sujak, B., "Exoelectron Emission in Vacuum in the Absence of Light During Plastic Deformation of Aluminum Thickly Coated With Oxide," Acta Phys Polon, Vol 28, 1965, p 311

Gonser, U., and Martin, Geo., "Möessbauer Spectrometry for the Measurement of Residual Stress in Steel," NR Science Center Memo 1963

Gonser, U., "Möessbauer Effect and Physical Metallurgy," NR Science Center Report SC-PP-68-77, August 1968

Gorshkov, G. A., and Postnikov, V. S., "Changes in Internal Friction of Aluminum, Cadmium, and Copper Produced by Cyclic Deformation," Russian Metallurgy (Metally), No. 1, 1965, p 67

Grosskreutz, J. C., and Benson, D. K., "The Emission of Exoelectrons From Aluminum During Fatigue," NASA CR-57918, 1963

Grosskreutz, J. C., Reimann, W. H., and Wood, W. A., "Correlation of Optical and Electron-Optical Observations in Torsion Fatigue of Brass," Acta Met., Vol 14, 1966, p 1549

Grosskreutz, J. C., and Rollins, F. R., "Research on the Mechanism of Fatigue," WADC TR 59-192, 1959

Grunberg, L., "A Survey of Exoelectron Emission Phenomena," Brit J Appl Phys, Vol 9, 1958, p 85

Grunberg, L., and Wright, K. H. R., "A Study of the Structure of Abraded Metal Surfaces," Proc Roy Soc (London), Series A, Vol 232-233, 1955, p 423

Gushcha, O. I., "Investigation of the Process of Fatigue Destruction of Metals by the Method of Magnetic Hysteresis and Eddy Current Losses," FTD-MT-65-421, 1965

Haxel, O., Houtermans, F. G., and Seeger, K., "Die Elektronenemission von Metalloberflächen als Nachwirkung einer mechanischen Bearbeitung oder Glimmentladung," Z Physik, Vol 130, 1951, p 109

Hanstock, R. F., "Damping Capacity, Strain Hardening, and Fatigue," Proc Phys Soc, Vol 59, 1947, p 275

Hanstock, R. F., "Fatigue Phenomena in High-Strength Aluminum Alloys," J Inst Metals, Vol 83, 1954-55, p 11

Hempel, M., Kochendörfer, A., and Tietze, A., "Untersuchungen über die Exoelektronen-Emission mechanisch beanspruchter Metalle," Arch Eisenhüttenwes, Vol 35, 1964, p 465

Herlescu, T., Bernath, A., and Safta, V., "Contributions a l'Etude Phénoméne de Fatigue par le Mesurage de la Variation des Constants Physico-Mecaniques," Rev Roum Sci Tech Serie Metall, Vol 12, 1967, p 269

Klesnil, M., and Lukáš, P., "Dislocation Arrangement in the Surface Layer of α-Iron Grains During Cyclic Loading," J Iron Steel Inst, Vol 203, 1965, p 1043

Kortov, V. S., and Mints, R. I., "Exoelectronic Emission as a Method of Studying the Deformed Surface of Metals," Physics of Metals and Metallography, Vol 19, 1965, p 72

Krogstad, R. S., and Moss, R. W., "Electron Emission During Metal Fatigue," Proceedings of the Symposium on Physics and Nondestructive Testing, September 28-30, 1965, Dayton, Ohio, p 9

Kryuk, V. I., Mints, R. I., and Kortov, V. S., "Exoemission From Ground Surfaces of Germanium and Silicon," Soviet Physics - Solid State, Vol 8, 1966, p 1295

Ku, T. C., and Pimbley, W. T., "Effect of Temperature on the Emission of Electrons From Abraded Surfaces of Beryllium, Calcium, Aluminum, and Magnesium," J Appl Phys, Vol 32, 1961, p 124

Kusenberger, F. N., Barton, J. R., and Donaldson, W. L., "Nondestructive Evaluation of Metal Fatigue," AFOSR-64-0668, 1964

Kusenberger, F. N., Leonard, B. E., Pasley, R. L., Barton, J. R., and Donaldson, W. L., "Nondestructive Evaluation of Metal Fatigue," AFOSR-66-0648, 1966

Laird, C., and Smith, G. C., "Crack Propagation in High-Stress Fatigue," Phil Mag, Vol 7, 1962, p 847

Lohff, J., "Die Elektronenemission bei der Oxydation mechanisch bearbeiteter Metalloberflächen," Z Physik, 1956, p 436

Lohff, J., "Die Energieverteilung der Elektronenemission mechanisch bearbeiteter Metalloberflächen," Z Naturforsch, Vol 12a, 1957, p 267

Meleka, A. H., and Barr, W., "A Possible Origin of Exoelectron Emission in Plastically Deformed Metals," Nature, Vol 187, 1960, p 232

Mints, R. I., and Kortov, V. S., "The Time Required to Reach Maximum Electron Emission From Deformed Metals," Russian Metallurgy and Fuels (Mining), No. 2, 1967, p 90

Mints, R. I., Kortov, V. S., Aleksandrov, V. L., and Kryuk, V. I., "Exoelectron Emission During Cyclic Loading of Austenitic Steels," Physics of Metals and Metallography, Vol 26, 1968, p 681

Mueller, H. J., "Exoelectron Emission and Related Electron Emissions," Research Report 1704-RR, U.S. Army Engineer Research and Development Lab, 1961

Mueller, R. K., and Pontinen, K., "Exoemission From Abraded and Etched Aluminum," J Appl Phys, Vol 35, 1964, p 1500

Nair, K. D., and May, I. Le, "Mechanisms of Fatigue Damage in Face-Centered Cubic Metals," Nature, Vol 217, 1968, p 634

Pimbley, W. T. and Francis, E. E., "Effect of Temperature on the Exoemission of Electrons from Abraded Aluminum Surfaces," J Appl Phys, Vol 32, 1961, p 1729

Ramsey, J. A., "Exoelectron Emission From Deformed Metal Surfaces," J. Australian Inst Metals, Vol 10, 1965, p 323

Ramsey, J. A., "The Emission of Electrons from Aluminum Abraded in Atmospheres of Air, Oxygen, and Water Vapour," Surface Sci, Vol 8, 1967, p 313

Ramsey, J. A., and Garlick, G. F. J., "Sensitized Photoelectric Emission During Oxidation of Aluminum," Brit J Appl Phys, Vol 15, 1964, p 1353

Seeger, K., "Die verzögerte Elektronenemission von Metallen," Z Physik, Vol 141, 1955, p 221

Seeger, K., "Verzögerte Elektronenemission und äusserer Photoeffekt von Germanium nach Elektronenbeschuss," Z Physik, Vol 149, 1957, p 453

Shlyapin, V. I., Vasserman, N. N., and Gladkovskii, V. A., "Study of the Fatigue Process by Means of Electric Impedance Measurements," Industrial Laboratory, Vol 33, 1967, p 1336

Sullivan, C. P., Averbach, B. L., and Cohen, M., "Repeated Tensile Loading of Iron and Steel," Trans ASM, Vol 54, 1961, p 299

Thompson, N., Wadsworth, N. J., and Louat, N., "Origin of Fatigue Fracture in Copper," Phil Mag, Vol 1, 1956, p 113

Truell, R., Chick, B., Anderson, G., Elbaum, C., and Findley, W., "Ultrasonic Methods for the Study of Stress Cycling Effects in Metals," WADC TR 60-920, 1961

Truell, R., Chick, B., Picker, A., and Anderson, G., "The Use of Ultrasonic Methods to Determine Fatigue Effects in Metals," WADC TR 59-389, 1959

Vogel, A., "Beiträge zur Excelektronenemission von Kristallen und Metallen," Z Physik, Vol 158, 1960, p 77

von Voss, W. D., and Brotzen, F. R., "Electron Emission From Plastically Strained Aluminum," J Appl Phys, Vol 30, 1959, p 1639

Wei, R. P., and Baker, A. J., "A Metallographic Study of Iron Fatigued in Cyclic Strain at Room Temperature," Phil Mag, Vol 12, 1965, p 1005

Williams, R. A., "An Investigation of Exoelectron Emission From Various Materials Using Abrasion and Ultrasonic Techniques," TM 630.328-04, Naval Ordnance Systems, Navy Department, 1966

Wood, W. A., "Some Basic Studies of Fatigue in Metals," Fracture, edited by B. C. Averbach, D. K. Felbeck, G. T. Hahn, and D. A. Thomas, John Wiley and Sons, Inc, New York, 1959, p 412

Wood, W. A., and Bendler, H. M., "Effect of Superimposed Static Tension on the Fatigue Process in Copper Subject to Alternating Torsion," Trans AIME, Vol 224, 1962, p 18

Wood, W. A., Cousland, S. McK., and Sargant, K. R., "Systematic Microstructural Changes Peculiar to Fatigue Deformation," Acta Met., Vol 11, 1963, p 643

Wood, W. A., Reimann, W. H., and Sargant, K. R., "Comparison of Fatigue Mechanisms in BCC Iron and FCC Metals," Trans AIME, Vol 230, 1964, p 511

Unclassified

Security Classification

DOCUMENT CONTROL DATA - R & D

(Security classification of title, body of abstract and indexing annotation must be entered when the overall report is classified)

1 ORIGINATING ACTIVITY *(Corporate author)* North American Rockwell Corporation International Airport Los Angeles, California 90009	2a. REPORT SECURITY CLASSIFICATION Unclassified 2b. GROUP NA

3 REPORT TITLE

The Early Detection of Fatigue Damage

4 DESCRIPTIVE NOTES *(Type of report and inclusive dates)*

Final Technical Report, July 1, 1968 to February 28, 1970

5. AUTHOR(S) *(First name, middle initial, last name)*

George Martin
Schillings Tsang

6 REPORT DATE May 31, 1970	7a. TOTAL NO. OF PAGES 137	7b. NO. OF REFS 64
8a. CONTRACT OR GRANT NO F33615-68-C-1706 b. PROJECT NO ARPA Order No. 1244 c. Program Code No. 8D10 d.	9a. ORIGINATOR'S REPORT NUMBER(S) NA-70-257 9b. OTHER REPORT NO(S) *(Any other numbers that may be assigned this report)* AFML-TR-70-124	

10 DISTRIBUTION STATEMENT This document is subject to special export controls and each transmittal to foreign governments or foreign nationals may be made only with prior approval of the Metals and Ceramics Division, MAMN, Air Force Materials Laboratory, Wright-Patterson Air Force Base, Ohio 45433.

11 SUPPLEMENTARY NOTES NA	12. SPONSORING MILITARY ACTIVITY Advanced Research Project Agency monitored by Air Force Materials Laboratory, MAMN, Wright-Patterson Air Force Base, Ohio

13 ABSTRACT

The fatigue process of 1100-0 aluminum was studied by means of exoelectron emission and ultrasonic surface wave measurements, and correlated with metallographic examination. Measurement of exoelectrons was accomplished by emission counts, amplified by a Channeltron electron multiplier and integrated over short time intervals. It appears that very early in the fatigue process there is an exoelectron emission peak, whose intensity is related to the intensity of the applied stress, coinciding with initial surface layer slip. The emission event lasts not more than a few percent of the fatigue life. No emission occurs thenceforth until in the final stages of fatigue, just prior to failure, when another emission period is observed. It was further noted that, at least at room temperature, light stimulation is necessary for exoelectron emission from 1100-0 aluminum. Preliminary ultrasonic surface wave measurements disclose a change in material response at about 50 percent of the fatigue life, which so far could not be correlated with metallographic observations.

DD FORM 1 NOV 65 1473

Unclassified

Security Classification

14 KEY WORDS	LINK A		LINK B		LINK C	
	ROLE	WT	ROLE	WT	ROLE	WT
Fatigue Process 1100-0 Aluminum Nondestructive Test Exoelectron Emission Ultrasonic Surface Wave						